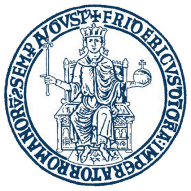

UNIVERSITÀ DEGLI STUDI
DI NAPOLI FEDERICO II

Ph.D. Thesis

Investigation for the Analysis of the Vibrations of Quasi-periodic Structures

Candidate:
Safiullah Timorian

Supervisors at UNINA:
Prof. Sergio De Rosa
Prof. Francesco Franco

Supervisors at UBFC:
Prof. Morvan Ouisse
Prof. Noureddine Bouhaddi

Submitted on January 2020 for cycle XXXII

2017/2020

To Asma, Rose and my Parents (Makrama and Bismullah)

Abstract

In this thesis, the definition and effects of quasi-periodicity in periodic structure are investigated. More importantly, the presence of irregularity in periodic structures and its significant impact in vibroacoustic responses of elastic systems are analyzed. In the extant literature, it has already shown that a sandwich panel, optimized for vibroacoustic performance with added random properties of the core, can exhibit stop band characteristics in some frequency ranges. Therefore, an additional target can exist in framing the abovementioned property under the Wave Finite Element Method (WFEM) for resulting in some design guideline. In this investigation, (1) the numerical studies of the vibrational analysis of 1D finite, periodic, and quasi-periodic beams are presented. The research's content deals with the finite element models of beams focusing on spectral analysis and the damped forced responses. The quasi-periodicity is defined by invoking the Fibonacci sequence for building the assigned variations (geometry and material) along the span of the finite element model in one direction. Similarly, the same span is used as a super unit cell with WFEM for analyzing the infinite periodic systems. (2) Variation method with a developed algorithm is considered to find the most efficient geometrical impedance mismatch of unit cells for vibration control. (3) Numerical studies and experimental measurements on 2D periodic and quasi-periodic lattices are thus performed. Experimental validations are performed by comparing the numerical quasi-periodic model with a prototype manufactured by laser machining. Based on the major findings, and considering both longitudinal and flexural elastic waves in 1D beams, the frequency ranges corresponding to band gaps are investigated. In the 2D structures, the wave characteristics in the quasi-periodic lattice introduce the possibility of designing wider frequency stop bands in low frequency ranges, and presents some elements of novelty; moreover, they can be considered for designing structural filters and controlling the properties of elastic waves. The results obtained in this study show that the beams with Fibonacci and panels with Thue-Morse characteristics can improve performances in terms of attenuation level without weight penalty, which can be an asset for meta-materials.

Acknowledgments

I am very pleased to thank and express appreciation to my family for providing me with their strong support and motivation in this journey. I would like to express my gratitude to Prof. Sergio De Rosa, Prof. Francesco Franco, for their patience and simplicity approach in scientific issues; Prof. Morvan Ouisse, and Prof. Nouriddin Bouhaddi, for their valuable time dedication to our meetings; and Dr. Giuseppe Petrone for his overwhelming support and daily discussions. The PASTA Lab (Laboratory for promoting experiences in Aeronautic structures) at the Università degli Studi di Napoli Federico II (UNINA), with its large wind tunnel and the fuselage section of a DC-10 is an iconic symbol that was a source of motivation every single day that I would cross the staircase to reach the office. I want to thank all the staff and members of the lab for their pleasant conversations and warm welcomes with superb cups of Neapolitan coffee from the cafe bars located close to the lab. I am very proud to be a member of this amazing group in the PASTA Lab'a leading Italian center that performs extraordinary experimental and numerical activities in the aerospace fields. The leader of the laboratory, Prof. Francesco Marulo, is an iconic inspiration for the entire group, and I thank him for those memorable conversations about the upcoming research development facilities in PASTA Lab.

I admire Prof. Morvan Ouisse and Prof. Noureddin Bouhaddi for the invaluable time they provided me during my secondment at the Université de Bourgogne Franche-Comte (UFC). They advised me to the path of pure numerical modelling and code development. This gave me the opportunity to develop the first tools (codes for the physics and mathematics of 1D beam structures and their vibroacoustics application). Similarly, I thank Prof. Morvan Ouisse and S.mart for giving me the opportunity to manufacture 2D meta-materials and test them in the ENSMM Lab in my next secondment. Thanks also to the DSMART team for their amazing weekly meetings and seminars. It was a great opportunity to learn and discuss ideas with the lab members.

Finally, many thanks are due to the VIPER (VIbroacoustic of PERiodic media) project and Marie Sklodowska-Curie Actions grants for their financial support over the duration of the project. The investigation in this thesis was performed in the framework of the VIPER project . The project has received funding from the European Union's Horizon 2020 research and innovation program under Marie Curie grant agreement No 675441 and EUR EIPHI (ANR 17-EURE- 0002) project. Special thanks are due to the S.mart platform for the manufacturing process.

I express my appreciation to all committee members of the VIPER project from all the consortiums, where they provide VIPER schools, conferences, and supervisory meetings. I further wish to thank them for the financial sponsorship during the conference, summer schools, seminars, and workshops. It was an excellent opportunity to meet people and learn in such a globally diverse environment during these three years.

Preface

This thesis first discusses the research and development of new methods and the state-of-the-art for designing periodic structures with irregularities (quasi-periodicity). Then, quasi-periodic structures are subjected to vibration and acoustic analysis. The final objective is to increase the vibroacoustic performances of these types of structures in applied industrial systems. It is well known that periodic structures introduce band gap effects. However, the presence of small degrees of irregularities may have a significant impact on the vibrational and acoustic response of the abovementioned elastic media. Therefore, the main objective of this thesis is to determine the significant impacts of quasi-periodicity in the vibroacoustic analysis using WFEM.

Periodic structures have been a topic of interest for researchers in aerospace, aeronautics, automotive, naval, and civil infrastructure industries for some decades. There are various methods that can be used for vibroacoustic analysis of periodic systems. The very first modern method was the receptance method, which has been applied to periodic beams and rib-skin structures by Mead et al.; it involves direct and inverse solutions of the wave equations. These solutions are used in the Floquet-Bloch theory, which has been applied to beams, plates, cylindrical shells, and sandwich panels. Dispersion relations can be used to represent the propagation and attenuation constants. For non-periodic and near-periodic structures, the transfer matrix method and space harmonics method can predict dispersion diagrams and sound transmission loss from vibrating periodic structures.

In the beginning of the 2000's, the first research was performed into elastic wave propagation in quasi-periodic structures by Veclasco et al. The full transfer matrix technique and surface Green function matching method was used to solve the transverse and sagittal elastic waves. Quasi-periodic structural design was proposed using mathematical sequences such as Fibonacci, Thue-Morse, and Rudin-Shapiro. The method was well established as providing proper response when using Fibonacci sequence patterns. Similar studies

using these types of sequences have been performed in the last decade, and many applications have been discovered in areas such as crystallography, photonics, heat insulation, elastic wave control systems, and vibroacoustic transmission properties.

The main advantage is that the irregularity can be optimized by the deterministic approaches to analyze the design. The use of finite structures with a limited number of cells in a span is rather useful compared to infinite systems, because the Floquet principle relies on strictly periodic patterns; thus, it is quite challenging to predict the dispersion analysis of quasi-periodic structures and compare them with the harmonic response of finite systems. Two approaches are proposed: the use of a super unit cell (identical periodic cell with different properties inside the cell); and the harmonic response of finite but continuous patterns following Fibonacci and Thue-Morse sequences. These two methods are very straightforward and robust.

Objective of the thesis

The aim of this thesis is to transform the developed state-of-the-art of the physics, mathematics, numerical simulations, and experimental research into quasi-periodic media, for the benefit of future generations. The tools developed from analysis of 1D and 2D structural design with vibration and acoustic application is intended to be of future academic benefit. It is intended to advance the understanding of this field, and influence the direction of future research.

Outline of the thesis

The first chapter is dedicated to an introduction to the topic and a discussion of the state-of-the-art. The motivation, scope, and outline of the thesis is presented. Furthermore, a comprehensive literature review of previous studies, quasi-periodic structures, their modelling strategy, and vibroacoustic effects is included.

Chapter 2 describes the modelling strategy of quasi-periodic structures. This section is a central part of the thesis, where modelling of 1D and 2D quasi-periodic structures based on Fibonacci sequences, Thue-Morse mor-

phism, perturbation methods, and fundamental findings on chains of spring mass oscillators are discussed.

Chapter 3 discusses vibration analysis using FEM. Starting from modal analysis using conventional FEM tools to spectral analysis of waveguide using WFEM techniques are discussed. The developed codes for WFEM methods on 1D beams, transfer matrix method, and frequency response of quasi-periodic 1D beams are detailed. Finally, the findings from dispersion diagrams and software-derived harmonic analysis of meta-materials are discussed.

Chapters 4 and 5 present the applied 1D and 2D WFEM techniques and forced response analysis. Chapter 4 describes spectral analysis and structural response of periodic and quasi-periodic beams. It concerns the use of increased orders of the Fibonacci sequence for the design of finite beams, super unit cells, and the method developed herein, called geometrical variations, applied on finite and finite beams.

In Chapter 5, numerical investigations and experimental measurements of the structural dynamic behavior of quasi-periodic meta-material are discussed. The COMSOL with MATLAB software package is utilized for solving the direct methods of wave propagation. Besides the dispersion diagrams, the forced response of meta-structures is also simulated, and the results of numerical simulations are experimentally validated. Chapter 6 contains the conclusion of the thesis.

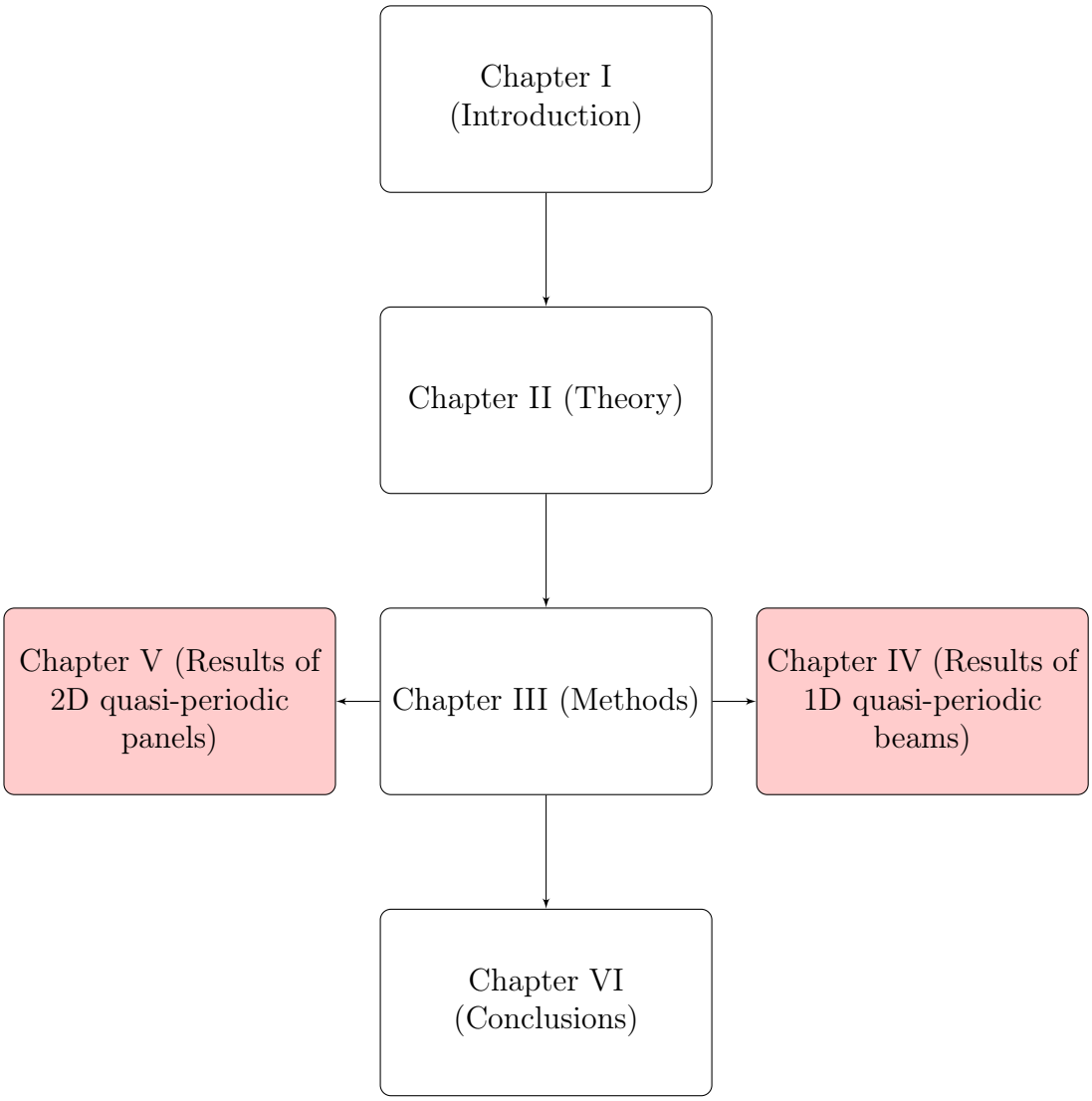
Chapter I
(Introduction)
Chapter II (Theory)
Chapter III (Methods)
Chapter V (Results of
2D quasi-periodic
panels)
Chapter IV (Results of
1D quasi-periodic
beams)
Chapter VI
(Conclusions)

Contents

List of Figures

List of Tables

Part I

Introduction

Chapter 1

Introduction and discussion of the state-of-the-art

Quasi is a word that is quite commonly used in Italian language culture. It is a suffix that when attached to a word, gives the meaning of (apparently but not really). Quasi-periodicity is clearly defined in physics and mathematics. In physics, it refers to the property of a system that displays irregular periodicity, whereas in mathematics, it indicates a function that has a certain similarity to a periodic function. For instance, if we see the plot of $sin(t)$, it is a regular curve in terms of amplitude and wavelength; further, if we see the plot of $sin(\sqrt{t})$, it is observed with regular amplitudes and irregular wavelengths. When we combine these two terms, we achieve a quasi-periodic function.

Periodic structures are of considerable interest in engineering applications because they introduce frequency band effects, due to the impedance mismatch generated by periodic discontinuities in the geometry, material, or boundary conditions, which can improve the vibroacoustic performances. However, the presence of defects or irregularities in the structure leads to a partial loss of regular periodicity (called quasi-periodic structure) that can have a noticeable impact on the vibrational and/or acoustic behavior of the elastic structure. From a physical point of view, the irregularity can be tailored to have an impact on dynamical behavior.

In aerospace applications, the study of structural vibrations is vital for designing structures with the highest safety margins. Aeronautic structures are subjected to external static or cyclic loads; for instance, airplane structures are subjected to random convected pressure fields, from jet noise at low speed and turbulent boundary layers at high speed. In another exam-

ple, space station structures are subjected to impulsive forces from control thrusters and docking impacts, and even to periodic forces from rotating machinery. According to Mead et al., when the natural force function, elastic wave motion is generated within the structure, the associated levels of vibroacoustic response must be predictable so that the structure can be designed with a minimum probability of catastrophic damage or malfunction in service [1]. In this thesis, the aim is to introduce irregularity into periodic structures and study if and how the presence of quasi-periodicity (irregularity) subjected to the aforementioned loading effects has significant impacts.

1.1 Motivation

Limiting the exposure of human beings to noise and vibration is being intensely researched to prevent discomfort and noise pollution. Many methods and solutions have been developed since the mid-21st century to control undesirable noise and vibration inside transportation facilities, bridges, oil and gas plants, automotive industries, power plants and civil structures. There are a wide range of challenges to be faced to overcome these problems. One of the main aspects is the nature and types of these structures that contribute to the induced vibroacoustic excitations.

Recent developments propose periodic media as a powerful design strategy for lightweight structures. Periodic structures are made of finite repetition of a single element in one, two, or three dimensions. In practice, examples of these types of structures include honeycomb lattices, sandwich panels, or repetitive structures formed from trusses, joists, and pipes. These types of structures can be included in metamaterials that exhibit properties not usually found in natural materials. These types of structures could also be easily manufactured.

1.2 Scope

The presence of defects or irregularity in a periodic structure leads to a partial loss of regular periodicity (termed quasi-periodicity) that can have a noticeable impact on the vibrational and/or acoustic behavior of the structure. The envisaged steps for this study are definition of the quasi-periodicity and its modelling, and analysis of the nature and size of the causes altering the perfect periodicity. The most important goal would be the analysis of

irregularity inside these models and to provide evidence whether it has significant impacts inside periodic structures or not.

The first work is focused on introducing a small degree of irregularity inside a perfect periodic pattern. For one-dimensional cases such as beams, the irregularities are straightforward; whereas for 2D cases, the system needs to be diagonally symmetric and must have a different composition of elements or cells in each direction. A more specific goal is the analysis of the influence of such effects on the vibroacoustic response. Modern numerical and analytical tools for investigating the most significant impacts of irregularities on the vibrational and acoustical response of a given structure are based on a combination of wave and finite element analysis, spectral finite elements, and transfer matrix methods. In addition, there are advanced tools such as laser machining for manufacturing, 3D vibro-scanning cameras for capturing the measurements, various types of actuators (i.e. coil/voice, and shakers) for inducing vibration and noise for experimental investigations.

1.3 State-of-the-art

This section will start with brief statements discussing the roots of the state-of-the-art, and link to the periodic, disordered and near periodic, and subject at hand. Later, this section will discuss the novelty and achievements of this study. There are various topics directly and partially related to the subject.

The analysis of the propagation of waves in structures is a fundamental task in many engineering applications. The knowledge of dispersion relations, providing information on the type and nature of propagating waves is of interest for the prediction of forced response, acoustic radiation, non-destructive testing and transmission of structure-borne sound. All these themes are nowadays the subject of many studies in order to improve the vibroacoustic comfort of passengers in aircrafts, trains and automotives; passive vibration reduction of bridges, pipelines, and space vehicles.

Wave propagation in simple structures can be investigated through analytical models, exact or approximated. However, this kind of analysis usually involves assumptions and approximations concerning the stress, strain and displacement states of the structure, and always more refined numerical models are required as the frequency increases since the wavelength may become comparable with the cross-section dimensions. For example, if the propagation of bending waves in a beam is investigated, Euler-Bernoulli, Rayleigh,

Timoshenko or 3-dimensional elasticity-based theories might be used, depending on the frequency range of interest [2, 3]. For complex structures, such as layered (composite and sandwich) beam [4–6] and plate [7–13], or cylinders [14–16], analytical formulations become quite difficult: beyond the required assumptions and approximations in the models, the resulting dispersion relations are usually transcendental and/or of high order, therefore their resolution is not straightforward or requires symbolic manipulation [16, 17]. For this reason, for the analysis of complex structural components, semi-analytical or numerical methods have been developed for the computation of dispersion curves. However, if the structure under investigation presents characteristics which are periodically repeated in one or more directions, the analysis procedure can take advantage of this property by exploiting the periodicity [18]. A generic structure obtained as an assembly of identical elements, called cells, can be considered as periodic. Several engineering structures can be assumed as periodic, starting from simply beams and plates, moving to stiffened plates or car tyres, up to aircraft fuselages, railways, tracks, etc. In this case the study of the wave propagation through the waveguide can be reduced to the analysis of a single cell by applying the periodicity conditions together with continuity of displacements and equilibrium of forces at the interfaces between two consecutive cells (Floquet-Bloch theorem) [19–21].

Periodic structures found a big interest in engineering applications because they introduce frequency band effects that can improve the vibroacoustic performances. In fact, in periodic structures, the impedance mismatch generated by periodic discontinuities in the geometry, acting as a waveguide, and/or in the material, can cause destructive wave interference phenomena over specific frequency bands called “stop band“ or “band gaps“ [22]. However, the presence of imperfections (i.e. defects or irregularity) in the structure, due to the manufacturing process or not exact reconstructions of the boundary conditions for example, lead to the loss of the periodicity of the structure: this can have a noticeable impact on the vibrational and/or acoustic behaviour of the elastic structure.

In this case it is more correct to speak about quasi-periodicity which is the property of a structure that displays irregular periodicity. A quasi-periodic structure can be idealised as repeated substructures which have asymmetric translations in any direction of the Euclidian space. It can be considered as an intermediate case between periodic and random elastic medium [23]. Quasi-periodic behaviour is thus a pattern of recurrence with a component of unpredictability that does not lend itself to a precise measurement.
An example of a natural quasi-periodic structure is a quasicrystal. It was

discovered in 1981 by Dan Shechtman [24, 25] and it is a structural form that are both ordered and non-periodic [17]. These structures are characterized by several properties, such as low coefficient of friction and low heat conductivity, just to cite some of them, that made them very attractive and interesting for technological applications, mainly in the fields of crystallography and photonics [24–29]. Quasi-crystals were used as non-stick coating on frying pans and cooking utensils [30] and to develop heat insulation, led and new materials able to convert heat to electricity [31–33].

In recent years there is a growing interest in the design possibilities offered by quasi-periodic structures also in the field of structural mechanics. This leads to some modelling issues which will be well analysed due to the impossibility of periodic simplifications, but an adequate design of the quasi-periodicity may offer new vibroacoustic properties to the structure [34–37], they also provide experimental verification of the transmission properties of one dimensional phononic crystals based on the quasi-periodic Fibonacci and Thue-Morse number sequence. Hou et al. [34] investigated the transmission properties and the band structure of Fibonacci binary composite material with different thickness ratio of two layers. Whereas in this investigation Fibonacci series is dedicated for 1D structures i.e. beams and the vibration properties and band structure of their unit cells are investigated. In term of analysis this research is mainly focused on Frequency Response Functions (FRF) and spectral analysis to study the dynamic behaviour of the structures [38–40]. Aynaou et al. [35] performed a theoretical investigation on acoustic wave propagation of one-dimensional phononic band gap structures made of slender tube loops pasted together with slender tubes of finite length according to a Fibonacci sequence. In this analysis Aynaou et al, found that besides the existence of extended and forbidden modes, some narrow frequency bands appear in the transmission spectra inside the gaps as defect modes. Similarly, in the results of the current investigation, there are narrow frequency peaks that appears in the frequency bands of the geometrical impedance mismatch case, especially on longitudinal frequency response. Aynaou et al consists a treatment procedure that spatial localisation of the modes lying in the middle of the bands and at their edges is examined by means of local density of states. In the other hand, Chen and Wang [36] studied band gaps of elastic waves propagating in one-dimensional disordered phononic crystals. Similar topological formation of Fibonacci and Thue-Morse are investigated in an experimental observation of the formation of phononic scattering band structure in one-dimensional periodically and quasi-periodically based on the Fibonacci and Thue-Morse number sequences by King and Cox [37]. Gei [41] shows that in the case of axial and

flexural vibration for systems based on different Fibonacci sequences, the number of stop/pass bands within a defined range of frequencies changes and follows the Fibonacci recursion rule, by showing also a self-similar pattern. From a design point of view the asymmetrical conditions in quasi-periodic structures can be built by following different sequences, such as: higher order generations of Fibonacci sequence, Thue-Morse, Rudin Shapiro sequences as well as Penrose lattices [42].

1.3.1 Periodic Structures

Periodic structures are made of a number of identical structural components joined together to form a global structure. In structural engineering, the mass and elasticity of the structural members are continuous; however, if these masses and elastic parts are arranged in regular patterns, it is called a periodic structure. Periodic structures can be defined in one, two, or three dimensions. They usually consist of straight and curved bars/beams, flat plates, and curved shells, each with different support conditions. Examples of periodic structures are ribbed plates on aircraft fuselages, multi-story buildings, multi-span bridges, multi-blade turbines and rotary compressors, chemical pipelines, stiffened plates and shells in aerospace and naval structures, space station structures, and layered composite structures.

Ideally, periodic structures should be designed with full consideration of the vibration to be encountered in service life; this could be caused by time dependent forces, pressure, or motion. For instance, this could be caused in buildings by earthquakes or proximity to heavy traffic, and for multi-blade turbines it could be caused by periodic or cyclic forces from reciprocating or rotating machinery.

1.3.2 Disordered and near periodic structures

These types of structures are periodic structures that contain either one element that is not identical to the others, known as a single disorder, or many elements that deviate from an average repeated by a small amount, known simply as disordered [43]. Mead and Bansal (1978) developed a general theory for mono-coupled periodic systems with a single disorder. The strategy is divided into three types of disorder systems: a beam element of non-periodic length; a rotary mass as a support; and a rotary spring at a support [44]. Each disorder has its own influences and impacts on the vibration analysis; thus, the dynamic behaviour of these types of periodic structures

is very complex. However, it is important to have a basic understanding of periodic structures to ensure safe, efficient, and economical design.

1.3.3 Quasi-periodic structures

We learned from sub-section 1.3.1 that periodic systems have an ordered and regular pattern. Despite of that, quasi-periodic systems with ordered pattern lacks regular translational symmetry in one or two directions. So, from practical point of view the definition of quasi-periodicity in the structure is the presence of defects or irregularity in the periodic structure, that leads to a partial lost of regular periodicity (called quasi-periodic structure). The previous definition of quasi-periodicity precisely points to the core of the problem.

Literature review

The quasi-periodicity concept which is investigated in this research can be interpreted as a certain degree of irregularity introduced in a periodic pattern. In fact, quasi-periodicity is the property of a system that displays irregular periodicity. Periodic behavior is defined as recurring at regular space and time intervals. Quasi-periodic behavior is a pattern of recurrence with a component of unpredictability that does not lend itself to precise measurements. It precisely points to the core of the problem. In fact, an increasing amount of literature is appearing on methods for the analysis of a given system by replicating only its elemental cell in space directions and time scale, thus simulating conditions of perfect periodicity. How to simulate systems, if perfect periodic conditions are violated, is still to be analyzed.

For periodic structures, the definitions of the effect of quasi-periodicity must be investigated in order to understand the physics, how this can be modelled, and what are the effects of the final design. In fact, it will be important to analyze if and how the presence of imperfections or irregularities, on a quasi-periodic basis, can have a significant impact on the vibro-acoustic responses of given components. It is expected and already shown that the effects on micro-scale can influence the performance on the macro-scale: the engineering design can receive important information if more light is shed in this link. Several analysis methods have been previously reported (the Anderson localization is one of the most famous), but some insights are now necessary in order to improve not only the simulation of quasi-periodic media,

but also to move to experimental prototypes that can demonstrate increased vibroacoustic performance (structural damping and/or acoustic transmission loss).

Starting from 1958 in an acoustical context, the discovery of Anderson localization phenomena showed that irregular vibration propagation could be impeded by lattice irregularities, giving rise on average to an exponential decay of vibrational level. Then, investigations in the 1980's and 90's founded periodic and non-periodic patterns, with a focus on random structures, and the response of the system caused an irregular vibration that was caused by irregularities impeding vibration in the system. In early 2000, Velascoe et al. investigated the elastic wave propagation in quasi-periodic structures and obtained the dispersion relations for elastic waves and spatial localization of the different modes. He proposed that the fragmentation of the spectrum (degree of split for a given portion of spectrum) for different sequences (Fibonacci, Thue-Morse and Rudin-Shapiro) is evident using intermediate generation orders; in the case of transverse and sagittal waves, higher generation orders are required to show the fragmentation clearly.

In 2010, Gei et al. investigated the band structures of dispersion diagrams for flexural and axial waves of quasi-periodic infinite beams. In conclusion, he indicated that tensile axial prestress promotes length reduction of pass bands while leaving the length of stop-band intervals almost unchanged. The design of quasi-periodic structures using Fibonacci sequences has attracted many researchers of structural design in recent years. In fact, modelling these types of structures may lead to some modelling issues which will be well analyzed due to the impossibility of periodic simplifications; however, an adequate design of the quasi-periodicity may offer new vibroacoustic properties to such structures. Both transmission loss and structural damping of quasi-periodic structures have been investigated. Hou et al. determined the band structure of a Fibonacci binary composite material with two layers of different thickness. In another theoretical investigation, Aynaou et al. simulated acoustic wave propagation in one-dimensional phononic bandgap structures made of slender tube loops pasted together with slender tubes of finite length according to a Fibonacci sequence. Chen and Wang then investigated the band gap of elastic wave propagation for a different structural design of one dimensional disordered phononic crystal. King and Cox developed a topology formation of Fibonacci and Thue-Morse sequence based on experimental observation of the formation of phononic scattering band structure in one-dimensional periodic and quasi-periodic systems.

There are interesting subjects in the literature partially linked to the current investigation which is intended mainly to the design of new architectured metamaterials (i.e. lightweight, easy-to-manufacture, and low frequency stop band properties, noise and vibration reduction) [45], [46].
Periodic structures create stop bands effect due to the geometrical and/or material impedance mismatches that can result in great vibroacoustic performances. In terms of material properties, there are various cases that show in-plane and out-of-plane elastic properties. For example the dynamical behaviour of a $2D$ periodic waveguide, which exhibits in-plane elastic properties (Young's and shear modulus) compared to out-of-plane ones, are described in terms of elastic wave propagation in [19, 47]. The possibility of designing such smart materials or structures, that can partially reduce mechanical waves on certain frequency ranges, is addressed in [21, 48, 49]. Geometrical discontinuity also plays a central role in creating stop band effects; as an example, sandwich beams with periodic auxetic core, exhibiting impedance mismatch generated by varying elastic and mass properties of the core, are able to produce stop band effects [50, 51].

According to the recent literature, there are also numerous examples of disordered periodicities and/or uncertainties in real structures, like bridges with column spans, and array of fuel tanks interconnected with each other by flexural links. The issues of the non-perfect periodicity in real structures can also be attributed to errors in manufacturing processes [52]. The presence of defects and imperfections in geometric and constitutive properties of the structures is generally referred as *disorder* [36]. Numerical solutions of these types of disordered systems can lead to the need of full stochastic approaches [53]. When the irregularity is localized in space (a 'defect'in the periodic arrangement), phenomenon of Anderson localization may occur, evidencing that the vibration propagation in a structure is not entirely regular and that could be impeded by the irregularities, giving rise on the average to an exponential decay of vibration level [54, 55]. They also demonstrates an example of a string with regular and irregular spacing of added masses in order to use it as a sort of passive vibration control.
On the other hand, the imperfections can be engineered and used as design parameters to tailor the dynamic behaviour. Among others, sequences of impedance mismatches built on numerical series like Fibonacci, Thu-Morse or Rudin Shapiro can be considered as design templates for the engineered irregularity [23].

In previous studies, it has already been shown that a sandwich panel, optimized for vibroacoustic performance by adding random properties of the core unit cell, can exhibit stop-band characteristics in some frequency ranges. An

additional target can consist in framing the aforementioned property under the Wave and Finite Element Method (WFEM) in order to lead to some design guidelines. The analysis could be performed by considering the presence of irregularities that have a significant impact on the vibrational and acoustic behavior. However, the standard finite element method is not very effective for utilizing the solution of the wave propagation problems [56]. The errors introduced in this method have been identified and analyzed, and they are due to the fact that wave propagation analysis is based on piecewise polynomial approximation: the accuracy of the numerical solution becomes rapidly worse with increasing wave number. Refs. [57] and [58] are good examples of how the use of periodicity and the WFEM can result in enhancement of the predictive quality. In [59], an enriched finite element method is presented to solve various wave propagations. The proposed method is an extension of the procedure introduced by Kohno, Bathe, and Wright for one dimensional problems [56]. The WFEM has been identified as the best approach for vibroacoustic analysis of periodic structures. The numerical method has been carried out via Bloch's theorem and imposing periodicity conditions to a single cell that represents a repetitive part of the whole structure. The results show promising agreement between WFEM and the Classical Finite Element Method (CFEM). Experimental testing and validating comparisons on stiffened cylinders are ongoing at Pasta-Lab.

In general, a generic structure obtained as an assembly of identical elements, called cells, can be considered a periodic structure. The modelling of a short section of the waveguide is expressed by supposing time harmonic motion; then, the equation of motion is implied by discrete coordinates, relating nodal degrees of freedom q and force f of the undamped section:

$$(\mathbf{K} - \omega^2 \mathbf{M})q = f \tag{1.1}$$

where $\mathbf{K}$ and $\mathbf{M}$ are the stiffness and mass finite element matrices [19, 58, 60, 61]. The analysis of periodic systems is thus well undertaken through WFEM. The analysis of transmission and diffusion at joints between waveguides as well as the damped periodical waveguides were investigated in several research works, [19, 61]. In [62–64], the first models to take into account the irregularities are presented: they are very recent and represent useful investigations to guide the next required steps. At the moment, the approach adopted in [57] seems the most promising for reproducing the forced response of periodic structures in presence of quasi-periodicity and variability effects. The flexibility of getting the $\mathbf{K}$ and $\mathbf{M}$ matrices from standard finite element codes and the definition of an external post-processing code appears as the most viable procedure even in view of the expected variations to be included

for simulating the quasi-periodicity.

1.3.4 Strategy

The envisaged steps for facing a such complicated problem are the following:

- *A*- Definition of the quasi-periodicity;
- *B*- analysis of the nature and sizes of the causes altering the perfect periodicity;
- *C*- definition of the required:
  analytical
  numerical
  experimental tools

The above are all challenging. In Fig. 1.1, a sketch of the possible problems/configurations is reported. The perfect periodic system (a) can be altered to get a (b) quasi-periodic system in terms of shapes, junctions, sizes, materials, etc.; These effects could be evaluated by adding each of them in a predictive environment. This will lead to development of a new class of software codes expected to be based on a combination of wave and finite element methods, spectral finite element methods, transfer matrix methods, and the adoption of stochastic variables, if needed. The possibility of using non-deterministic (possibilistic) algebra should also be considered, such as those associated to fuzzy-logic or interval algebra.

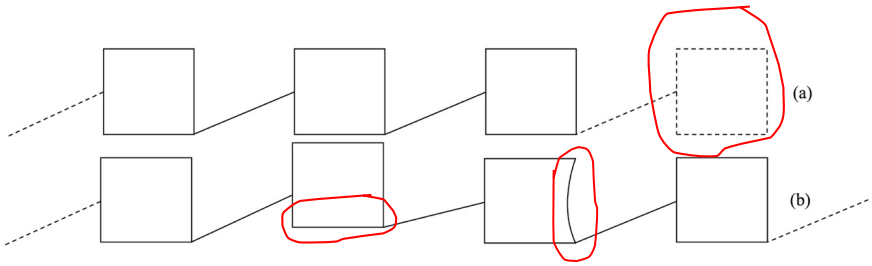

Figure 1.1: Sketches of the periodic and quasi-periodic distribution of repeated cells, (a).Periodic System, (b) Quasi-periodic System.

The first design proposal in this thesis is for 1D beams. In this design, the quasi-periodicity is defined by invoking the Fibonacci sequence for building the assigned variations (geometry and material) along the span of a finite element model [65]. Similarly, the same span is used as a super unit cell (an

identical unit cell with different properties) with Floquet-Bloch boundary conditions for analyzing infinite periodic systems. The frequency ranges corresponding to band gaps are investigated by considering longitudinal and flexural elastic waves. The wave characteristics in quasi-periodic beams present some novel properties and could be considered for designing structural filters.

The second proposal is for 2D lattices. In this part, a WFEM and harmonic response analysis of a meta-material structure is considered. A deterministic approach is used to introduce a 2D Thue-Morse sequence for creating a quasi-periodic metamaterial to improve the vibroacoustic performance [66]. Some sequences such as the Thue-Morse are intrinsically ready to be used for 2D cases, whereas the Fibonacci sequence is more suitable for 1D cases. Two dimensional lattices are built with the conventional finite element method (FEM) to comply with the Thue-Morse sequence in order to explore the opportunities offered in terms of reduction of the forced response in some frequency bands. Specifically, the work presents a modified version of a starshaped concave unit cell. The tailored quasi-periodicity is defined by invoking a bi-directional Thue-Morse morphism sequence on the meta-material. The geometrical impedance mismatch results in asymmetry and follows a combination of two different star-shape elements by variation of different corner angles. The main target of the study is structural stop band/filters in order to isolate the maximum vibration level at certain frequency ranges.

Part II

Theory

Chapter 2

Modelling strategy of quasi-periodic structures

2.1 1D systems

To start modelling strategy, a simple spring mass system is modelled using MATLAB. The system consists of multiple masses and connected to each other by springs. The main objective is to design a quasi-periodic mass oscillating system.

Perturbed spring mass oscillators

A multiple spring mass system is designed, that consists of 12 objects, with the same masses and 13 objects, with the same stiffnesses.

Four cases are considered for the periodicity pattern, with each single case itemized in below: The first case models 4 inhomogeneous masses i.e. mass (read: density) vary throughout the individual element and repeats three times up to object number 12, and similarly for stiffnesses. The second case models triple inhomogeneous masses repetition. The third case models double inhomogeneous mass repetition. Finally, the fourth case is similar to case three, except with a double perturbation in mass 5 and 6 (middle) of the oscillator system. The perturbation in the last case is simply defined as a small change in the masses number 5 and 6, to be called (*quasi-periodic*) oscillator. Cases 1, 2, 3, and 4 are respectively displayed in Figs. 2.1, 2.2, 2.3, and 2.4.

- $(m_1 \neq m_2 \neq m_3 \neq m_4 = m_5 = m_1 ... m_{12},)$

- $(m_1 \neq m_2 \neq m_3 \neq m_4 = m_1 ... m_{12},)$
- $(m_1 \neq m_2 \neq m_3 = m_1 ... m_{12},)$
- $(m_1 \neq m_2 \neq m_3 = m_1, m_4 \neq m_6 ... m_{12},)$

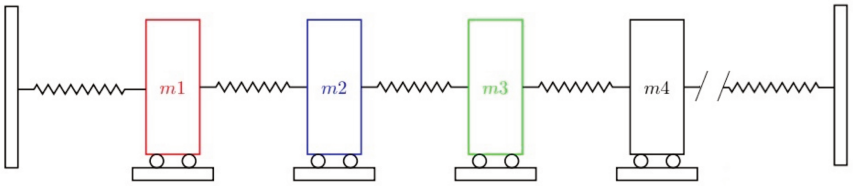

Figure 2.1: Schematic of the finite periodic spring mass oscillator with 4 inhomogenous masses and similar for stiffnesses repeated all along the span

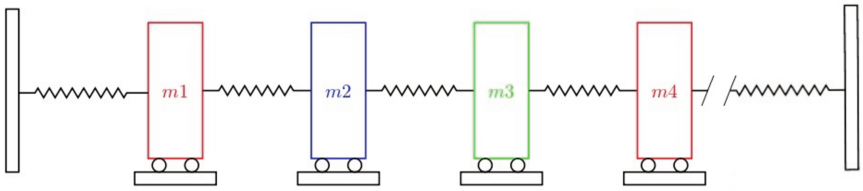

Figure 2.2: Schematic of the finite periodic spring mass oscillator with three inhomogenous masses and similar for stiffnesses repeated all along the chain of oscillator

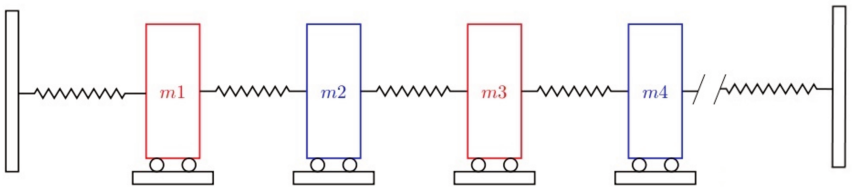

Figure 2.3: Schematic of the finite periodic spring mass oscillator with two inhomogenous masses and similar for stiffnesses repeated all along the chain of oscillator

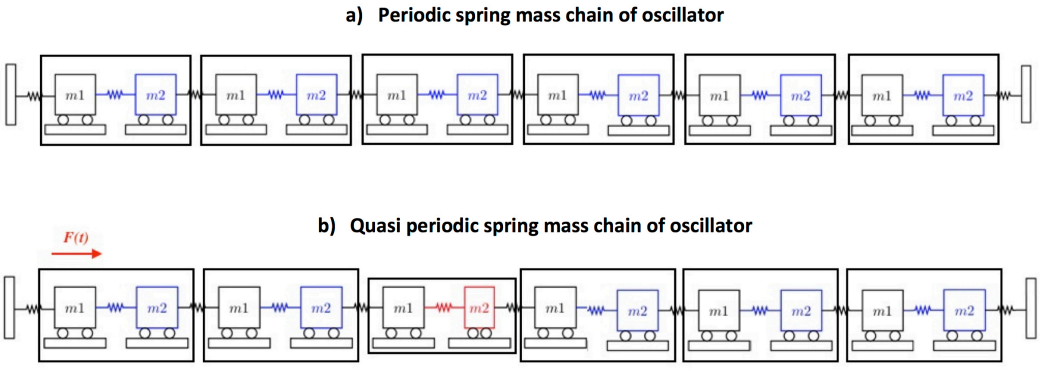

Figure 2.4: Schematic of the finite periodic spring mass oscillator with two inhomogenous masses and similar for stiffnesses repeated all along the chain of oscillator. This diagram is similar to case 3, except with a double perturbation in mass 5 and 6 (middle) and similar for stiffnesses of the oscillator system. The perturbation in this case is simply defined as a small change in the mass and stiffness of the oscillator in the exact location

Fibonacci Sequence, Perturbation and Nomenclature

The well-known sequence called Fibonacci [67] is a series of integer numbers such that:

$$\boldsymbol{S_n = S_{n-1} + S_{n-2}} \tag{2.1}$$

For instance the Fibonacci sequence starting with 1 and 2 is 1, 2, 3, 5, 8, 13, 21,....The configuration of the quasi-periodic structures is here carried out by using a sequence of two possible variations according to Fig.2.5.

The variations can typically be due to the sections, materials or boundary conditions. The first cell coincides with $\boldsymbol{S_1}$, then the cells can be assembled, forming a sequence defined by a simple integer (order). The $\boldsymbol{S_n}$ denote the n-th sequence:

This series is used as a mathematical configuration for building an assigned periodic bars/beams (Fig. 2.5), plates, and even complex structural configurations. Recently researchers are mainly focusing on studies of the physical properties of the solid systems having long-range orders and lacking translational symmetry [23]. Therefore recent developments in quasi-periodic systems as an intermediate sequence between periodic and random are of inter-

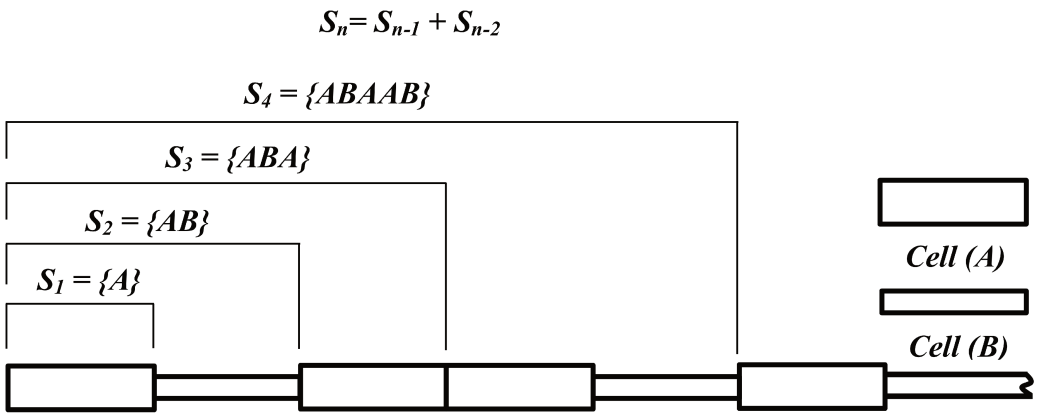

Figure 2.5: Configurations of quasi-periodic beam following a Fibonacci pattern

est. Perturbation is used to model finite beams with deterministic approach, introduced in one of its elements alongside the beam span, see Fig. 2.6.

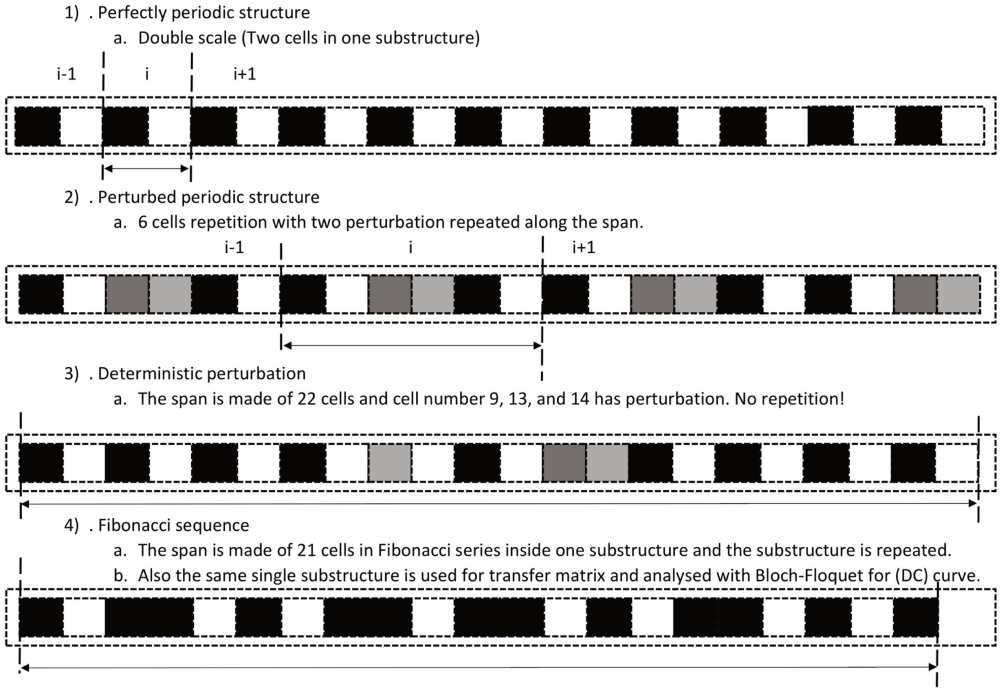

Figure 2.6: Configuration of periodic and quasi-periodic beams using Fibonacci and perturbation

Thue-Morse Sequence and Nomenclature

Thue-Morse sequence is based on binary arrays (an infinite sequence of A_s and B_s). Starting from a $1D$ example, the sequence can be a function s from the set of binary sequences by replicating every A in a $1D$ sequence with AB and every B with BA [68]:

$$s(x, y) = s(x)s(y). \tag{2.2}$$

Eq. 2.2 defines a map s for all strings x, y. The sequence starts with A then AB, $ABBA$, $ABBABAAB$, and so on, [69]. Defining the Thue-Morse morphism $s(A) = AB$, leads to the relations for increasing the quasi-periodicity pattern in one direction. See Fig. 2.7.

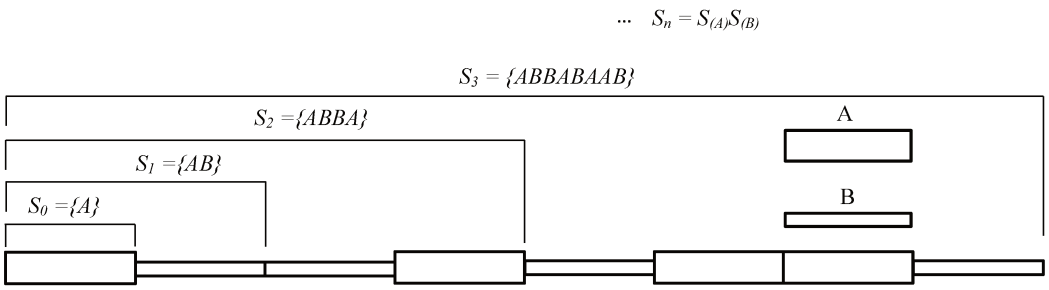

Figure 2.7: Configuration of quasi-periodic beam using Thue-Morse sequence. The beam is modelled from the combination of two different unit cells A and B. The configuration contains the first 3^{th} order of the sequence that includes combination of 8 unit cells A and B

Super Unit Cell

A super unit cell is a cell that hosts a single order of the Fibonacci or Thue-Morse sequences and it hosts given order of deterministic quasi-periodic pattern in a single cell. Although it will be repeated in a periodic way, the cell itself has a quasi-periodicity replication inside the super unit cell. The super unit cell is always identical but with a different properties. Two types of periodicity are considered.

The first identical cell has multiple sub-cells following Fibonacci series . The second identical cell is similar to that used for the biatomic approach used in the rod cases of the previous sections. This time the structure has a periodicity pattern with a combination of double cells with different properties. For illustration, the substructures are described in details for super cell, Fig. 2.8, and for double cell, see Fig. 2.9.

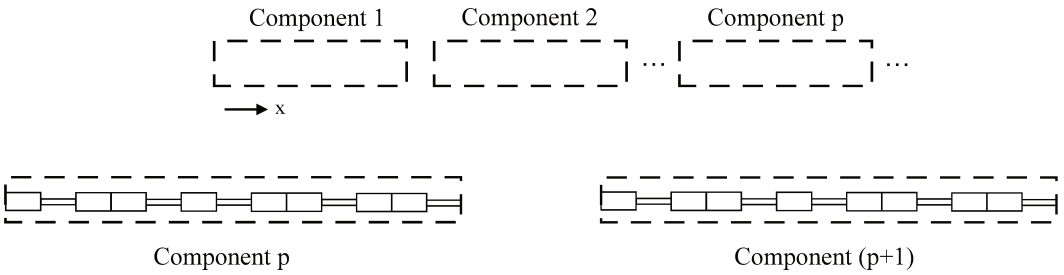

Figure 2.8: Periodic wave-guide (Super unit cell with 6^{th} order of the Fibonacci sequence)

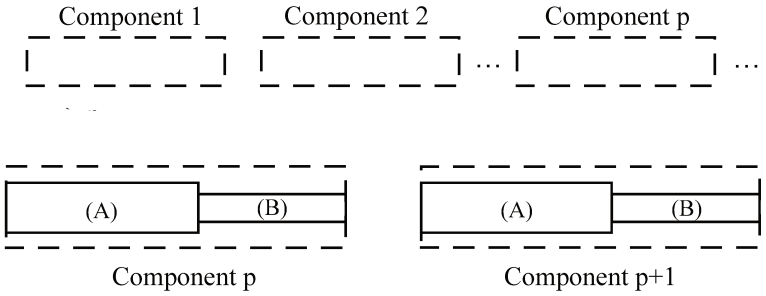

Figure 2.9: Periodic wave-guide (reference double unit cell)

2.2 2D systems

The study of 2D systems are based on shell plates, lattices, and 3D panels. The design strategy consists of the replication of unit cells in two folds. First fold with square periodicity and second one hexagonal or triangular periodicity. In this case study, only square periodicity are considered.

2.2.1 Design of a lattice structure

Considering the Thue-Morse sequence in 2D, a pattern is designed, composed of two different elements A and B and replicated in two directions. Depending on the orders of the sequence, different lattices could be modeled. The first order starts from a 2×2 matrix containing [A,B;B,A] that is equivalent to the second order s^2(A). In the next part of the algorithm, the second order matrix is translated to the right, left, and diagonal directions in order to build s^3(A) and so on. A loop is generated to translate the same order to the right and left with the opposite entries and similar entries to the diagonal direction to fulfil the pattern of the Thue-Morse sequence. The orders are detailed below:
$s(A) = AB$
$s^2(A) = s(s(A)) = AB \mid BA$
$s^3(A) = s(s(s(A)) = ABBA \mid BAAB$
$s^4(A) = s(s(s(s(A)))) = ABBABAAB \mid BAABABBA$

Each A and B represents cell A and cell B, respectively. In the present model, only 64 combined unit cells are used: the Thue-Morse morphism map stops at s^4. The designed quasi-periodic lattice is shown in Fig. 2.10.

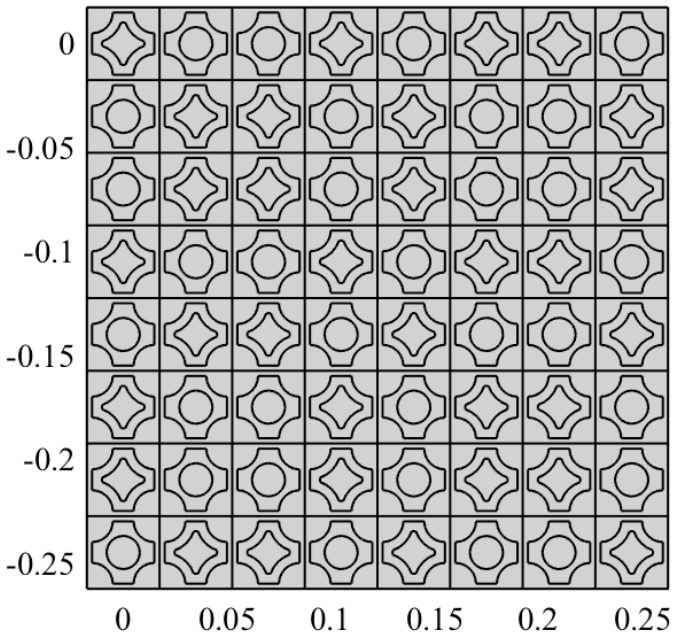

Figure 2.10: Schematic of the Thue-Morse sequence in 2D

The replication of the two unit cells starts form the second order with 4×4 elements and continues to infinite orders.

2.2.2 Quasi-periodic metamaterials

Metamaterials are human made typical structures that has specific properties which is not found in the nature. These types of materials are assembled out of multiple elements. They are usually made of metals, plastics, and woods. These materials are formed into assemblies of multiple panels in plates and lattices. In this thesis, a 2D meta-material lattice is designed to be used as a filter junction for the elastic wave propagation (Fig. 2.11). The elastic wave propagates from one portion of this structure to the other portion. The metamaterial is located at the interface between the two substructures.

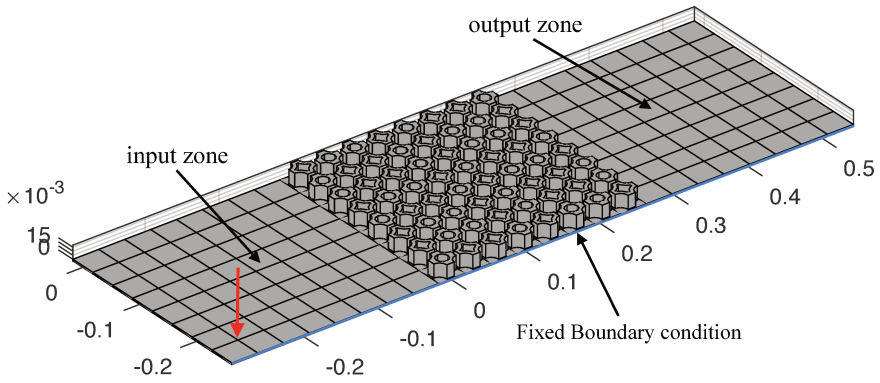

Figure 2.11: Quasi-periodic meta-material model

2.2.3 Quasi-periodic Phononic Crystals

A study of recent literature revealed many theoretical, numerical and experimental studies based on vibration reduction and acoustic transmission loss of small and large scale elastic structures using 2D Phononic Crystals (PCs). The very existence of band-gaps in PCs was predicted theoretically by [70–73]. The quasi-periodic model is defined by a small degree of irregularity in the PCs super-cells. In this study two unit cells are modelled for wave finite element analysis, and two finite periodic panel and one quasi-periodic

panel are modelled for forced response analysis shown in Fig. 2.13

Semi-Sierpinski carpet PCs

Semi-Sierpinski carpet (SSC) is a plane fractal curve and it has a technique of subdividing a shape into smaller copies of itself, removing one or more copies, and continuing recursively can be extended to different shapes. The (Semi) suffix in the definition of this topic concerns that instead of removing one piece from the center of the cell, it removes 5 pieces and continuing recursively follows the Sierpinski carpet. In this modal the location of SSC reveals the position of local resonators (Fig. 2.12).

Phononic Crystals Super-cell

The super-cell is made of 25 cells, each of which is comprised of a square matrix with circular scatterers as inclusions, in which 9 of these circles of these square unit cells are filled with metal scatterers and the rest are hollow air holes all around the super-cell. Cell A, B, C, and D are designed as two different cases. In case 1(quasi-periodic 1) shown in the left side of Fig. 2.13, the quasi-periodicity is applied by considering cell A ($r = 5$ mm), cell B ($r = 3$ mm), cell C ($r = 5.5$ mm), and cell D ($r = 2.5$ mm). The 9 middle cells follow the SSC model, and the other circles with the air holes follow the Thue-Morse sequence. The SSC model controls the filling rate of resonance material by reducing the inclusion of cell A (45 steel) and at the same time increasing the inclusion of cell B (45 steel), using different circular radius in order to keep the same mass as the reference model. In contrast, case 2 (quasi- periodic 2) shown in the right side of Fig. 2.13 deals with a super-lattice of cell A and cell B ($r = 4$ mm) as in the reference model, but the coordinates of the circles in the entire lattice is changed using the Thue-Morse sequence. For instance, the coordinates of the constant cell B are the base position $p(\vec{\mathbf{i}}, \vec{\mathbf{j}})$, in this method unit cell-A is displaced to $\rho(2\vec{\mathbf{i}}, -2\vec{\mathbf{j}})$. In this case cell-A and B is replicated by Thue-morse sequence in two directions (Fig. 2.13).

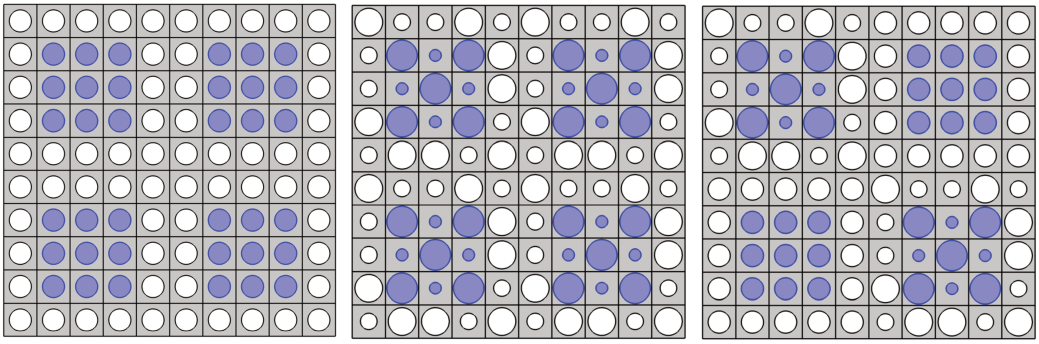

Figure 2.12: Finite quasi-periodic PCs model

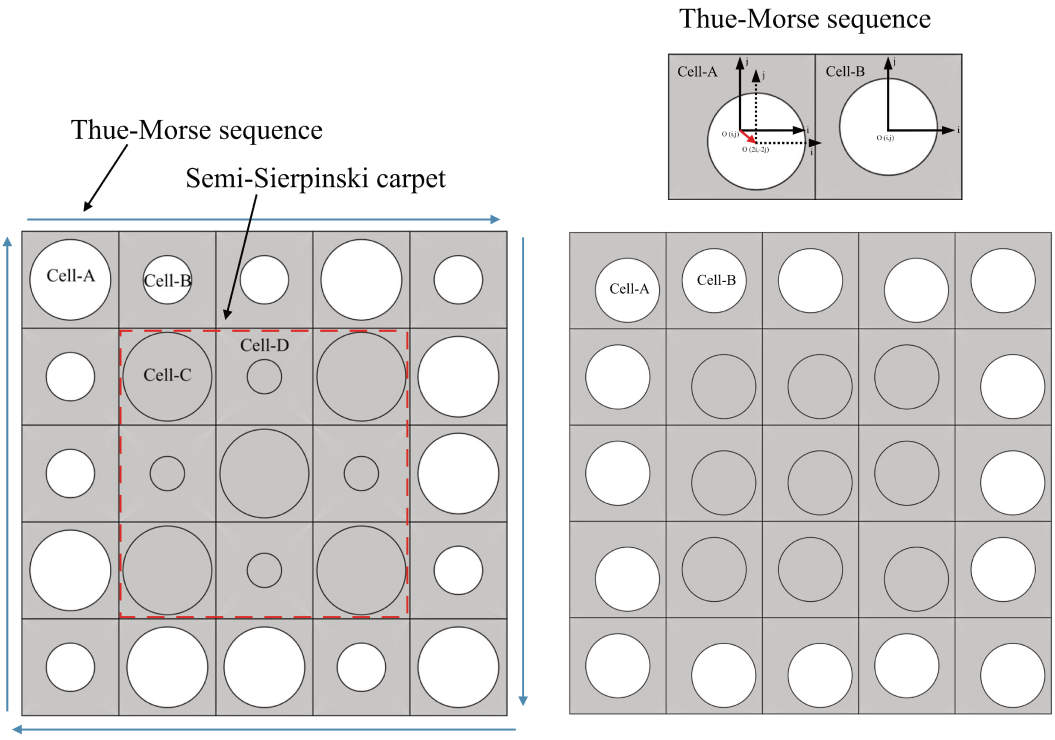

Figure 2.13: Infinite quasi-periodic PCs model

Part III

Methods

Chapter 3

Vibration analysis using FEM

In the pervious chapter sub-section 2.1.1, we learned how to model a multi-Degrees Of Freedom (DOF) system from finite to infinite DOF. It was a fundamental approach towards designing very simple geometry and boundary conditions. However, complex structures may require very complicated exact solutions. Practically speaking, these types of structures can be represented in three dimensional geometries, and consequently the mathematical models may not be very simple. Theoretical models of these complex structures cannot accurately model nonlinearity and anisotropic materials. Therefore, the best way to find solutions is the use of numerical methods. Numerical methods are able to represent a continuum of infinitesimal material particles using an approximate equivalent assembly of inter-connected discrete elements. Each discrete element can be treated individually as mathematical continua. The numerical analysis can involve various methods such as differential equations, finite differences, finite elements, boundary elements, and relaxation techniques [74]. In this chapter, we focus on the use of the Finite Element Method (FEM) and Wave Finite Element Method (WFEM) to perform vibrational and spectral analysis.

3.1 Finite Element Method (FEM)

The FEM is a powerful numerical technique in which a continuum elastic structure is discretized into small but finite substructures. The finite substructures are called elements, and are interconnected with nodes, which means that a continuum beam with infinite number of DOFs can be modelled with a set of elements having finite number of DOFs. The size of the elements depends on the scale and type of structures. The size could also be

small enough that the deformation within the finite element can be approximated by relatively low-order polynomials. In this section, modal analysis and harmonic analysis of 1D beams are presented.

3.1.1 Modal analysis

This subsection presents a simple modal analysis of beams. The beams have configurations of periodic, perturbed, and quasi-periodic systems. A FE model of a periodic beam is simulated using the FEMAP NX-Nastran commercial software package to solve the eigenvalue problem of all three types of periodic structures. In addition, another method called the semi-analytical approach of beam structure is also studied for solving a homogenous beam and periodic beams. The geometrical characteristics of the periodic model are reported in Table.3.1.

Table 3.1: Geometrical description of FEM model

Discrete beam	**Periodic beam Figure 2**	**Perturbed beam Figure 4**	**Quasi-periodic beam Figure 5**
Number of substructures	10	10	10
Configuration of substructures	Double cell	Double cell	Fibonacci sequence
Mesh size of substructures	6 elements	6 elements	3 elements single cell

Three cases are under investigation. The first is a periodic beam, the second a perturbed beam, and the third a quasi-periodic beam. The mechanical properties of each substructure of the periodic beam are kept uniform. The only change in double cell substructure is the cross-section moment of inertia of each single cell. This property is also applied in the quasi-periodic beam. The configuration of the quasi-periodic beam is designed using a Fibonacci sequence [67].

The perturbed beams have similar mechanical properties, but the cells, with perturbed properties, have variations of modulus of elasticity and cross section, of one, two, three, and fifty percent. This statistical variation is used in the modal analysis to observe the transfer of potential energy from one substructure to the next one, and whether the substructure or unit cell acts

as destructive (propagating wave) or constructive (non-propagating wave). Fig.3.1 shows the geometric description of the periodic, perturbed, and quasi-periodic beams following the cross-section and material variations given in Table.3.2.

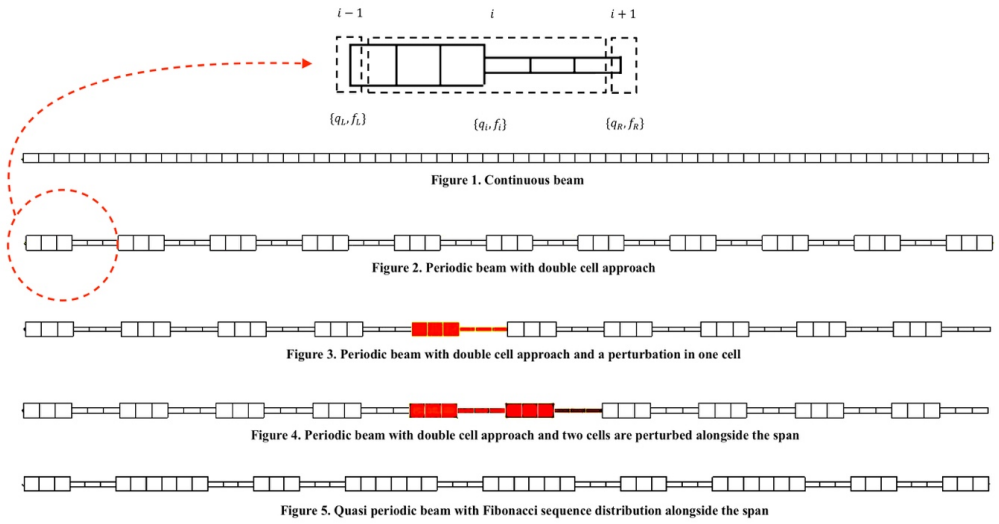

Figure 3.1: Geometric description of the periodic, perturbed, and quasi-periodic beams. Fig.1: continuous beam, Fig. 2: periodic, Fig. 3 and Fig. 4: perturbed periodic beam, and Fig. 5: quasi-periodic beam using Fibonacci sequence.

The two sub-figures 3, and 4 in Figure 3.1 are designed considering virtual manufacturing defects. Figure 3 with low degree of perturbation and figure 4 with higher degree of perturbation.

Table 3.2: Geometrical and material variation description of beams

Beam type	$\boldsymbol{E}$ $(N/m^2)\times10^{-11}$				**Cross section** (m^2)	
Periodic	2				First cell	Second cell
					1×10^{-4}	9×10^{-4}
Perturbed	1%	2%	3%	50%	3%	50%
	1.98	1.96	1.94	1	8×10^{-4}	5×10^{-5}
Quasi-periodic	2				First cell	Second cell
					1×10^{-4}	9×10^{-4}

In this numerical simulation, the periodic beam span is 6 m long for all

models. The numerical model is designed using 1D 2-node beam element type 188. Mesh setting with beam element (188 2-node) with the number of element per wavelength 4, 5, and 10 are checked. As the beam span is 6 m, 19 elements per wavelength was more accurate to converge the exact natural frequency of 5000 Hz. A modal analysis is invoked to extract the eigenfrequencies and mode shapes of the models. The eigenfrequencies of each types of structure are plotted with respect to the length of substructure for visualization of band gaps. In this part of the analysis, only flexural wave modes are under investigation.

Eigenfrequency characterisation

Fig.3.2 shows eigenfrequencies of finite structure with the dispersion relations of beams explained in analytical terms. Eigenfrequencies of all three types of structures are plotted with respect to the same number of substructures in Fig. 3.2. The grey series of circles corresponds to the eigenfrequencies of quasi-periodic beam and the orange circles are the eigenfrequencies belonging to the perturbed periodic beam. Beside that the light blue circled dots are the eigenfrequencies of the perfectly periodic beam and the dark blue dashed lines in the far left of the graph corresponds to the stop bands of the analytical WFEM. The regions bounded by red dash line boxes are band gaps for which the wave does not propagate, roughly between $1500-1800$ Hz and $2800-4200$ Hz. The band gap of span of finite element modelling agree with the band gaps of the wave finite element in the range of $0-5000$ Hz. The analytical model solution shows a good agreement with numerical model.

For higher frequencies, the spectral analysis of Bloch waves in periodic system is used to evaluate the frequency intervals for the finite discrete system. [75] indicates that the main distinction between finite and infinite models is that the former reduces to linear systems with eigenvalues equal to the square of the frequency, whereas infinite models necessarily involves finding roots of transcendental equations.

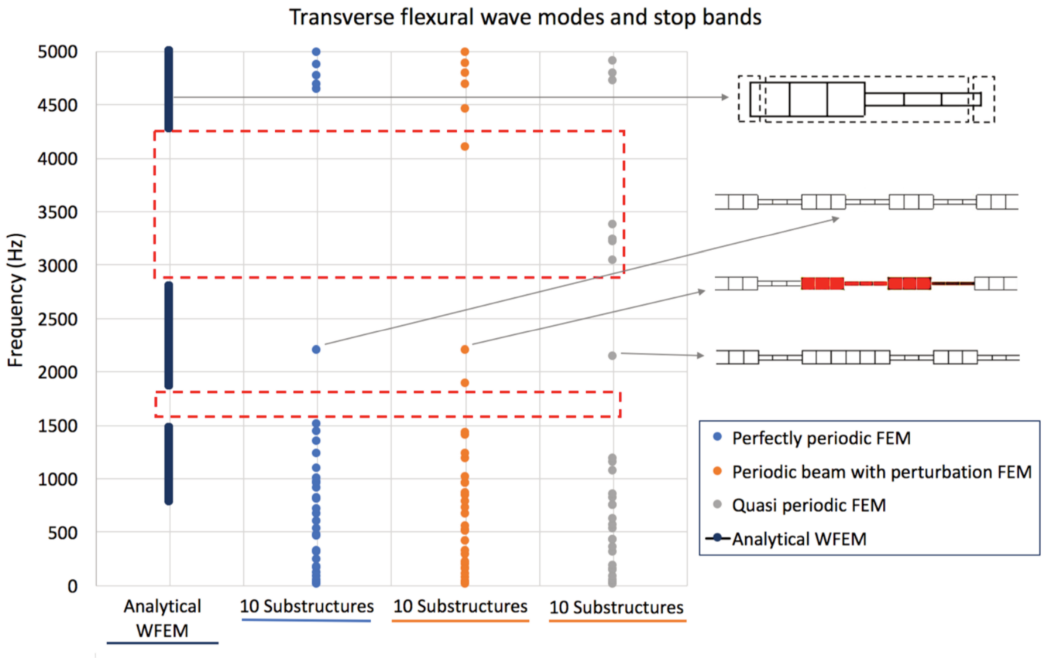

Figure 3.2: Eigenfrequency of finite element is linked with the band gaps of infinite model

3.1.2 Harmonic analysis

The harmonic response of structure can be computed by commercial FE software. In this study, the focus is on harmonic analysis of beams. For 1D beams, there are two types of harmonic analysis, the first is forced response and the second is transmissibility.

Frequency Response Function of Finite beams

The Frequency Response Function (FRF) is calculated by modal analysis of a periodic beam with 10 unit cells as described in Table. 3.1. The analysis consider only the bending wave modes. The FRFs are then compared with the analytical solution of the infinite beams. The aim is to verify the localized waves inside the band gaps of the finite models. In the post processing the velocity magnitude of the response of each case are extracted and plotted with respect to the frequencies. The study of band gaps is clarified, and it is thus more understandable that dynamics of periodic structures create

band gaps and substructure localized resonance. This can be verified in the perturbed and quasi-periodicity cases to find and investigate the localized resonance.

Fig.3.3 shows the velocity magnitude of the response observed in a point very close to the applied input force with respect to the frequency. The zone of excitation is node 16. A force with a white spectrum is applied in the middle of the (substructure number 3) of fully periodic zone.

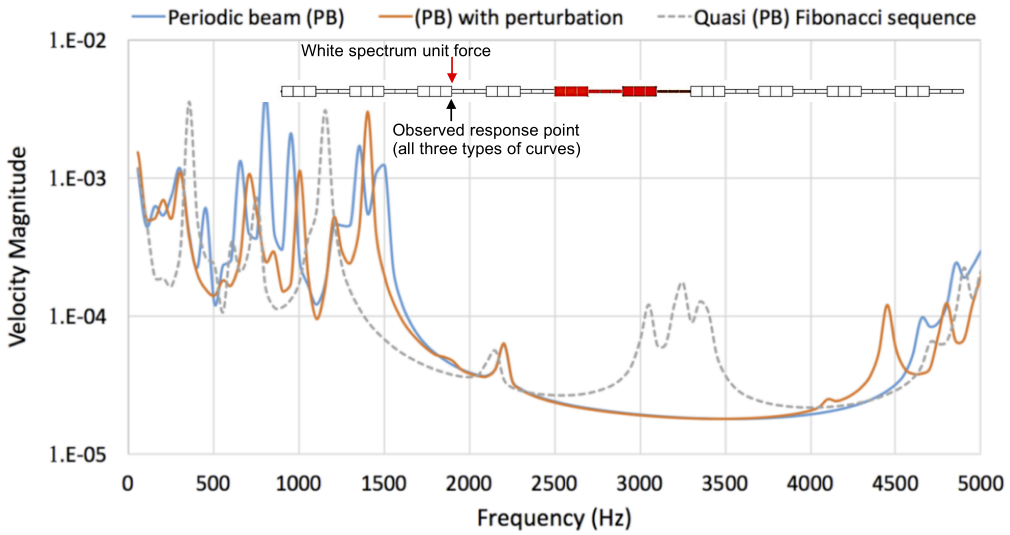

Figure 3.3: Frequency response in terms of velocity magnitude of beams with an applied unit spectrum force in node 16

In Fig. 3.3 The orange curve shows the velocity magnitude of periodic beam with perturbation, which behaves similarly to the periodic beam in the blue plot but with lower amplitude. In the quasi-periodic beam (plot with grey dashed lines), the curve behavior is different. It has a wider band gap that shift to lower frequency, and lower attenuation level compared to its counter parts. There are three localized waves inside the large band gap zone in the frequency range of 3000-3500 Hz.

For the perturbed domain, the response velocity in a location in the periodic region and a location in the perturbed region is plotted in Fig. 3.4. The blue line shows the velocity magnitude propagation of the periodic beam. It

can be observed that there is a stop band in the range of 1500-2100 Hz, and just after 2200 Hz, a peak appears inside the band gap zone that shows a localized wave. Orange curve in Fig.3.4 corresponds to the FRF of perturbed beam for which the velocity magnitude is observed in the second perturbed substructure position, element 27, node 28 middle of 5^{th} unit cell of the perturbed beam. In addition, there is also the blue curve that displays a response velocity in the location of perfectly periodic zone position: element 15, node 16 middle of the 3^{rd} unit cell.

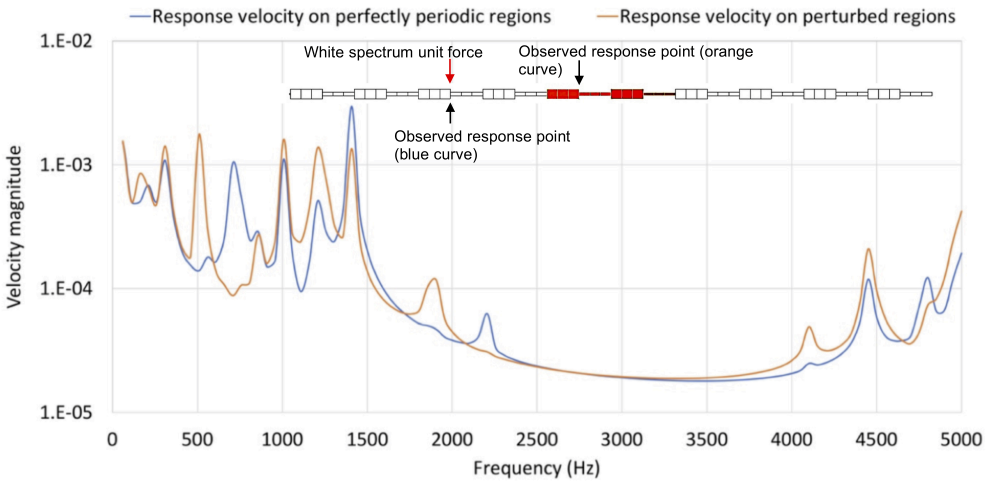

Figure 3.4: Frequency response in terms of velocity magnitude of beams with an applied unit spectrum force in node 28

Transmissibility

Transmissibility is the ratio of output (applied white noise) to input (observed response). In this topic two cases are covered. First a forced response is observed in the input (where white spectrum force is applied) and in the output, where the response is observed in the last node of the beam. Second, the harmonic displacement of the same structure is calculated using APDL-ANSYS finite element software. The response in both cases shows that in the case of harmonic displacement, the forcing frequency and natural frequency of the system coincides. The measurements does not have units but sometimes it refers to Q factor. Fig. 3.5 shows a simple diagram of Q factor. The bandwidth Δf is the difference between frequency f_2 and f_1 of a damped oscillator, with f_c being the central frequency between f_2 and f_1. Then the Q factor can be computed by $\frac{f_c}{\Delta f}$. The higher the Q factor, the narrower and sharper the peak is.

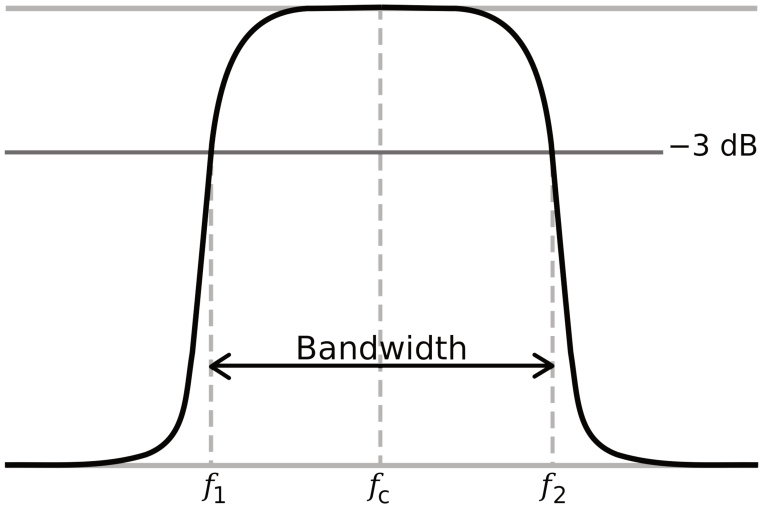

Figure 3.5: Diagram of Q factor and bandwidth discription

Here in Fig.3.6 an example of observed FRF at the input and output is shwon. It can be seen that the FRF of red line coincides with blue line in the peak located in the frequency range of $2400 - 2640$ Hz. The transmissibility is calculated by the Q factor.

Furthermore, in Fig.3.7 harmonic displacement response of a Thue-Mores beam is considered. In this analysis, an initial displacement is introduced instead of force. The response is observed at the end of the finite beam.

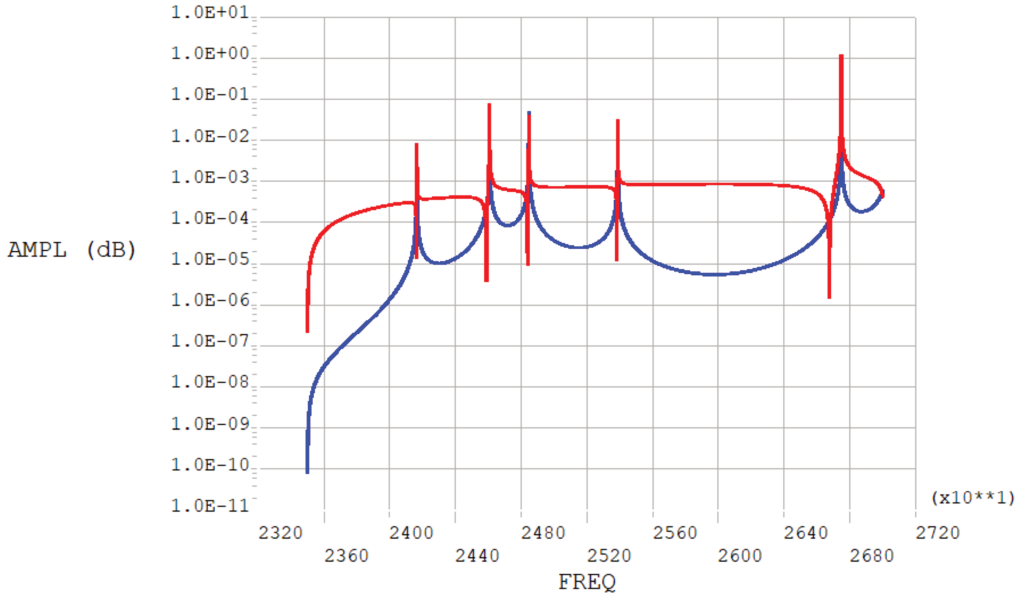

Figure 3.6: Magnified portion of the FRF of the simple beam observed in two points

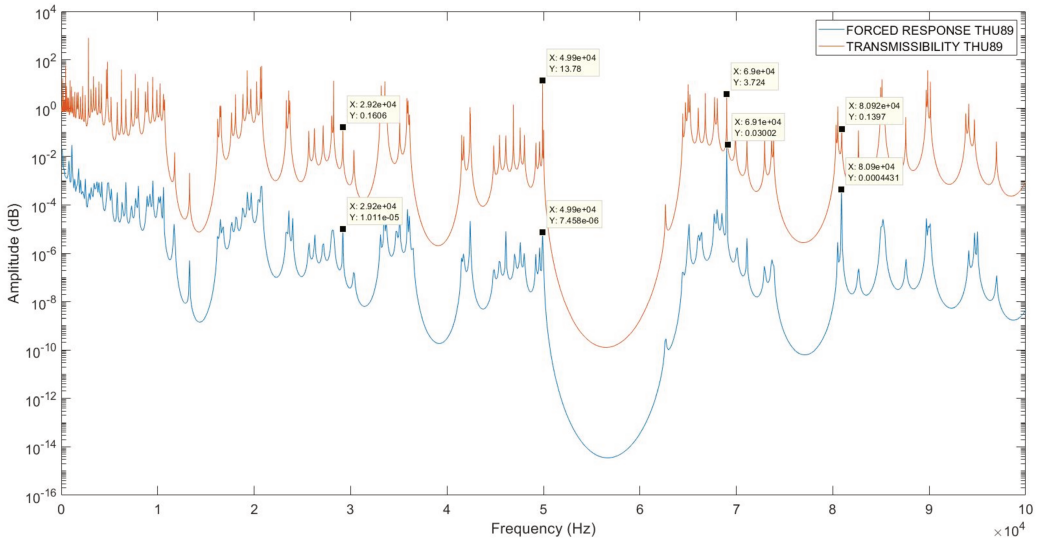

Figure 3.7: Transmissibility curve of Thue-Morse beam.

3.2 Wave Finite Element Method

Wave Finite Element Method (WFEM) is a powerful method for predicting the response of a simple or complex waveguide using a conventional finite element model. The waveguide can be a short segment of the continuous structure. The method is applied for any types of structures, from bars/beams to curved beams and from shell plates to sandwich panels. In the beginning of the section the method is applied for the phononic crystals and continuous to beams and finally to shell structures and lattices.

3.2.1 1D WFEM

In this study 1D WFEM is mainly considered for longitudinal, and flexural wave analysis of 1D systems. The analysis includes, dispersion curves using direct methods. The method combines wave and finite element tools using Floquet-Bloch (FB) boundary conditions. In this section spring mass systems with beams are investigated.

Infinite periodic spring mass chain of oscillators

The objective of studying PCs in this investigation is mainly focused on designing metamaterials to obtain band gap effects. PCs consist of a series of materials that are designed to act as a metamaterial and manipulate sound waves. Here in this numerical simulation, a Bravais lattice of mono-atomic and di-atomic unit cells are considered for modelling a periodic chain. The first step is to create a band gap and localize the characteristics of the wave in the first Brillouin zone. Secondly, the wave propagation can be classified in periodic media, but the question will still be to find if and how the quasi-periodicity has a significant impact in creation of stop bands.

A system consisting of a chain of springs and masses is assumed as an infinite Bravais lattice in this problem. This continuous oscillator is discretized into finite elements and the medium is an elastic solid with density, ρ, modulus of elasticity, E, rod cross-section, A, and reciprocal distance between the two masses, d, as shown in Fig. 3.8. The rod structure has a set of discrete translation operation that defines the lattice vector and number of counting integrals as: $R = n_1 d_1 + n_2 d_2 + n_3 d_3$, where R is the discrete lattice and n, d corresponds to the number of masses and distance between each mass respectively. The schematic diagram of mono atomic spring mass is shown

in Fig. 3.8

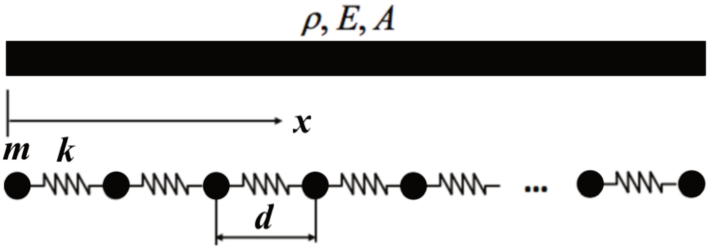

Figure 3.8: Mono atomic spring mass system considered as a rod

Analytical solution of infinite mono-atomic lattice

The equation of motion of discrete system for the n^{th} number of mass is:

$$m\ddot{u}_n + 2ku_n - k(u_{n+1} + u_{n+1}) = 0 \tag{3.1}$$

By assuming wave solution, there are two terms to be considered. The time harmonic motion and the travelling wave: time harmonic motion is the propagation of a wave in the time domain, whereas a travelling wave propagates in space.

- Time harmonic motion in finite systems is mainly considered in the discrete time domain.

$$u_n = U_n e^{(i\omega t)} \tag{3.2}$$

$$-M\omega^2 u_n = k(u_{n+1} + u_{n+1} - 2u_n) \tag{3.3}$$

- In the frequency domain, a travelling wave is imposed, as it is in space domain, the resulting curve could be defined by wave vector with respect to frequency.

$$U_n = Ue^{ink} \tag{3.4}$$

$$-M\omega^2 U_n = 2kU_n[cos(k) - 1] \tag{3.5}$$

where U is constant and by imposing the Eq. 3.6 into Eq.3.3, we get the dispersion equation.

$$\omega^2 - \frac{2K}{M}[1 - cos(k)] = 0 \tag{3.6}$$

The dispersion curve is plotted for a single cell approach in Fig. 3.9; the use of a single cell means that the dispersion curve is without the second curve that corresponds to optical branch. Only the acoustic part of the wave propagation is contained in this plot. The vertical axis is eigenfrequencies of the system with respect to the wave numbers in the horizontal axis

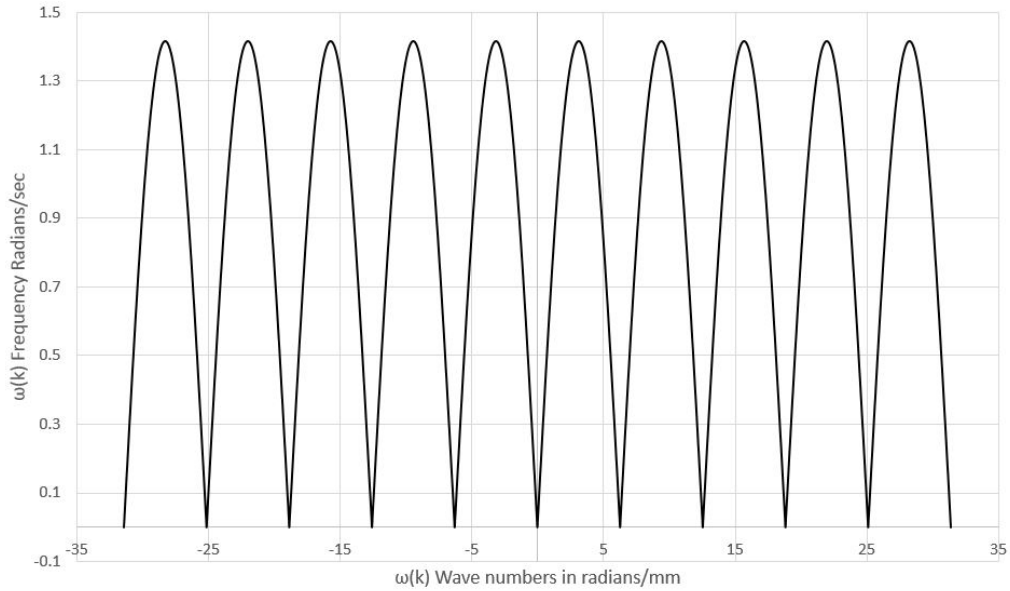

Figure 3.9: Dispersion curve of spring mass system based on mono-atomic lattice

Analytical solution of infinite bi-atomic lattice

The double cell approach models a chain of bi-atomic oscillators. In this case, two different stiffnesses are introduced with constant mass. The study of the double cell approach is intended to aid understanding of the interaction of the closest neighbor cells. The variation of both mass and stiffness that is modelled in the double cell approach is presented in Fig. 3.10. Here, only the modulus of elasticity variation is used.

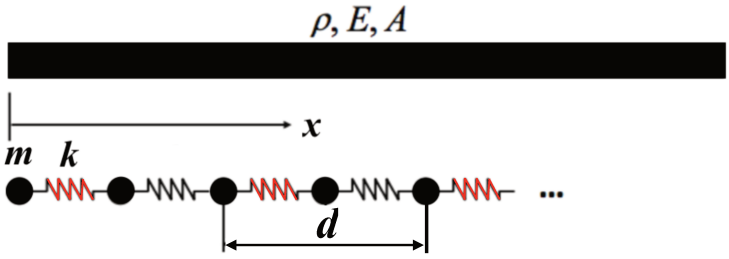

Figure 3.10: Bi-atomic (two different masses) spring mass system considered as a rod

For the bi-atomic chain of oscillator, we consider two equations of motion.

- In analytical solution, the first concentration is on the two-continuum equation of motion for each cell.

$$m_1 \frac{\partial^2 u_n}{\partial t^2} = k(v_n + v_{n-1} - 2u_n) \tag{3.7}$$

$$m_1 \frac{\partial^2 v_n}{\partial t^2} = k(u_n + u_{n-1} - 2v_n) \tag{3.8}$$

- By imposing the travelling wave solution in equations of motion, it leads to the dispersion curve equation: :

$$u_n = Ue^{inkD-\omega t} \tag{3.9}$$

$$v_s = Ve^{inkD-\omega t} \tag{3.10}$$

where V and U are constants and by imposing the assumed travelling equation into the equation of motion, we obtain the dispersion equation.

$$\frac{(M_1M_2)}{K^2}\omega^4 - 2\frac{(M_1M_2)}{K}\omega^2 + 2[1 - cos(kD)] = 0 \tag{3.11}$$

By solving the fourth order quadratic Eq.3.11 explicitly, we can obtain the dispersion equation that provides the relation between wave numbers as a function of eigenfrequencies. Indeed, there is a fourth-order quadratic equation that gives the roots for both acoustic and optical wave propagation inside the lattice.

$$\omega_1^2 = K\frac{[M_1 + M_2 + \sqrt{(M_1 + M_2)^2 - 2M_1M_2(1 - cos(kD))}]}{M_1M_2} \tag{3.12}$$

$$\omega_2^2 = K\frac{[M_1 + M_2 - \sqrt{(M_1 + M_2)^2 - 2M_1M_2(1 - cos(kD))}]}{M_1M_2} \tag{3.13}$$

The perfectly periodic structure is analyzed with FB theory. The aim of the wave analysis was to create meta-materials. A stop band is created in this periodic infinite structure with the same parameters used in the finite structure. The dispersion curve of infinite spring mass with bi-atomic lattice is shown in Fig. 3.11. The results of the analytical solution shows the stop band and pass band zones in both single and double cell approaches. It is found that by having the same values for both parameters, there will be no stop band. Whereas, if we keep the density constant and vary the modulus of elasticity a band gap will appear in the results. Furthermore, from deriving Eq. 3.12 and Eq. 3.13 there is a term that can be used to control the band gap interval by the following relation:$\sqrt{\frac{2K_1}{M}} - \sqrt{\frac{2K_2}{M}}$.

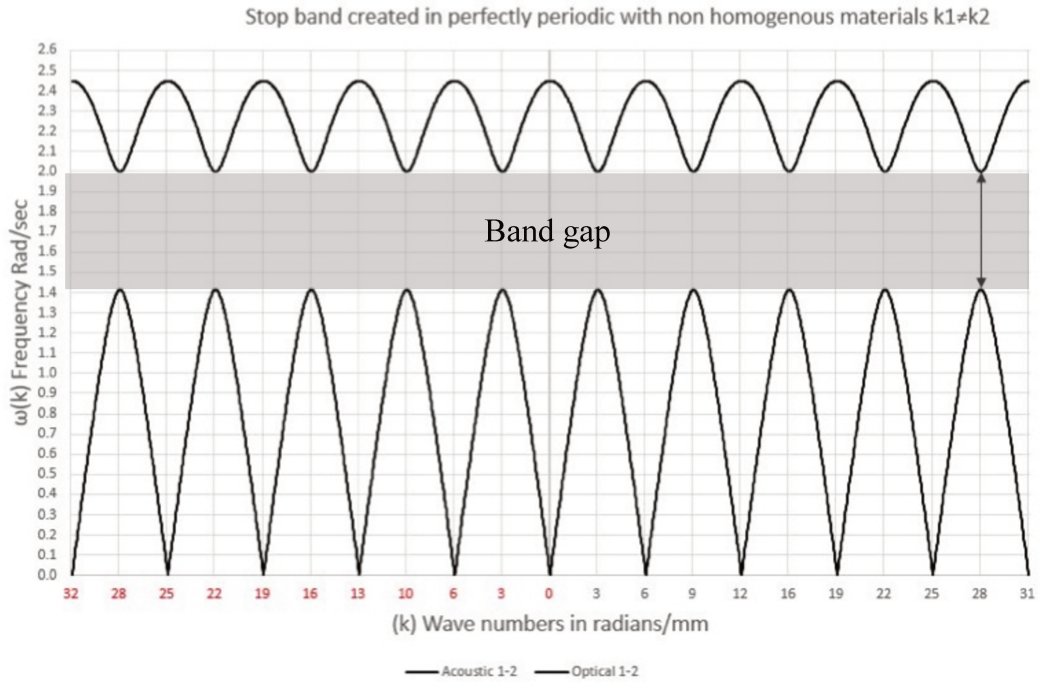

Figure 3.11: Bi-atomic dispersion curve of spring mass system

3.2.2 Spectral Analysis of Beams

FB theory is a powerful method to solve the elastic wave propagation in periodic structures. A unit cell (waveguide) in an infinite periodic beam structure is enough for this type of analysis. This method uses a classical approach for perfectly periodic structures. However, the main objective is to predict spectral analysis of quasi-periodic structures; therefore, double cells and super unit cells are used in this analysis.

3.2.3 Transfer matrix of super unit cell:

The transfer matrix is a square matrix of even dimension and is function of frequency of the disturbance propagating in the structure [76]. For a given structure, each super unit cell composed of n individual cells, has the same transfer matrix $[\mathbf{T}]$ such that;

$$\mathbf{x}_n = \mathbf{T}\mathbf{x}_0 \tag{3.14}$$

where $\mathbf{x}_n$ is the state vector on the left-side of the cell (i.e. on the left-side of the super unit cell), $\mathbf{x}_0$ is the state vector on the right-side of cell 1 (i.e.

on the right-side of the super unit cell), and $\mathbf{T} = \mathbf{T}_n\mathbf{T}_{n-1}, ...\mathbf{T}_1$ where $\mathbf{T}_j$ is the transfer matrix of cell j. In order to obtain the transfer matrices, both mass and stiffness matrices are extracted from APDL-ANSYS.
The dynamic behaviour of the cell number j is described by:

$$\mathbf{D}^j\mathbf{q}^j = \mathbf{f}^j \tag{3.15}$$

where $\mathbf{D}^j$,$\mathbf{f}^j$, and $\mathbf{q}^j$ define respectively the dynamic stiffness matrix, force and displacement vector. The dynamic stiffness matrix writes

$$\mathbf{D}^j = -\omega^2\mathbf{M}^j + \mathbf{K}^{j*} \tag{3.16}$$

with $\mathbf{K}^{j*} = \mathbf{K}^{j*}(1 + i\eta)$ where $\mathbf{M}^j$,$\mathbf{K}^j$, and η are respectively the mass matrix, the stiffness matrix and the loss factor corresponding to the structural damping. The matrices and vectors are partitioned according to the degrees of freedom: $\mathbf{q}_L^j$, $\mathbf{q}_I^j$, and $\mathbf{q}_R^j$ respectively refer to the left-side, internal, and right-side parts of the super unit cell number j. The corresponding terms in the matrices are written

$$\begin{bmatrix} \mathbf{D}_{LL}^j & \mathbf{D}_{LI}^j & \mathbf{D}_{LR}^j \\ \mathbf{D}_{LI}^{jT} & \mathbf{D}_{II}^j & \mathbf{D}_{IR}^j \\ \mathbf{D}_{LR}^{jT} & \mathbf{D}_{IR}^{jT} & \mathbf{D}_{RR}^j \end{bmatrix} \begin{Bmatrix} \mathbf{q}_L^j \\ \mathbf{q}_I^j \\ \mathbf{q}_R^j \end{Bmatrix} = \begin{Bmatrix} \mathbf{f}_L^j \\ \mathbf{0} \\ \mathbf{f}_R^j \end{Bmatrix}. \tag{3.17}$$

The internal degrees of freedom can then be condensed using the second row of Eq.3.17, in order to retain the analysis to the left and right boundary displacements and forces.

$$\mathbf{q}_I^j = -\mathbf{D}_{II}^{j^{-1}}(\mathbf{D}_{LI}^{jT}\mathbf{q}_L^j + \mathbf{D}_{IR}^j\mathbf{q}_R^j). \tag{3.18}$$

it leads to

$$\begin{bmatrix} \mathbf{D}_{LL}^j - \mathbf{D}_{LI}^j\mathbf{D}_{II}^{j^{-1}}\mathbf{D}_{IL}^j & \mathbf{D}_{LR}^{j^T} - \mathbf{D}_{LI}^j\mathbf{D}_{II}^{j^{-1}}\mathbf{D}_{IR}^j \\ \mathbf{D}_{RL}^j - \mathbf{D}_{RI}^j\mathbf{D}_{II}^{j^{-1}}\mathbf{D}_{IL}^j & \mathbf{D}_{RR}^j - \mathbf{D}_{RI}^j\mathbf{D}_{II}^{j^{-1}}\mathbf{D}_{IR}^j \end{bmatrix} \begin{Bmatrix} \mathbf{q}_L^j \\ \mathbf{q}_R^j \end{Bmatrix} = \begin{Bmatrix} \mathbf{f}_L^j \\ \mathbf{f}_R^j \end{Bmatrix}. \tag{3.19}$$

The reduced dynamic stiffness matrix is written as follow:

$$\begin{bmatrix} \tilde{\mathbf{D}}_{LL}^j & \tilde{\mathbf{D}}_{LR}^j \\ \tilde{\mathbf{D}}_{LR}^{jT} & \tilde{\mathbf{D}}_{RR}^j \end{bmatrix} \begin{Bmatrix} \mathbf{q}_L^j \\ \mathbf{q}_R^j \end{Bmatrix} = \begin{Bmatrix} \mathbf{f}_L^j \\ \mathbf{f}_R^j \end{Bmatrix}. \tag{3.20}$$

One define state vectors for the boundaries of the component j:

$$\mathbf{u}_L^j = \begin{Bmatrix} \mathbf{q}_L^j \\ \mathbf{f}_L^j \end{Bmatrix}, \mathbf{u}_R^j = \begin{Bmatrix} \mathbf{q}_R^j \\ \mathbf{f}_R^j \end{Bmatrix}. \tag{3.21}$$

The transfer matrix is hence obtained by reorganising the degrees of freedom according to the state vector:

$$\mathbf{u}_R^j = \mathbf{T}^j \mathbf{u}_L^j \tag{3.22}$$

where, $\mathbf{u}_L^k$ and $\mathbf{u}_R^j$ are the displacement vector of the right and left component of the unit cell, and $\mathbf{T}^j$ is the transfer matrix in Eq.3.22:

$$\mathbf{T}^j = \begin{bmatrix} -\tilde{\mathbf{D}}_{LR}^{j^{-1}} \tilde{\mathbf{D}}_{LL}^j & -\tilde{\mathbf{D}}_{LR}^{j-1} \\ \tilde{\mathbf{D}}_{RL}^j - \tilde{\mathbf{D}}_{RR}^j \tilde{\mathbf{D}}_{LR}^{j^{-1}} & \tilde{\mathbf{D}}_{LL}^j \quad \tilde{\mathbf{D}}_{RR}^j \tilde{\mathbf{D}}_{LR}^{j^{-1}} \end{bmatrix}. \tag{3.23}$$

The transfer matrix of the super unit cell is then obtained in Eq.3.23.

3.2.4 Dispersion analysis:

Periodicity conditions applied on the super unit cells are then written as

$$\mathbf{u}_L^{p+1} = e^{\mu} \mathbf{u}_L^p \tag{3.24}$$

where μ is the propagation constant. Combining Eq.3.22 and Eq.3.24,yields to the eigenvalue problem:

$$\mathbf{T}^p \phi_i = \lambda \phi_i. \tag{3.25}$$

where $\lambda = e^{\mu}$.

Depending on the nature of the eigenvalue of $[\mathbf{T}^p]$, the waves propagating in a periodic structure are described as travelling waves and attenuating waves which occur in alternating frequency bands known as pass-bands and stop-bands. If the eigenvalues of $[\mathbf{T}^p]$ are complex and of the form $e^{\pm ikL}$, $k \in \mathbb{R}$ the corresponding wave is in a pass-band and the wave travels in the form of $e^{\pm ikL}$, where k is a real wave number, the positive and negative signs indicating left and right travelling waves, respectively. On the other hand if all eigenvalue of the $[\mathbf{T}^p]$ are of the form $e^{\pm\beta}$ or $e^{\pm\beta+i\pi}$, $\beta \in \mathbb{R}$, is pure real exponent, the corresponding frequency is in a stop-band and the wave amplitude after travelling n elements are attenuated by the factor $e^{(\pm\beta n)}$, in which the real exponent β implies attenuated waves [76].The dispersion curves are computed by imposing frequency and computing k according to the given eigenvalue problem.

3.2.5 2D WFEM

Similar to the 1D case, 2D WFEM is also used to predict band gaps of a 2D complex waveguide using a conventional finite element model. The struc-

tural design of phononic crystals and metamaterials that are manufactured artificially with periodic constitutive or geometric properties may influence the characteristics of mechanical wave propagation. These types of structures have geometrical and material discontinuities that may reduce the vibration attenuation level. It is possible to isolate the unwanted vibration within a certain frequency range referred to as the band gap. Optimization of band gaps of phononic crystal and metamaterials can be challenging [77]. The eigenfrequency analysis of a single super-cell containing the reduced global dynamic stiffness and mass matrices is solved by applying the Floquet theory [18,19,78]. The displacement $\mathbf{v}$ of the position of a unit cell with respect to the wave propagating at frequency ω can be expressed as:

$$\mathbf{v}_{(\mathbf{d}_q)} = \mathbf{v}_{q0} e^{i(\omega t - \mathbf{k}\cdot\mathbf{d}_q)} \tag{3.26}$$

where $\mathbf{v}_{(\mathbf{d}_q)}$ is the displacement of point d of the reference unit cell, $\mathbf{v}_{q0}$ is the amplitude, $\mathbf{k}$ is the wave vector, and $i = \sqrt{(}-1)$. The displacement between reference point d and the position $\mathbf{f}_q(n_1, n_2)$ could be written following the Floquet theory as follows:

$$\mathbf{v}_{(\mathbf{f}_q)} = \mathbf{v}_{(\mathbf{d}_q)} e^{i\mathbf{k}\cdot(\mathbf{f}_q - \mathbf{d}_q)} = \mathbf{v}_{(\mathbf{d}_q)} e^{i(n_1 k_1 + n_2 k_2)} \tag{3.27}$$

In the first Brillouin zone direct lattice vector by the basis $o = (\mathbf{a}_1, \mathbf{a}_2)$ describes the spatial periodicity of the periodic domain, while reciprocal vector by the basis $r = (\mathbf{p}_1, \mathbf{p}_2)$ defines the periodicity of the frequency wave numbers, as shown in Fig. 3.12. The direct lattices are function of reciprocal lattices which is written as following:

$$\vec{p_1} = \frac{2\pi}{a_1}\hat{a_1}, \vec{p_2} = \frac{2\pi}{a_2}\hat{a_2} \tag{3.28}$$

The wave vector $\mathbf{k} = 2\pi\lambda$ inside the reciprocal lattice can be expressed as:

$$\mathbf{k} = k_1\mathbf{p}_1 + k_2\mathbf{p}_2, \tag{3.29}$$

The method can be applied for any type of structure, from shell plates to sandwich panels. The classical FB method is also used for the band diagram analysis of the strictly periodic infinite panel through COMSOL Multiphysics. The analysis uses the Floquet periodicity that is defined in the four side boundaries of the unit cell. The unit cell represents a bi-directional spatial periodicity in the given infinite structure. The band diagram is computed along the three symmetry directions of the first Brillouin zone shown

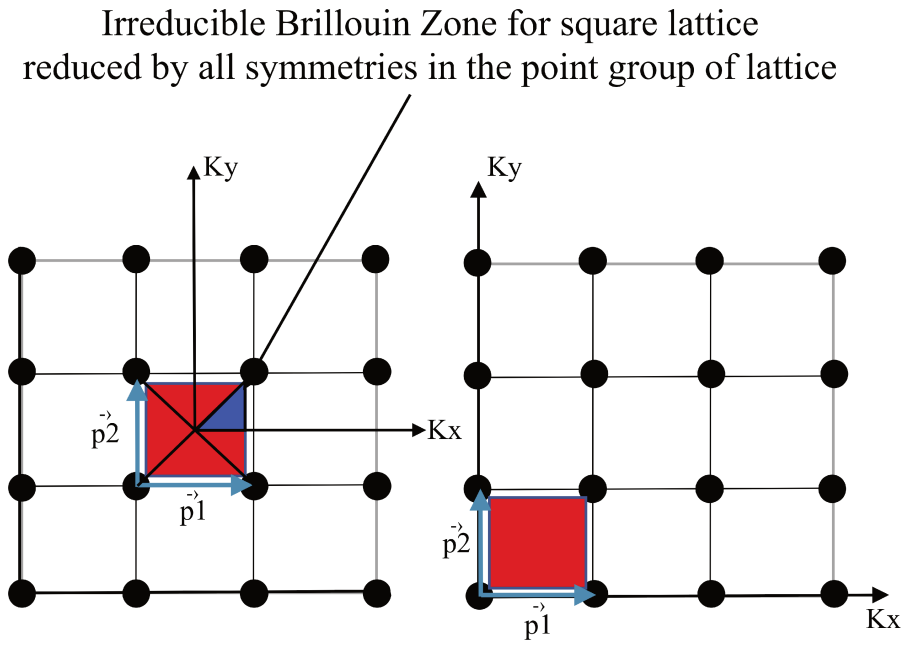

Figure 3.12: First Brillouin zone reduced by all symmetries in the point group of the lattice

in Fig. 3.13. The periodicity boundary conditions at the four sides of the lattice are:

$$u_{dest} = e^{[j\mathbf{k}_F \cdot (r_{dest} - r_{sour})]} u_{sour} \tag{3.30}$$

where (r_{dest} - r_{sour}) is the reciprocal distance between the two periodic cells, and k_F is the wave vector. The source and destinations can be selected by choosing the periodic boundary condition. For 2D lattices, the source and destination are applied once on the right and left of the unit cell and once on the top and bottom of the unit cell. The FB boundary condition can easily solve the complex eigenvalue problem using the direct method by giving the wave numbers in the input, and getting the eigenfrequency in the output, depending on the nature and number of desired Bloch modes. The periodicity condition can be applied to the both directions of the unit cell:

$$u_R = e^{[-jk_x L]} u_L \tag{3.31}$$

$$u_U = e^{[-jk_y L]} u_B \tag{3.32}$$

where, u_R and u_L are the displacement in the right and left side of the x axis, respectively, and u_U and u_B are the displacement in the upper and bottom of the y axis. L is the length of reciprocal element, and k_x and k_y are the wavenumers in the $x-$ and $y-$directions.

Band diagrams are analysed by setting up inputs in the eigensolver analysis using parametric sweep fucntion giving, k wave number as an input that varies between 0 and π. The elastic wave direction from 0 to π is divided into three portions. The first portion spanning the $A-R$ edge (wave propagation on $x-$direction), the second portion spanning the $R-S$ edge (wave propagation on $y-$direction), and last portion spanning the diagonal direction $S-A$ edge of the first Brillouin zone.

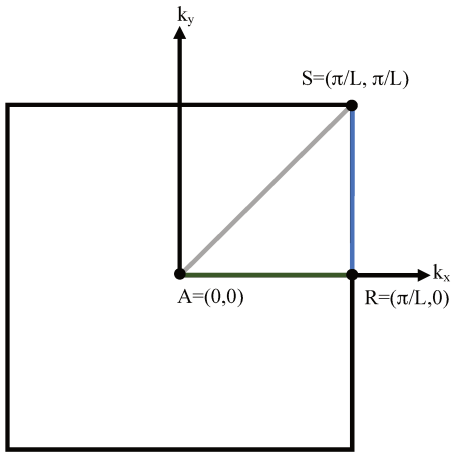

Figure 3.13: Diagram of the first irreducible Brillouin zone for a square lattice

Here in Fig. 3.14, an example of a dispersion diagram for two different unit cells is considered. Cell A and cell B have commonalities in terms of mass, volume fraction, material, and structural properties, in order to be useful periodic tools to be compared with the quasi-periodic counterpart. The results predicted by these two cells could lead to the design of a quasi-periodic lattice, which is a finite panel with a tailored irregularity that is invoked by the Thue-Morse morphism deterministic approach. The results of the numerical analysis are shown in the band diagram in Fig. 3.14. There are two complete frequency band gaps in each sub-figure. Cell A is predicted to have a small resonance band gap with $\Delta\omega = 570$ Hz, and a larger Bragg band gap at $\Delta\omega = 2.9$ kHz at around 11 kHz. Cell B in the right hand side of Fig. 3.14 shows almost similar dispersion behavior but with a wider

resonance band gap of $\Delta\omega = 754$ Hz around 4 kHz and a slight wider Bragg band gap of 3.1 kHz. According to a sensitivity analysis of both cells, the wall thickness of the cell A is set to 4.8 mm and the radius of the resonator shape of cell B is set to 8 mm to isolate the maximum vibration level.

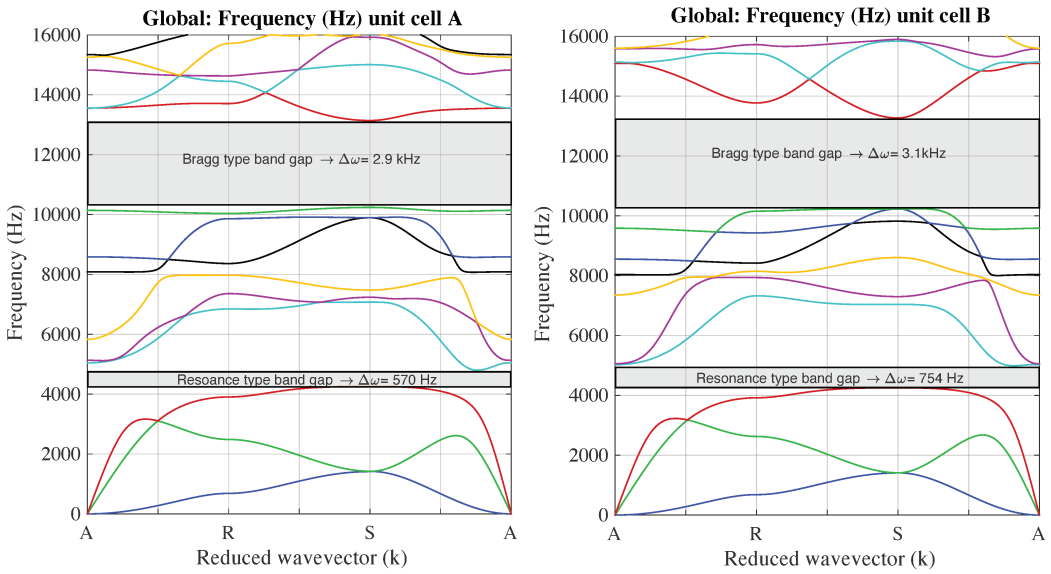

Figure 3.14: Band diagram of infinite panels with a representative, left cell A and right cell B

Part IV

Results and discussion

Chapter 4

Spectral analysis and structural response of periodic and quasi-periodic beams

4.1 Introduction

In this investigation the modelling of simple quasi-periodic structures is built with the conventional finite element method (FEM) to fulfil the generation of quasi-periodic patterns since these are based on an asymmetrical distribution of identical cells [79, 80]. Finite, periodic and quasi-periodic structures are thus proposed and compared by using the Fibonacci sequence to investigate about the possibility to have and control useful frequency bands in which the response can be reduced as much as possible. In Section 2 the models and their specific lexicon are presented. Section 3 contains the methods and tools used for the numerical investigations. The main results obtained are commented in Section 4 and finally, some concluding remarks are given in Section 5.

4.2 Models and Lexicon

In this study, quasi-periodic beams with a finite number of cells are analysed. In these models specific sequences like Fibonacci series will be used to generate impedance mismatches in view of the desired degree of quasi-periodicity [43, 81].
The degree of quasi-periodicity might be controlled with mathematical rules described in theory section.

Tab.4.1 shows the number of unit cells necessary to generate a given order of Fibonacci sequence.

Table 4.1: Example of number of cells according to Fibonacci orders.

Fibonacci orders function of number of cells								
Orders	4^{th}	5^{th}	6^{th}	7^{th}	8^{th}	9^{th}	10^{th}	11^{th}
Number of Cells	5	8	13	21	34	55	89	144

The numerical models is identified by the order of the Fibonacci sequence, and thus the length of the n-th order sequence, $\boldsymbol{S_n}$, will be greater than $\boldsymbol{S_{n-1}}$. As example, Fig.4.1 shows a Fibonacci ($\boldsymbol{S_6}$) beam with a sequence of 13 [ABAABABAABAAB] cross-sections.

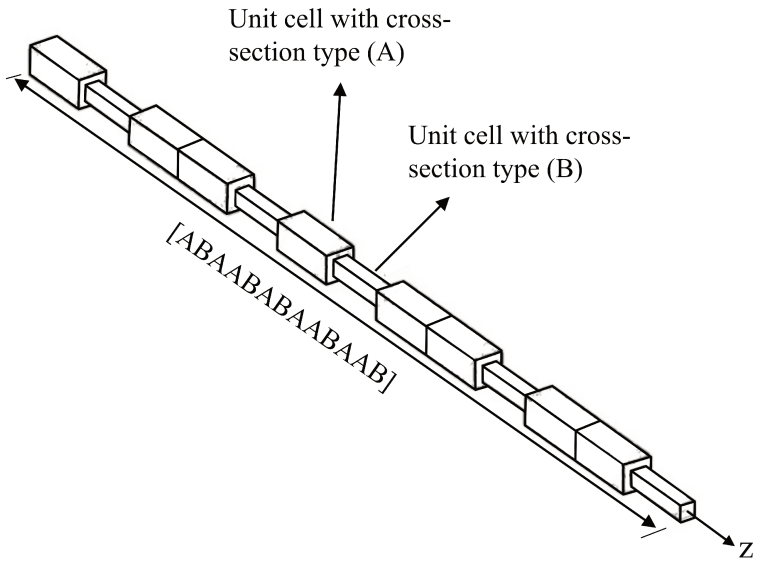

Figure 4.1: Fibonacci configuration of 6^{th} order

4.2.1 Cases

In this framework, two types of unit cells are defined: cell A and cell B. Variations between cells A and B will be obtained through impedance mismatch. Two cases will be considered:

Case M1: impedance mismatch due to geometrical discontinuity, as in Fig. 4.2(Case M1);

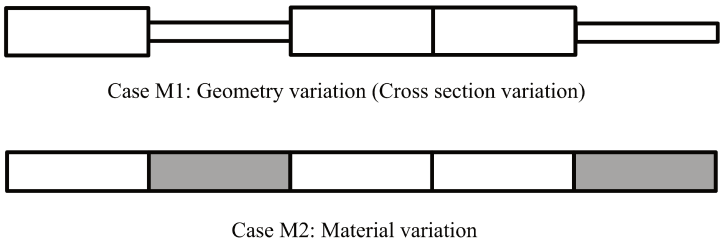

Figure 4.2: Configuration of discontinuities: (M1) and (M2).

Case M2: Case M2: impedance mismatch due to material discontinuity, as in Fig. 4.2(Case M2).

The various configurations considered for M1 will be described in the next section. Without loss of geometry, the material used in case M1 is steel $A-36$ whose properties are provided in Table.4.2
For the typical quasi-periodic structure case M2 the material variation is reported in Table.4.2.

Table 4.2: Mechanical properties of quasi-periodic bi-material beam.

Material	Young's modulus (Pa)	Poissons Ratio	Density ($\mathrm{kg} \cdot \mathrm{m}^{-3}$)
Steel A-36	2×10^{11}	0.26	7800
Al 2045-T4	73×10^{9}	0.33	2700
Magnesium	45×10^{9}	0.35	1770
Copper	110×10^{9}	0.355	8960

4.2.2 Geometrical variations of case M1

A comparison of four configuration types displayed in Fig.4.3 for the case M1 is considered. In this case the mass of the sum of cells A and B are kept constant in order to compare the equal mass beams. The aim is to find the most efficient geometrical variation behavior of unit cells (A) and (B) for vibration control. The factors prescribed in Table 4.3 are the ratio of the length of section edges. The configuration Type IV has no impedance mismatch, and Type II will be first analyzed as a reference.

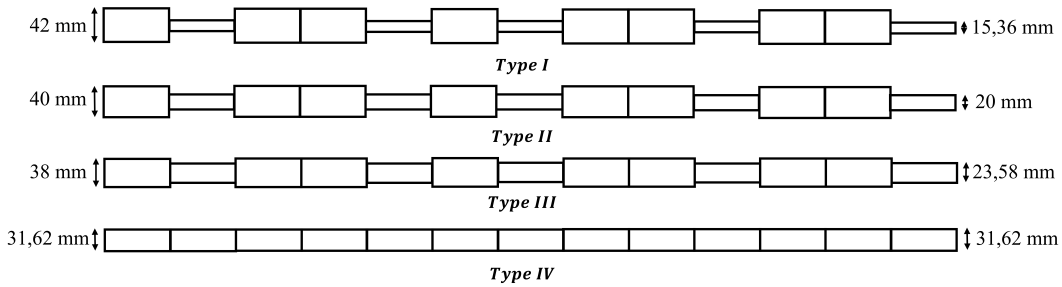

Figure 4.3: Comparison of case M1 by keeping constant the mass and the length of sum of the A and B cells (the beams have square cross sections).

Table 4.3: Sizes of cells A and B as sub-cases for M1.

Geometrical variation				
Type	Cell	width [mm]	height [mm]	Factor
I	A	42.00	42.00	2.7
	B	15.36	15.36	
II	A	40.00	40.00	2
	B	20.00	20.00	
III	A	38.00	38.00	1.6
	B	23.58	23.58	
IV	A	31.62	31.62	1
	B	31.62	31.62	

4.3 Methods and Tools

Two numerical methods are used: FEM is used for analyzing the Frequency Response Functions (FRF) of the finite beam, while the Wave Finite Element Method (WFEM) together with spectral analysis is used for computing the dispersion diagrams.

4.3.1 Finite Element Analysis

The analysis is performed with the conventional FE method to obtain the frequency response functions (FRF) of damped quasi-periodic beams. The FE analysis was carried out using ANSYS-APDL linked with MATLAB. The elements used are Beam 188, which is a linear 2-node beam element. Both cells (A and B) are composed of 4 nodes (three beam elements) and each node has three degrees of freedom: longitudinal in the axial direction (x-axis), bending in the lateral direction (y-axis), and torsional rotation around

the x-axis. The distance between each cell is 100 mm. The FRF of quasi-periodic beams are computed from Eq. 4.1.

$$H_{kj}(\Omega) = \sum_{p=1}^{N} \frac{\psi_{pk}\psi_{pj}}{m_p(\omega_p^2 - \Omega^2 + i2\xi_p\omega_p\Omega)} \tag{4.1}$$

where $H_{kj}(\Omega)$ is the transfer function, m_p the modal mass, ω_p the eigen-frequency, Ω the forcing frequency; ξ_p is the modal damping, ψ_{pk} and ψ_{pj} are the components of the p-th eigenvector evaluated at the source and receiver points and N the number of retained eigenmodes. Accordingly, the FRF of the quasi-periodic beams are computed.

These forced response analysis are performed with free-free boundary conditions shown in Fig. 4.4. The input force is located at one end of the beam in the transverse direction and the response is computed at the other end of the beam in the same direction.

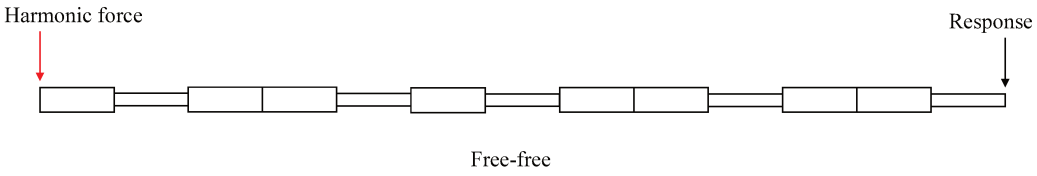

Figure 4.4: As a sample from many orders of the Fibonacci beams used in this analysis, a schematic diagram of beam with 6^{th} order of Fibonacci is picked for numerical analysis.

4.3.2 Spectral analysis of infinite beam (waveguide)

The FB conditions can be applied to simulate waveguides that are modelled as infinite periodic beams. This is classical for perfectly periodic structures. In order to perform spectral analysis on quasi-periodic structures, super unit cells are used. In this example, the super unit cell is defined according to the 6^{th} order of Fibonacci sequence (type ABAABABAABAAB) and double unit cell, as a reference. The super unit cell and double unit cells are used in the Wave Finite Element Method (WFEM) analysis presented in the next section.

After obtaining the transfer matrix of super unit cell, the periodicity condition is applied on the super unit cell. Solving the eigenvalue problem, the dispersion curves are computed by imposing frequency and computing k according to the direct solution of eigenvalue problem.

4.4 Frequency response function of finite beams using FEM

FRFs of finite structures are analyzed for cases M1 and M2. The FRFs are plotted in the frequency ranges of $0-10$ kHz for flexural and $0-25$ kHz for axial vibration. The frequency ranges for flexural and axial modes are chosen based on modal analysis of the first 22 desired modes. This investigation is carried out to fulfil the criterion for sufficiently accurate number of element per wavelength. The boundary condition is free-free and mesh setting with two different beam elements (1882-node and 1893- node) with the number of elements per wavelength 4, 5, and 10 are checked. The span of the beam is 1300 mm and 39 elements per wave length was found to be more accurate when using beam element 188 with 2 nodes to determine the exact natural frequency, which is 9700 Hz.

The harmonic response function of periodic beams is computed in MATLAB. A script is created to define the finite element model of the periodic double cell with an arrangement of 13 unit cells. In the FRF analysis, the boundary condition is too considered as free-free and white noise (i.e., harmonic force of 1N from $0-10$ kHz with a bandwidth of 10 Hz) is applied to one end of the beam. The white noise is applied in vertical z- and horizontal x-directions, respectively, for flexural and longitudinal vibrations.

4.4.1 FRF results for Case M1-Type II

A first analysis of M1-Type II is performed, considering increasing orders of the Fibonacci sequence (4^{th}, 5^{th}, 6^{th}, 7^{th}, 8^{th}, 9^{th}, 10^{th}, and 11^{th} orders). It should be noted that the structure is not periodic, and that an increase in Fibonacci order is associated with an increase in the length of the beam. All results are carried out in the frequency range $0-10000$ Hz. The results in Fig. 4.5 shows multiple stop bands that remain coherent from one order to the other, for instance, around $600-900$ Hz, $1900-2300$ Hz, and a larger

frequency stop band around $2900 - 4000$ Hz.

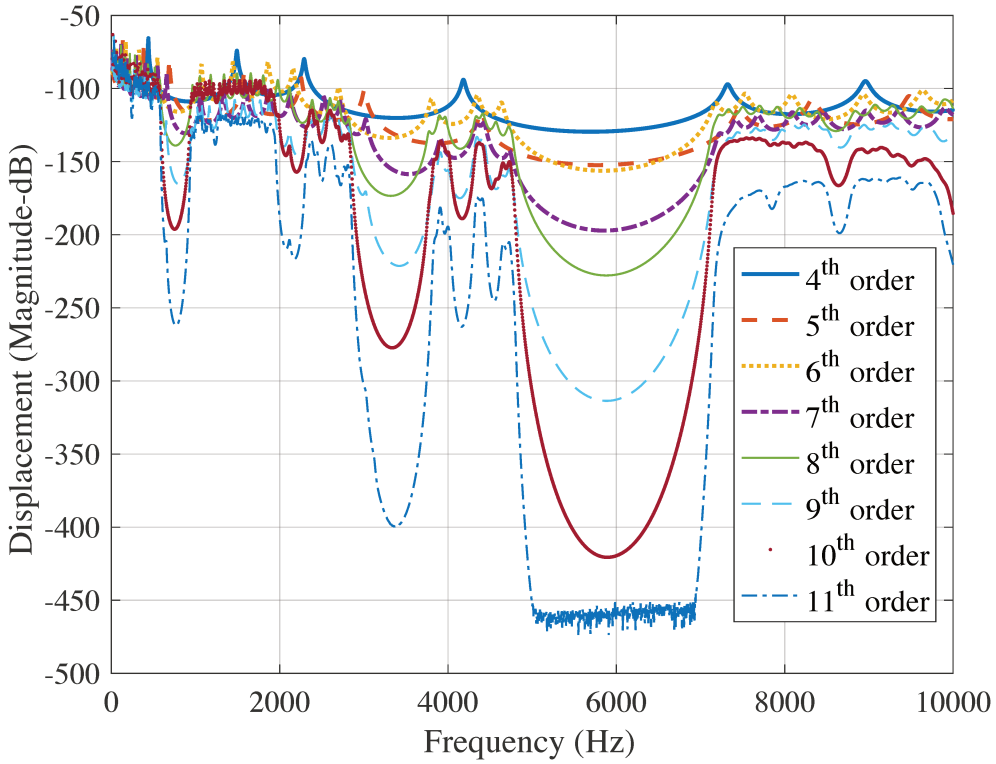

Figure 4.5: FRFs of the flexural waves for given orders of Fibonacci beam with geometrical variation

The trend is similar to periodic structures when the number of cells increases: the band gap locations do not change, but the trough in the FRF is becoming larger. The largest frequency stop band appears around $4900-7100$ Hz. The lowest depth of the amplitude that exceeds (-450) decibels corresponds to the precision of the numerical tool and is obviously not measurable in practice. The dark blue curve corresponds to the highest generated Fibonacci order, which is the 11^{th} order in this investigation, and shows the deepest gaps. Other curves follow an equal increment in the depth as the generation order is increasing. The peaks that can be observed in Fig. 4.5 correspond to the resonances of the finite beams.

Beside the flexural response shown in Fig. 4.5, a similar analysis is per-

formed for the longitudinal waves. Fig. 4.6 shows responses of the beams with an applied force in the axial direction. There are only two stop bands around $4300 - 4800$ Hz and $6600 - 10000$ Hz.

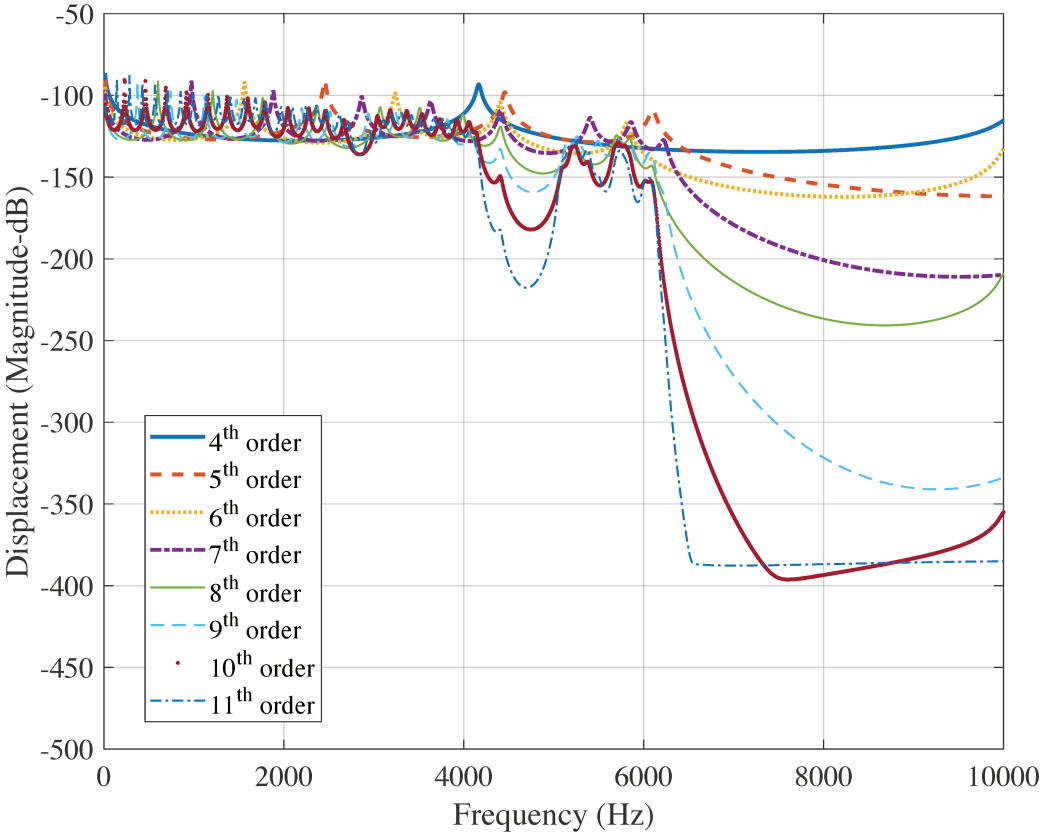

Figure 4.6: FRFs of the longitudinal waves for given orders of Fibonacci beam with geometrical variation

The trend is similar to the flexural waves shown in Fig. 4.5 when the number of cells is increasing: the band gap locations do not change, while the trough in the FRF is becoming larger. There is also a localized mode that appears inside the band gap of longitudinal waves. The effects of dynamic behavior of the beam-spans when increasing the number of cells following Fibonacci orders is emphasized by this analysis. In practice, these types of beam-spans can be used as junction filters between structures. The induced vibrational energy transfers through this junction, and it acts as a metamaterial that filters the elastic waves due to the impedance mismatch in geometry and material.

4.4.2 Frequency response function of double cell and super unit cell structure using WFEM:

In this section, FRFs of periodic beams are analyzed. Two cases are considered: a double cell variation with a span of 13 unit cells having perfect periodic order, and a 6^{th}-order Fibonacci super unit cell with 13 unit cells, which has non-symmetric repetition of cells inside the periodic super unit cell. Four variations of geometry are modelled in both cases. The aim of this analysis is to investigate the effect of the geometric variation on width and shift in frequency of band gaps and comparing the two models in order to find an optimized design for vibration control. The application is based on flexural and longitudinal waves in the perfectly periodic models shown in Fig.4.7 and Fig.4.8, respectively.

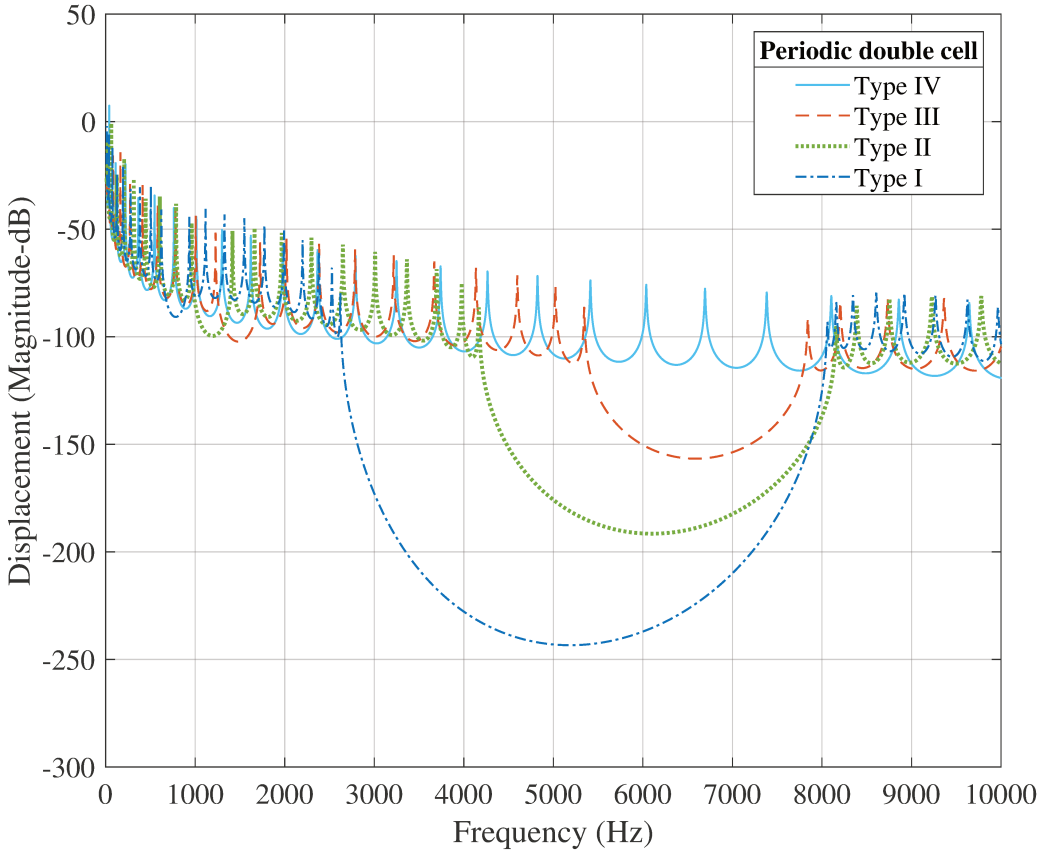

Figure 4.7: WFEM frequency response function of periodic double cell beam for flexural waves

The analysis is applied for four types of geometrical variations as a test cases. Both flexural and longitudinal waves are investigated under the FB periodicity condition. The frequency range of FRF of flexural waves in Fig. 4.7 is considered up to 10 kHz, whereas the frequency range for longitudinal waves in Fig. 4.8 is up to 25 kHz, depending on the frequency stop bands zone. The response shows that the width of the stop band increases as the height of the cross-section (B) decreases and the width of the stop bands increases from almost 2.5 kHz up to around 8 kHz. Similarly, the FRF of the same periodic double cell is considered for longitudinal waves to describe the dynamic behavior of the beam in compression conditions.

Fig. 4.8 shows an enlargement of frequency stop bands in lower and higher frequencies. The results of type I, II, and III shows an enlargement of frequency stop bands compared to continuous beam type IV, which has no stop bands. The wide of frequency band gap in the axial vibration direction is almost 15 kHz.

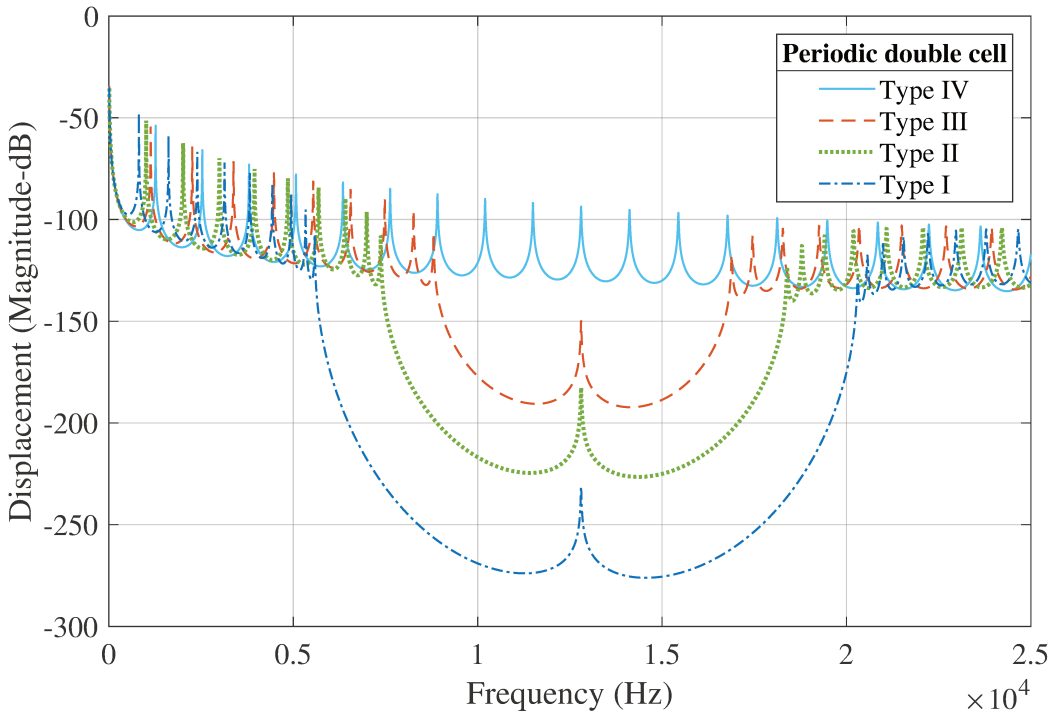

Figure 4.8: WFEM frequency response function of periodic double cell beam for longitudinal waves

Now we consider a super unit cell. Fig.4.9 shows the FRF for the fre-

quency range of $0-1$ kHz. The results shows a shift of frequency band gaps and enlargement of width of the band gaps. Fig.4.9 shows the FRF of a 6^{th} order beam. It can be noted that band gaps move to higher frequencies when increasing the height of the second cell (B). For instance, the subplot for Type I (B height=15.36 mm) has a band gaps around $400-650$ Hz. For type II (B height=20.00 mm) the band gap is shifted to higher frequencies.

Ultimately, the use of the super unit cell has significant advantages compared to the double unit cell. The first point that can be noticed in the FRFs in Fig.4.9 is that there is a tremendous shift of frequency stop bands from lower to higher frequency ranges. The second point is that there is a frequency stop band appearing in lower frequency ranges below 1 kHz, which is not the case in the double unit cell approach.

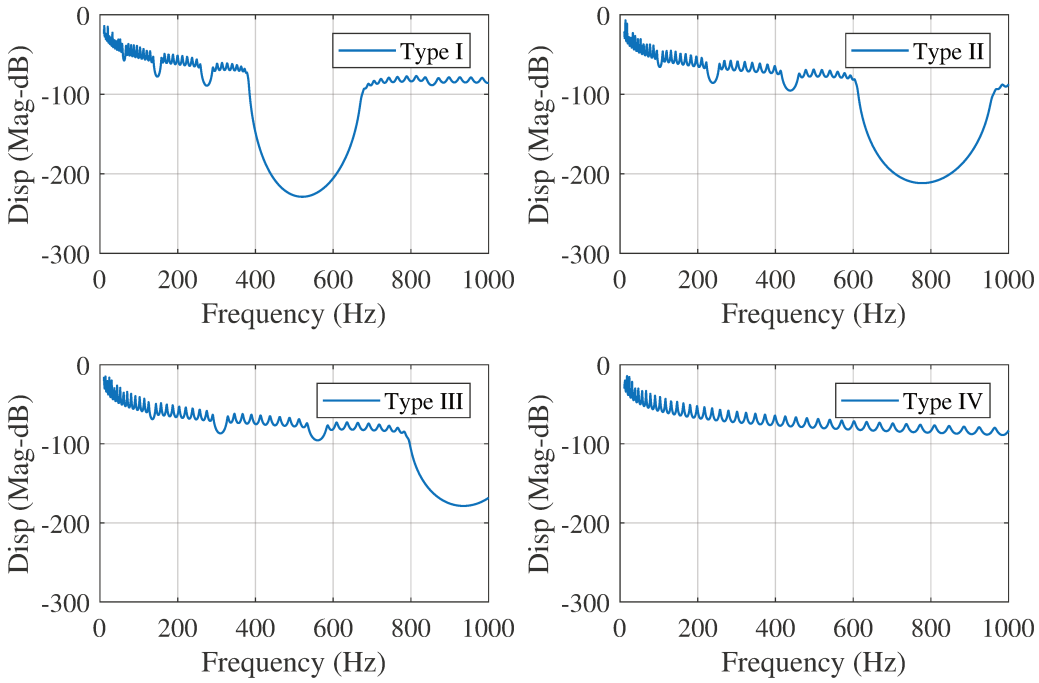

Figure 4.9: WFEM FRF for flexural waves of super unit cell with 6^{th} order of Fibonacci sequence

In conclusion, the characteristics of the beam with Fibonacci series periodicity (or simply quasi-periodic beams) is that the geometrical impedance mismatch between the non-symmetrical interfaces in these types of beams

efficiently reduces the response, especially in lower frequency regimes compared to the standard double cell (ABABABABABABA) periodic case. It does not show an efficient result in creating wider stop bands, but it has multiple attenuation levels in lower and medium frequency ranges. The results obtained in this study show that the beam with Fibonacci characteristics can improve performances in terms of attenuation level without weight penalty, which can be an asset for metamaterials.

4.4.3 Frequency response function of quasi-periodic beam with geometrical variations of type II:

This FRF of Fig. 4.10 is influenced by the previous test case results shown in Fig. 4.7, Fig. 4.8, and Fig. 4.9. As it can be seen from previous results, there are evident band gap shifts and width enlargement, when the factor of the cross sections demonstrated in Table 4.3 increases from (1 - 2.7). Now in this sub-section, the same procedure is applied to the 11^{th}-order Fibonacci quasi-periodic beam using four types of geometrical variation. The FRF of four types of geometrical variation is shown in Fig. 4.10. Types I, II, and III all have stop bands, but at different frequency ranges, whilst Type IV does not show any stop bands over the modelled frequency range. It should be noted that increasing the factor of the geometrical variation increases the width of the band gaps. There are some band gaps that exist in Type II and III, but are not as deep as those in Type I.

In conclusion, the FRF results for case M1-Type II in sub-section 4.4.1 shows significant impacts on vibration control of the beam span. Flexural analysis shows that by increasing the number of Fibonacci orders, the trough of the band gaps increases and it is also demonstrated in longitudinal waves. Then, the FRF results of double cell and super unit cell using four type of variations shows more width enlargement in double cell approach, and shift in frequency of band gaps for super unit cell approach. The second advantage of super unit cell approach is that it has frequency stop band in lower frequency ranges below 1 kHz. In the last sub-section 4.4.3, the FRF of quasi-periodic beam with Type-II geometrical variations shows width enlargement and an increased attenuation level using higher orders of Fibonacci sequence compared to lower orders.

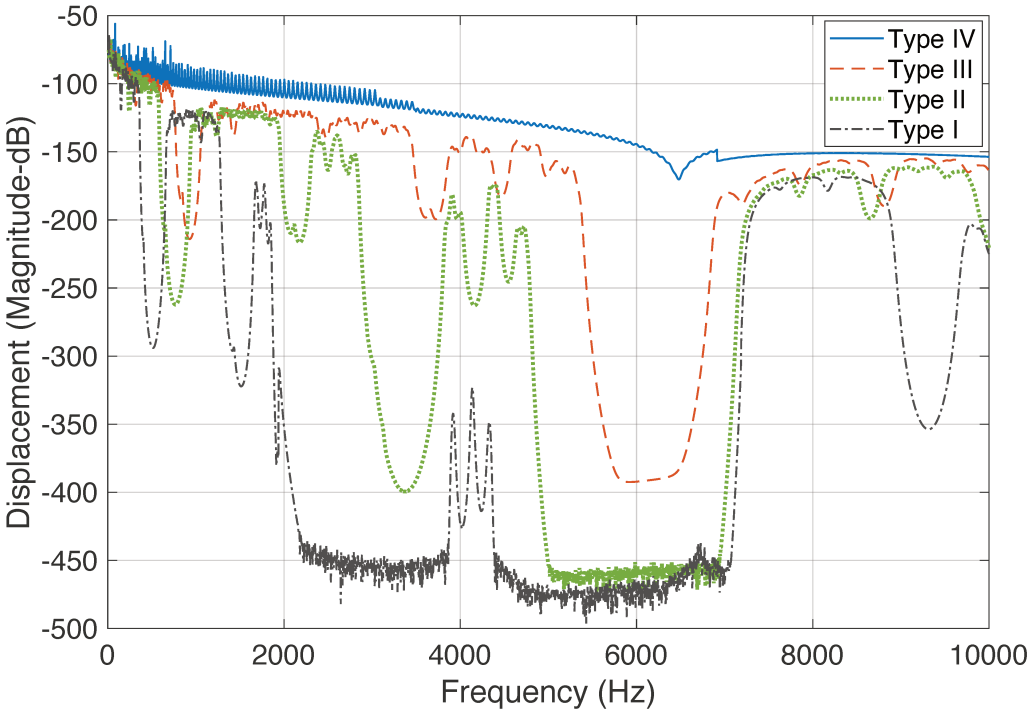

Figure 4.10: FRFs of the flexural waves for 11^{th} order of Fibonacci beam with geometrical variation

4.4.4 FRF results for Case M2

The second quasi-periodicity configuration is based on the impedance mismatch of material constituents. The beam is analyzed as a continuous span (with no cross-section variation). The mass of the system for all Fibonacci orders is kept the same, while the length of the beam is changed, and the number of cells are increased according to the Fibonacci sequence. The length of the structure varies from 0.5 m to 14.4 m to include the [4^{th},5^{th}, 6^{th}, 7^{th}, 8^{th}, 9^{th}, 10^{th}, 11^{th}] Fibonacci orders with [5, 8, 13, 21, 34, 55, 89, 144] cells, respectively. The results of the dynamic analysis for flexural waves in Fig.4.11 shows similar behavior as those for the geometrical impedance mismatch in terms of increase of the depth of the band gaps when the order increases.

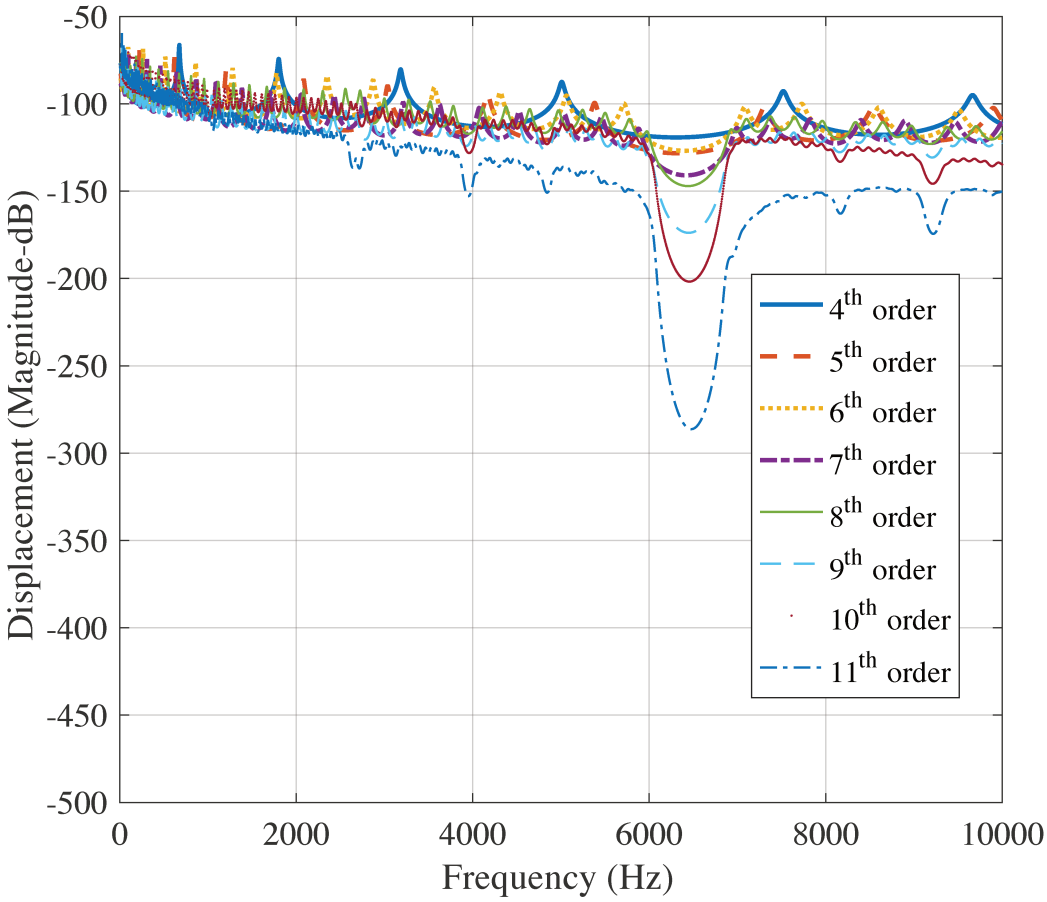

Figure 4.11: FRFs of the flexural waves for given orders of Fibonacci beam with material variation.

The main result from this analysis is that material constituent discontinuity does not have as much influence as cross-section variance in the depth growth of frequency stop bands. Analyzing again the numerical results in comparative way (i.e., without paying attention to the absolute values), the growth of depths in the frequency band gaps is less than those computed for the variation of cross-sections. Fig. 4.12 shows results of modelling the longitudinal waves for case M2, demonstrating a change in the location and width enlargement of band gaps compared to flexural waves. The band gaps can be observed in two ranges between $4400 - 4800$ Hz and $6700 - 10000$ Hz. The FRF of the longitudinal waves has much better influences in terms of numbers and width of the band gaps compared to the flexural waves and also the band gap trough is gradually becoming larger.

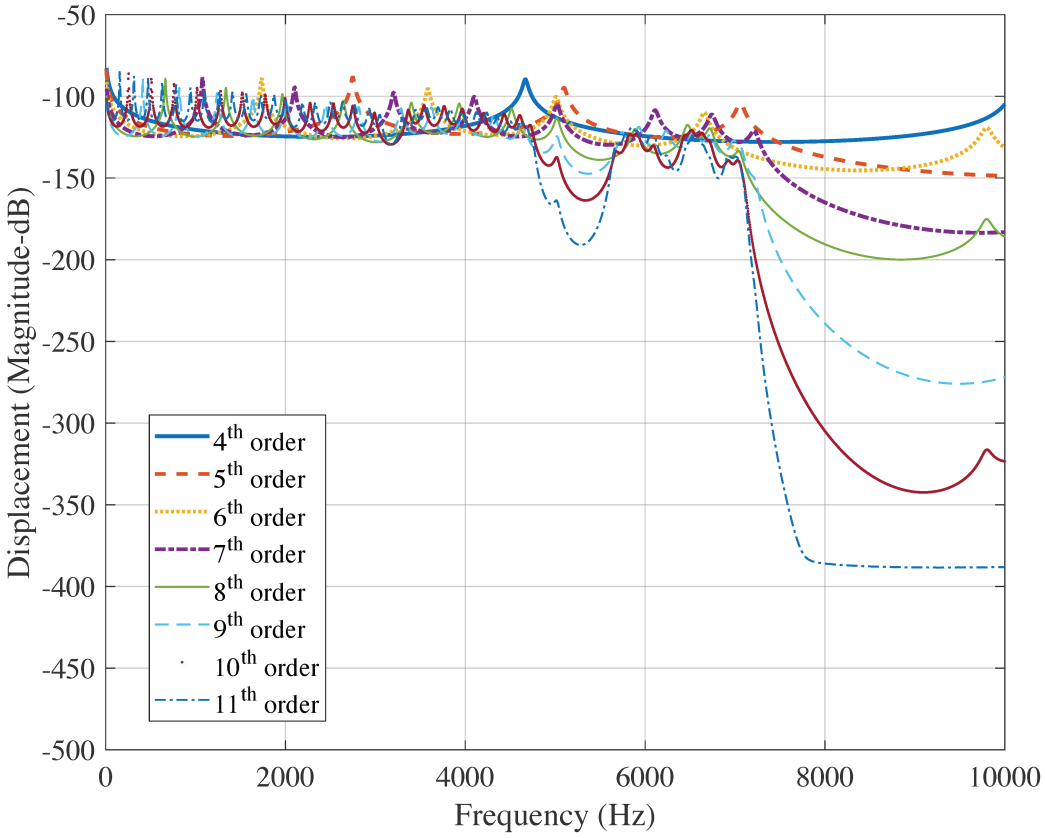

Figure 4.12: FRFs of the longitudinal waves for given orders of Fibonacci beam with material variation.

The FRF of the 11^{th}-order Fibonacci beam shows a flat curve in the band

gap at higher frequency (without any higher dynamics), that is caused by the longer length of the beam. Beside the flexural and longitudinal (FRFs) of case M2, another extra sub-case scenario has been investigated by considering a combination of lower and higher sound velocity materials. As there was not a big difference between the sound velocity of (aluminum 2045-T4) and (A36 steel), the flexural FRFs of the 11^{th}-order Fibonacci sequence periodic beam were also calculated for copper and magnesium.

Fig. 4.13 shows three curves, corresponding to the material combinations of case M2. A36 Steel is selected as a constant material (cross-section (A)) and copper, aluminum, and magnesium are chosen according to the Fibonacci sequence along the axial direction as (cross-section (B)). The results shows that combination of steel and copper with velocities of $5063m/s$ and $3503m/s$, respectively, has a very low attenuation and narrower band gaps, as marked by the solid line between $5000 - 7000$ Hz. In contrast, the combination of steel with aluminum and magnesium with velocities of $5199m/s$ and $5042m/s$, respectively, are shown by the dashed and dot-dashed lines, and have larger depth and wider band gaps compared to the copper case.

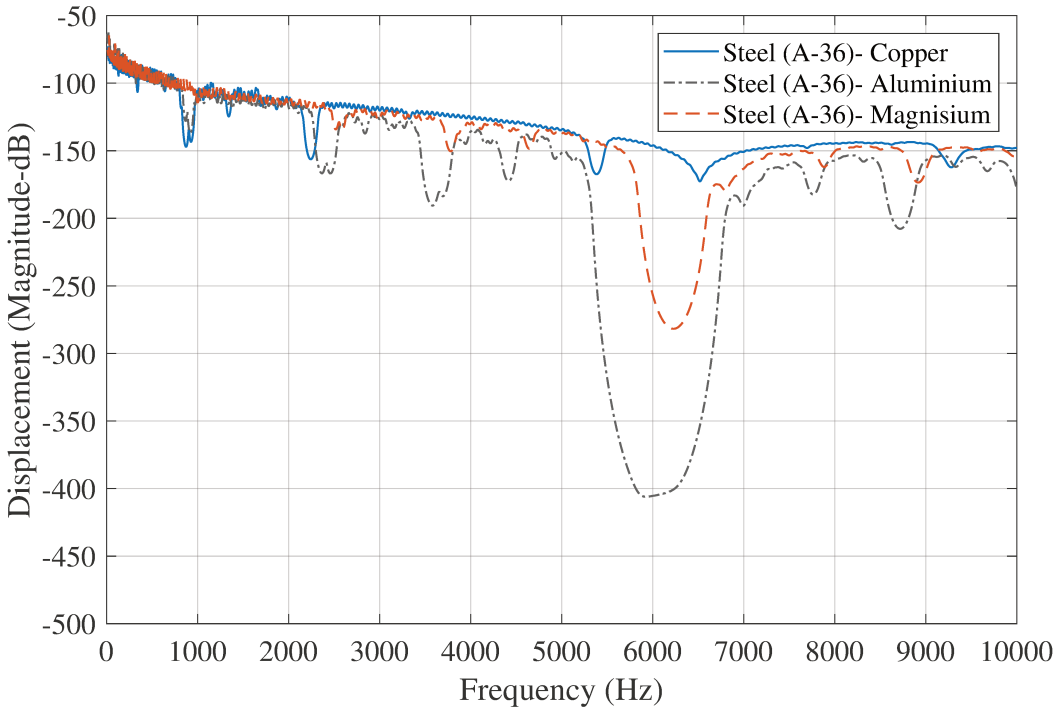

Figure 4.13: FRFs of the 11^{th} order of Fibonacci beam with Case M2.

In conclusion of section 4.4, the dynamic response of a quasi-periodic finite span reduces when using the four types of variations. The effectiveness of case M1 compared to case M2 depends on sound velocity. It seems from the lexicon that the sound velocity of case M2 with constant cross-sections and material variation is simply the ratio between modulus of elasticity and density. In contrary, the sound velocity of case M1 with constant material and cross-section variation is the ratio of modulus of elasticity with respect to density multiplied by the square of the height of the cross section. Thus, it explains why M2 is less efficient in terms of change in the impedance mismatch.

4.5 Spectral analysis of the M1 waveguides

4.5.1 Double cell

The same transfer matrix in Eq.3.23, extracted for the FRFs of the previous results based on a periodic double cell, is used again for dispersion curves computation. Frequency-shift of the stop/pass band positions is quantified, using the real solution of waves [41]. Herein, for quantifying the frequency shift of stop bands, the dispersion curves are plotted considering only the real parts of propagative waves. In Fig. 4.14, three types of cross-section variation for double cell periodicity are plotted. Type I, used as a reference, and the other Types are varied in all four subplots. The investigated frequency range is restricted to $0-2$ kHz in order to precisely visualize the band gap frequency shifts. Concerning Type I geometrical variation, again the band gaps move to higher frequencies for increased height of cross-section B. The frequency stop bands for Type I are around $650-850$ Hz, whereas for Type II they shift to higher frequencies at around $1000-1350$ Hz with greater width compared to Type I.

For Type III, the band gap moves to even higher frequencies $1300-1600$ Hz. In the numerical analysis the boundary condition is considered as free-free and a white noise (i.e., harmonic force of 1N from $0-10$ kHz with a bandwidth of 10 Hz) is applied to one end of the beam. The Type III band gap gradually shifts as the height of the second cross section (B) is reduced, until it reaches the zero-impedance mismatch in Type IV.

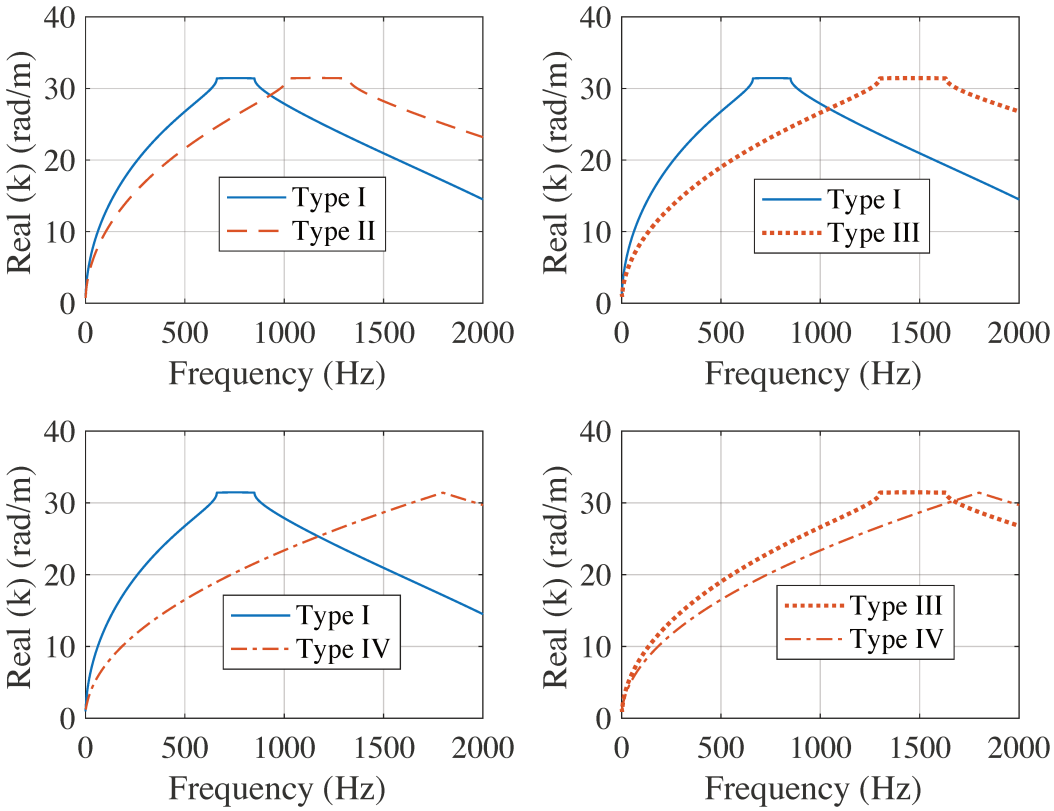

Figure 4.14: WFEM frequency response function of periodic double cell beam for flexural waves

4.5.2 Super unit cell

In this sub-section spectral analysis of super unit cell is studied. The super unit cell is identical and has a periodic pattern. The only difference is that each super unit cell contains different properties in terms of geometrical impedance mismatch. The geometrical properties of the super unit cell is based on the Fiboancci orders. Fig.4.15 shows the dispersion curves of 6^{th}-order Fibonacci. The same technique used for the dispersion of fully periodic double cell is also used for this system. Again, the comparison is plotted between Type I, used as a reference, and the other Types of geometrical variation.

The results are compared in terms of the real part of the wave number, of the periodic beam shown in Fig. 4.14 and the quasi-periodic beam in Fig. 4.15. In both cases, the stop bands shift to higher frequencies, but for

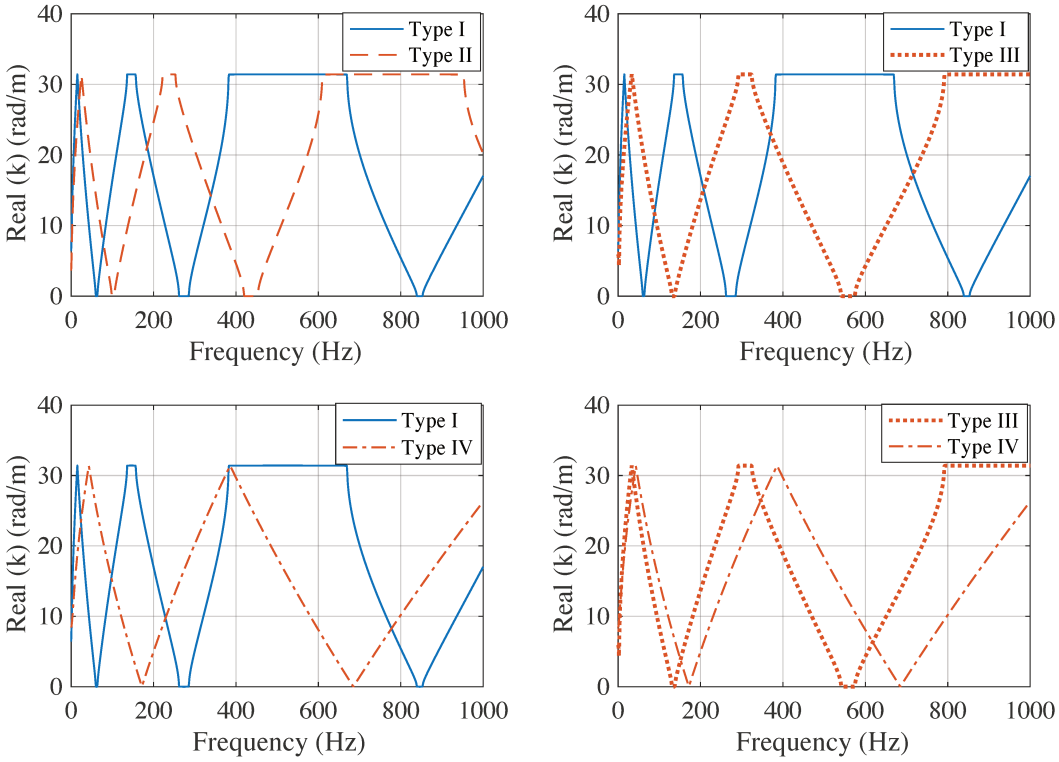

Figure 4.15: Dispersion curve of super unit cell with 6^{th} order of Fibonacci periodicity

the quasi-periodic beam the change is more dramatic. In fact, comparing the same band gap for the two beams, the band gap of the quasi-periodic beam is almost two times larger than for the periodic beam. This is made more clear in Fig. 4.16, which shows a comparison between the band gaps of the periodic and quasi-periodic beam, at the same cross-section ratio. The horizontal axis of the plot shows an average frequency that corresponds to the band gap interval Δf over the overall selected range of frequency f from Fig. 4.14 and Fig. 4.15.

In Fig. 4.16, the blue curve corresponds to the double-cell periodic beam, whereas the red curve corresponds to the 6^{th}-order Fibonacci quasi-periodic beam; and including the four types of geometrical cross-section in both cases. The band gap width of the quasi-periodic beam is higher than the periodic one up to (ratio of cross section variation) 2. After that, the band gap width of the periodic beam increases by increasing the ratio of cross section variation, while the band gap width of the quasi-periodic case decreases.

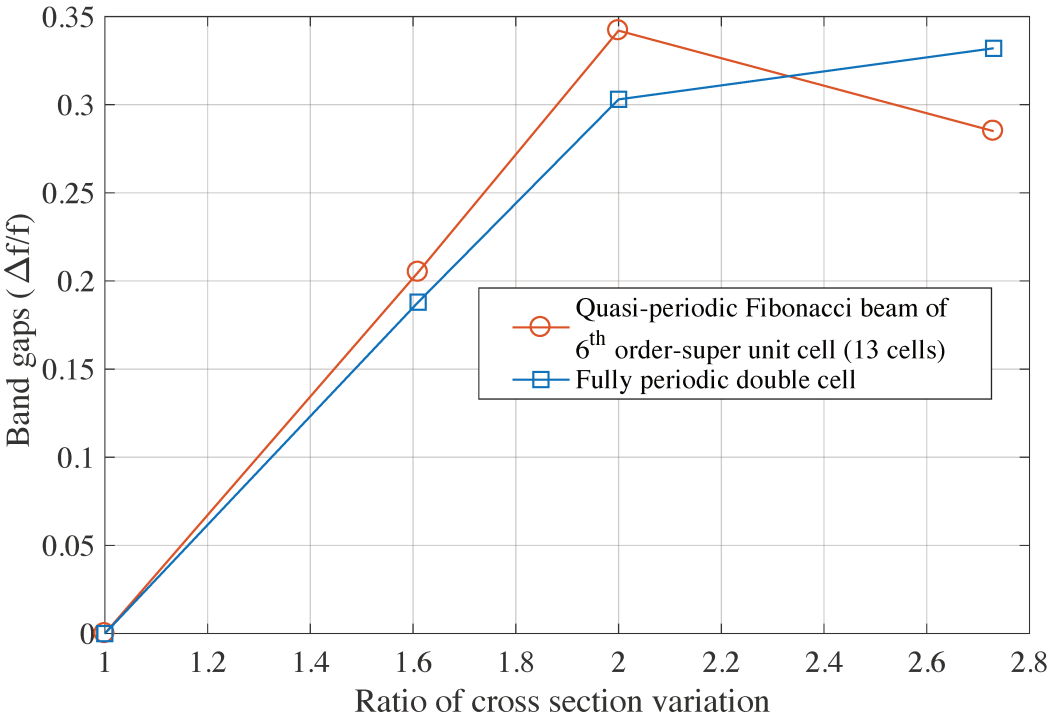

Figure 4.16: Spectral behaviour of band gaps for periodic and quasi-periodic embedded beams

4.6 Comparison of two quasi-periodic models (Fibonacci & Thue-Morse)

In this section, a comparison of flexural waves obtained by investigating two different quasi-periodic models, Fibonacci and Thue-Morse sequence [23], is discussed. The Thue-Morse sequence can be obtained within the present approach by always invoking the [A] and [B] base modules. In order to compare beams having the same mass, since the two models follow different sequences, the two models have two different orders: 5^{th} for Fibonacci and 3^{rd} for Thue-Morse. For the Fibonacci case, the beam is composed of 8 unit cells with the sequence [ABAABABA]; however, for the Thue-Morse case, the beam consists of 8 units cells following the sequence [ABBABAAB]. Hence, the beams have identical mass and length, but different material properties. Cell(A) is made of A36 steel, whereas cell(B) is made of $2045-T4$ aluminum

alloy. The length of the beam is 80 mm. They have free-free boundary conditions and are forced with a white noise applied in the first node while the response is taken from the last node of the beams.

Comparison is made by comparing FRFs and spectral analysis and results are reported respectively in Figs.4.17 and 4.18. The results from both models are good, showing different levels of attenuation with some differences in frequencies of stop bands. In fact, focusing on the FRF results plotted in Fig.4.17, both curves show a large stop band around $7800 - 8800$ Hz, but with the Fibonacci case having 10 dB lower attenuation level compared to the Thue-Morse case. However, in the remaining frequency range, there is another stop band (smaller in both width and depth) that locates in a frequency range of $4600 - 5000$ Hz for Thue-Morse beam and in another frequency range $3200 - 3600$ Hz for Fibonacci beam.

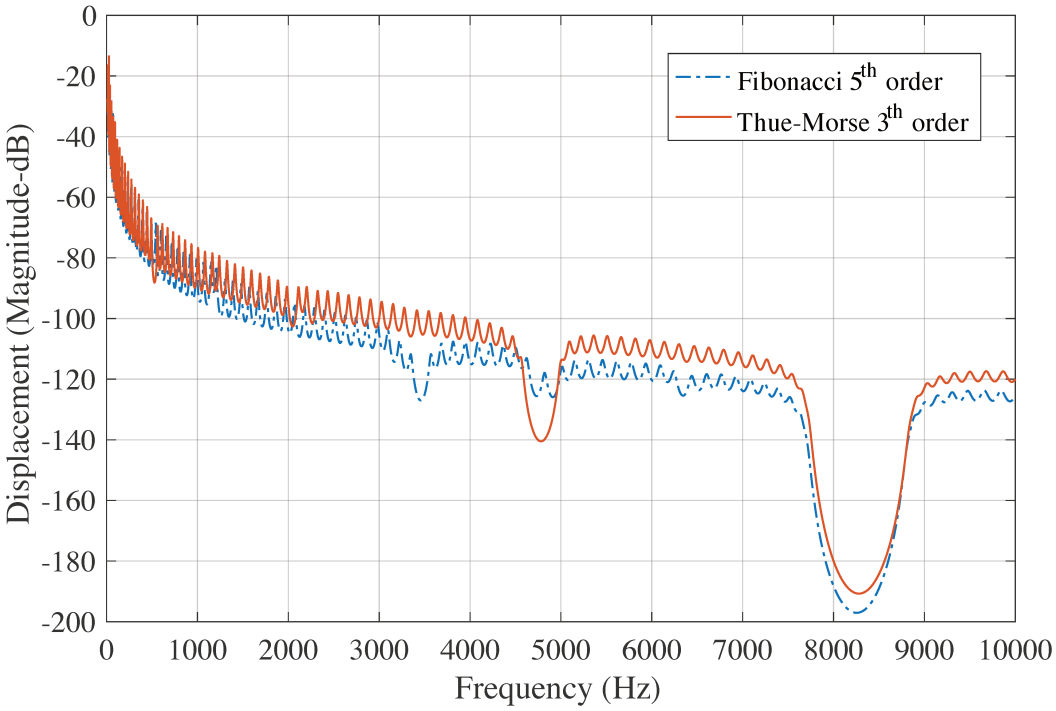

Figure 4.17: FRFs of the beams with material variations according to the Fibonacci and Thue-Morse sequences.

This is more evident in Fig.4.18, where the real and imaginary parts of the wavenumber are plotted. This plot is much illuminating, and it can be noted that the number of stop bands for both curves are the same, but the

width and the depth of the bands gaps for the Fibonacci and Thue-Morse models is different. For instance, in the frequency range $2000 - 2500$ Hz, the stop bands of the Thue-Morse model outperforms, both in width and in depth, the Fibonacci case. However, in the frequency range $3000 - 4000$ Hz the opposite behavior is observed.

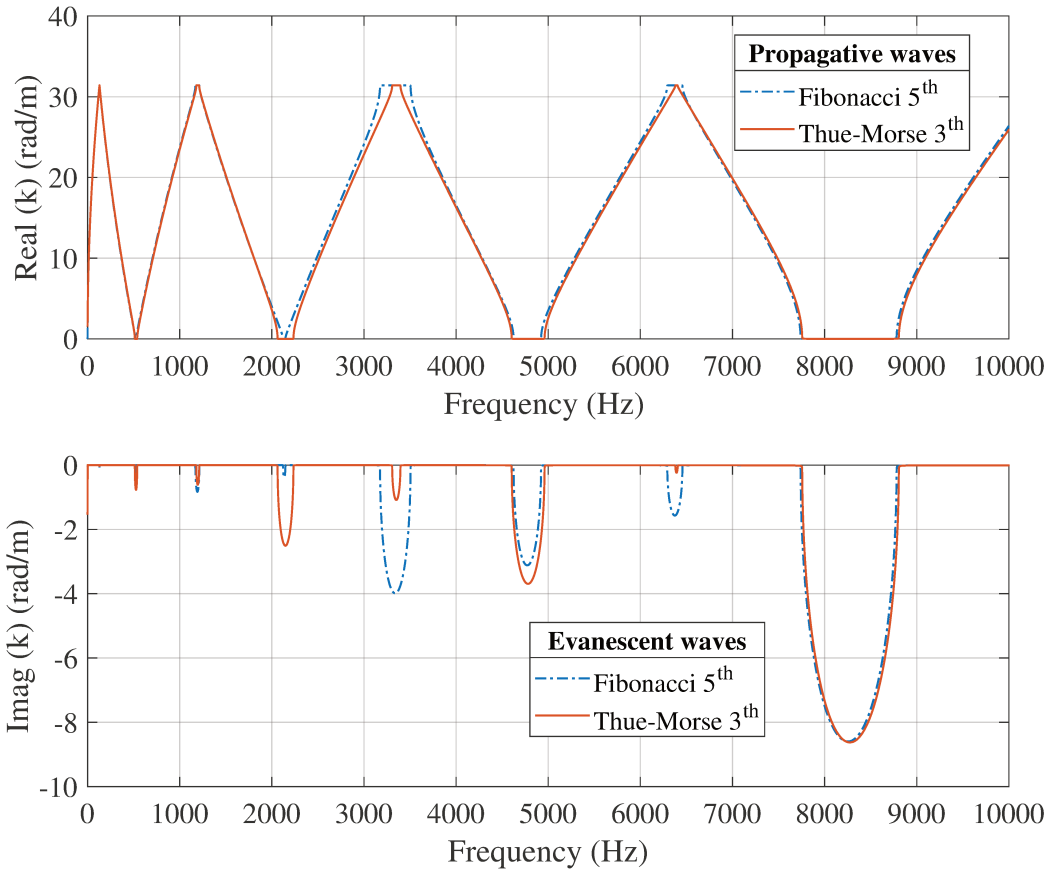

Figure 4.18: Dispersion curve of the flexural waves in the Fibonacci and Thue-Morse beam cases.

In conclusion, it should be noted that both Fibonacci and Thue-Morse models have similar band gap performances, with slightly different width and attenuation level. The Fibonacci model has lower attenuation levels and wider stop bands, which could lead to increase the vibration control performances of beam spans.

4.7 Conclusions

The structural response of periodic and quasi-periodic beams were investigated, by modelling numerical deterministic approach. The periodic beams were made of two different cells in terms of mass and cross-section dimensions. In contrast, the quasi-periodic beams used the same two cells, but the replication of periodic cells followed the Fibonacci sequence pattern.

First, the harmonic response of quasi-periodic beams with increasing orders (length) of Fibonacci sequence was investigated using the finite element method. In this case, beams were made up of cells (constant length) whose cross-section areas and material properties followed the Fibonacci sequence.

Then, four types of geometrical variations were investigated. Case M1 with a geometrical impedance mismatch were applied in the periodic and quasi-periodic beams of double and super unit cells, for which the global mass of the beams were kept constant and cross-sections varied.

Finally, spectral analysis was performed of the wave propagation behavior of periodic structures with WFEM. In this case, beams were made up of identical super-unit-cells that were composed of cells whose properties followed a 6^{th}-order Fibonacci sequence.

4.7.1 Main results

It can be noted that increasing the number of Fibonacci orders of the quasiperiodic structure leads to band gaps with increased attenuation.

Study of the geometric variation applied to a quasi-periodic beam is extended in the WFEM method. The case M1 with geometrical variation by reducing the volume fraction of cross-section (A) and increasing the volume fraction of cross-section (B) proportionally, while keeping the total mass of both cells constant is studied. Four types of numerical models are designed for spectral analysis of the flexural and longitudinal waves.

A quasi-periodic beam is designed using the 6th-order Fibonacci sequence and placed in a super unit cell for FB waves analysis. Four types of cross-section variations in the beams are considered. The main results, obtained for the 6th-order case, show that a larger difference between the cross-sections (i.e., cross-section (A) is much larger than cross-section (B)) leads to three

main effects: i) change in extension/enlargement of frequency band gaps, ii) shift of frequency band gaps to lower frequency, and iii) an increase in the attenuation levels of frequency stop bands.

Overall, the investigation of quasi-periodic structures with geometrical impedance mismatch in this chapter have an efficient impact on attenuating acoustic waves in lower frequency regimes as compared to strictly periodic counterparts. Although, quasi-periodic structures does not create wider stop bands, but by combining case M1, can shift the stop bands drastically compared to the strictly periodic spans. The results obtained also show that the quasi-periodicity examined with specific material and geometrical properties can improve performance, because attenuation in a given frequency range, can be obtained without weight penalty, which can be an asset for lightweight structures.

Chapter 5

Numerical investigations and experimental measurements on the structural dynamic behaviour of quasi-periodic meta-material

5.1 Introduction

The current work is focused on the analysis of quasi-periodic 2D structures. A deterministic approach is used to introduce a two directional Thue-Morse sequence for creating a quasi-periodic meta-material to improve the vibroacoustic performances. In the literature there are various previous studies of dynamic analysis of 1D quasi-periodic systems; in contrast, study of 2D quasi-periodic systems is very rare. Some sequences are intrinsically ready to be used for 2D cases, such as the Thue-Morse, while others like Fibonacci are well adapted to 1D cases.

In this research, 2D lattices are built with the conventional finite element method (FEM) to comply with the Thue-Morse sequence in order to explore the opportunities offered in terms of reduction of the forced response in some frequency bands [79, 80]. Specifically, the work presents modified versions of star-shaped concave unit cells.

The tailored quasi-periodicity is defined by invoking a bi-directional Thue-Morse morphism sequence on the meta-material. The geometrical impedance mismatch results in asymmetry and follows a combination of two different star-shape elements by variation of different corner angles. The main target

of the study is the design of structural stop band/filters in order to optimize the isolation of vibration at certain frequency ranges.

The contents of this chapter are as follows. In Section 5.2, quasi-periodic structure is presented. Section 5.3 introduces the Wave Finite Element Models and dispersion analysis. Then in Section 5.4, experimental results are validated. Section 5.5 describes structural dynamic analysis using Finite Element models. A closing section summarizes the conclusions of this work.

5.2 Quasi-periodic structures

In this chapter, the focus is on the application of the Thue-Morse sequence to 2D domains for introducing irregularity in both directions. In this section, a possible approach is presented to analyze the vibration performance of quasi-periodic 2D structures.

This section contains three sub-sections. The first is dedicated to description of the cells. Second sub-section introduces the Thue-Morse morphism sequence, while the third sub-section concludes with the periodic sequence.

5.2.1 Cells

The waveguide modelled in this analysis is a star-shaped lattice. The meta-material is made of two different unit cells (A and B). Fig. 5.1 shows the geometry of the two cells inspired from [82].The two unit cells differ in terms of the corner angle α.

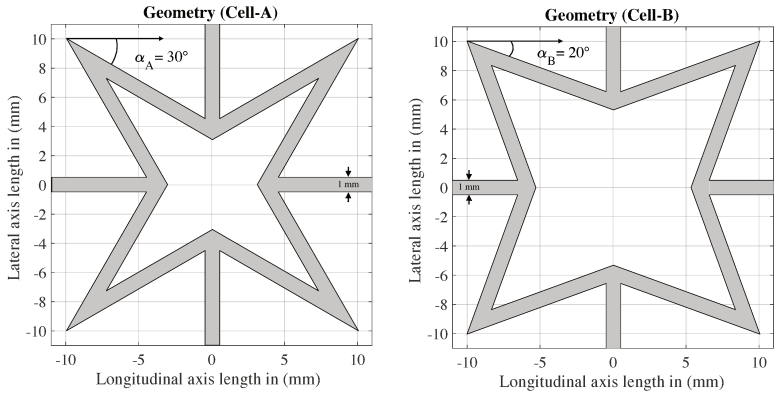

Figure 5.1: Meso-scale unit cell A and B preliminary design stage

Unit cells A and cell B have equal sides distance of 22 mm, and the internal core with star shape covers an area of $20 \times 20mm^2$. The thickness of the base plate is 3 mm and the wall thickness of the cells is 1 mm. Cell A has an angle $\alpha_A = 30°$ and Cell B has an angle $\alpha_B = 20°$. The angles are variables of the sequences according to the generating order of the developed sequence. Cells A and B will be arranged in a specific sequence presented in the next section.

The properties of the materials used in all the analysis in this chapter are given in Table. 5.1. Shell elements with free triangular mesh are used in the FE model shown in Fig. 5.2. Each unit cell has a total of 28 nodes, where only 8 nodes are connected with the adjacent element along the x- and y-directions. In addition, each node has 6 degrees of freedom.

Table 5.1: Material properties

Material	**Polymer**
Modulus of elasticity(Pa)	1.68×10^9
Density $(\mathrm{kg} \cdot \mathrm{m}^{-3})$	818
Poisson's ratio	0.38
Structural loss factor	2.5 %

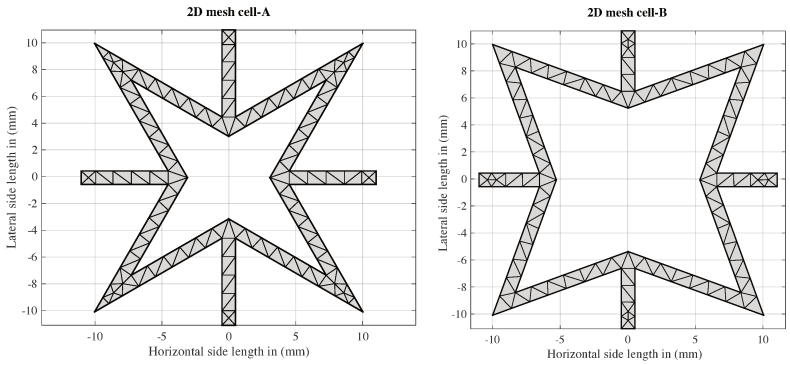

Figure 5.2: 2D mesh of cell-A and cell-B

5.2.2 Quasi-periodic lattice

According to the section 2.2.1 (design of lattice structure), 2D lattice is designed using the Thue-Morse sequence in 2D, for star-shape structures.

The finite quasi-periodic lattice has 8×8 units of cell-A & B, see Fig. 5.3.

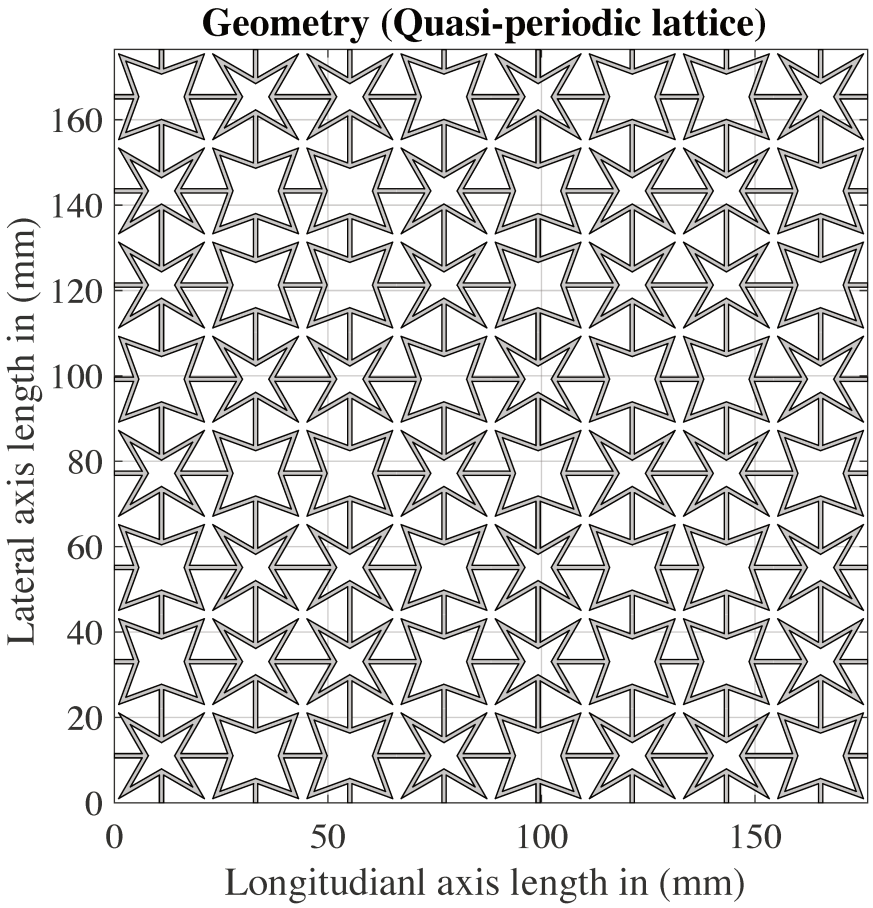

Figure 5.3: Quasi-periodic lattice combining unit cells A and B: following Thue-Morse sequence in two directions

5.2.3 Periodic lattice

For comparison purposes, two strictly periodic arrangements are also considered: two finite panels composed of 8×8 units of cell-A and 8×8 units of cell-B. Both periodic lattices are shown in Fig. 5.4.

Fig. 5.5 shows another periodic lattice with alternated unit cells A and B. As for the previous cases, the whole geometry includes 64 unit cells, in which 32 of them are cells A and 32 cells B.

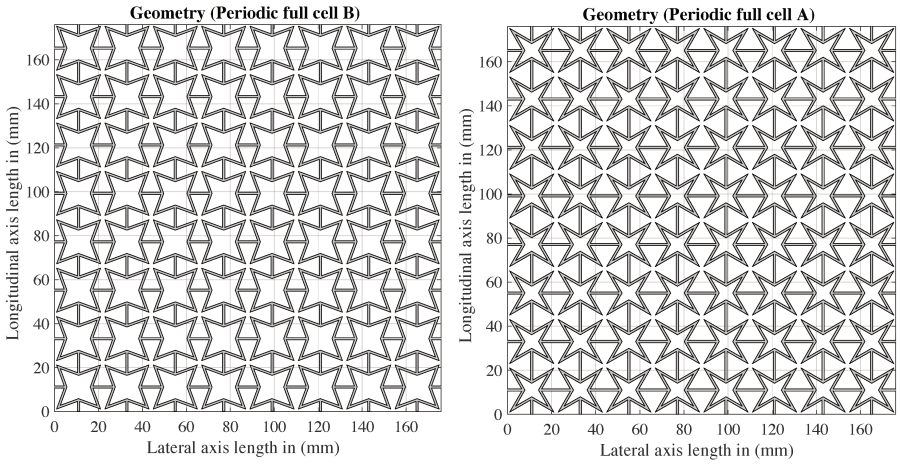

Figure 5.4: Finite periodic lattices, right with cell A and left with cell B

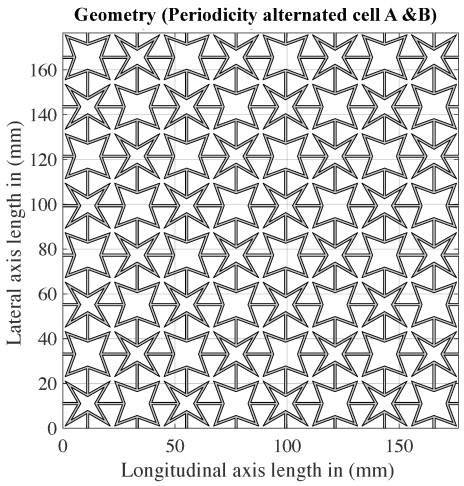

Figure 5.5: Periodic lattice with combined unit cell A and B in alternating pattern

5.3 Wave and finite element models: dispersion analysis

This section is divided into two sub-sections. The first is related to the analysis of the behavior of infinite periodic 2D lattices by computing the dispersion curves of unit cells, for full cell-A and full cell-B configurations as depicted in Fig. 5.4. The second is dedicated to other infinite periodic 2D lattices by computing the dispersion curve of alternated (mixed periodic) A-B periodic lattice structures, as depicted in Fig.5.6.

Eigenfrequency analysis is used to compute the band diagram of periodic structures for the first 25 Bloch modes for single cells and the first 120 Bloch modes for the second case with combined (mixed periodic) A-B [18,58]. The FB method is used, for which the periodic boundary conditions are written as:

$$u_{Rx} = e^{-jk_x D} u_{Lx}, \tag{5.1}$$

$$u_{Ry} = e^{-jk_y D} u_{Ly}, \tag{5.2}$$

where u_{Rx} and u_{Lx} are the right and left side displacement along the x-axis, and u_{Ry} and u_{Ly} are the displacement along the y-axis, respectively. D is the length of reciprocal or unitary repeated element, k_x and k_y are the wavenumbers in the x- and y- directions.

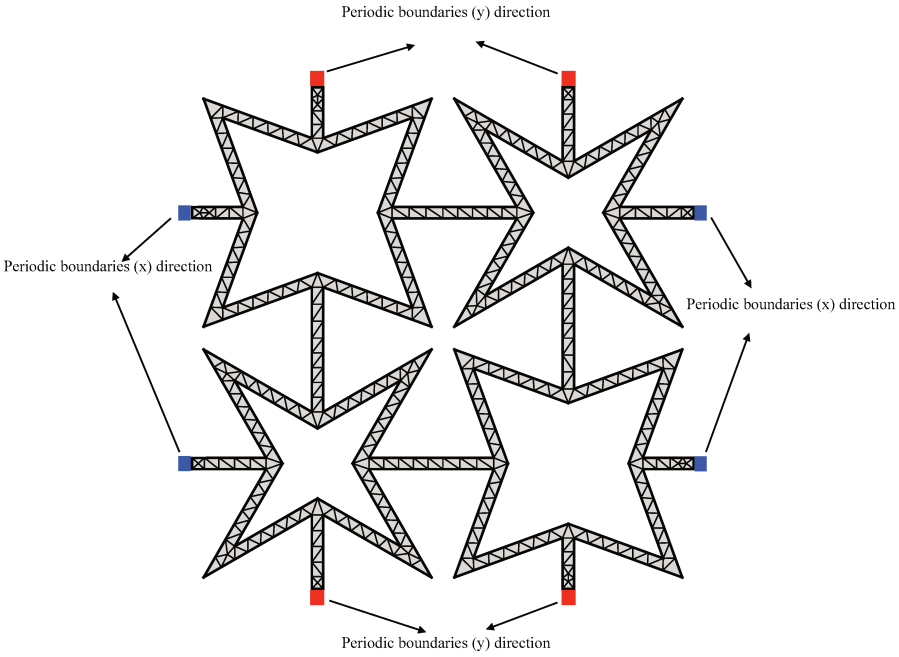

Figure 5.6: FE model of the combined (mixed periodic) A-B structure with periodic conditions

The FE model of the combined (mixed periodic) A-B unit cell in Fig. 5.6 is made of four single A and B cells. The pattern is periodic and dispersion diagram results will be compared to the FRFs of the quasi-periodic pattern in the following sections. The parametric eigenvalue analysis is performed

according to the edges of the first irreducible Brillouin zone Fig. 5.7. It starts from (Γ) towards the x-direction to M, and from M towards y-direction to K and then back to (Γ) [18].

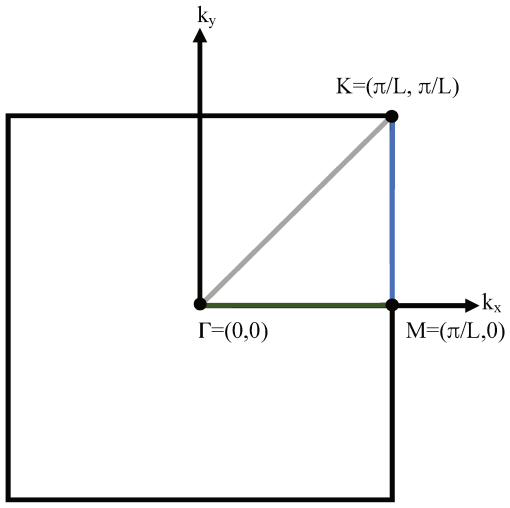

Figure 5.7: Schematic of first irreducible Brillouin zone

The band diagrams of cell A and cell B are presented in Fig.5.8. In the dispersion diagram, all types of waves (i.e., bending, longitudinal, and shear) are considered [77, 83–85]. The analysis of cell A shows three frequency stop bands between 0 and 18 kHz. The first band gap with a bandwidth $\Delta f = 2.6$ kHz appears at $2808 - 5431$ Hz, then the second one has a slight wider band $\Delta f = 2.64$ kHz at $7081 - 9725$ Hz, while the third frequency band gap with $\Delta f = 1.86$ kHz is located at $11480 - 13340$ Hz.

Over the same frequency range, cell B has a completely different behavior in terms of band gaps, with only one wide band gap with $\Delta f = 1.73$ kHz being observed at $3157 - 4892$ Hz. The second band gap starts at 5149 Hz and ends at around 5975 Hz, with further small frequency stop bands at around 6896 Hz, 8623 Hz, and 9809 Hz.

The dispersion diagram shown in Fig. 5.9 corresponds to the combined A and B cells. The first complete stop band is observed at $3000 - 4500$ Hz, and the second one is between $5000 - 5800$ Hz. There is too a narrow band gap from 5800 Hz to 6000 Hz. The fourth one starts from 7000 Hz to 8000 Hz that is much wider and the fifth one with $\Delta f = 2$ kHz. There is also a very nar-

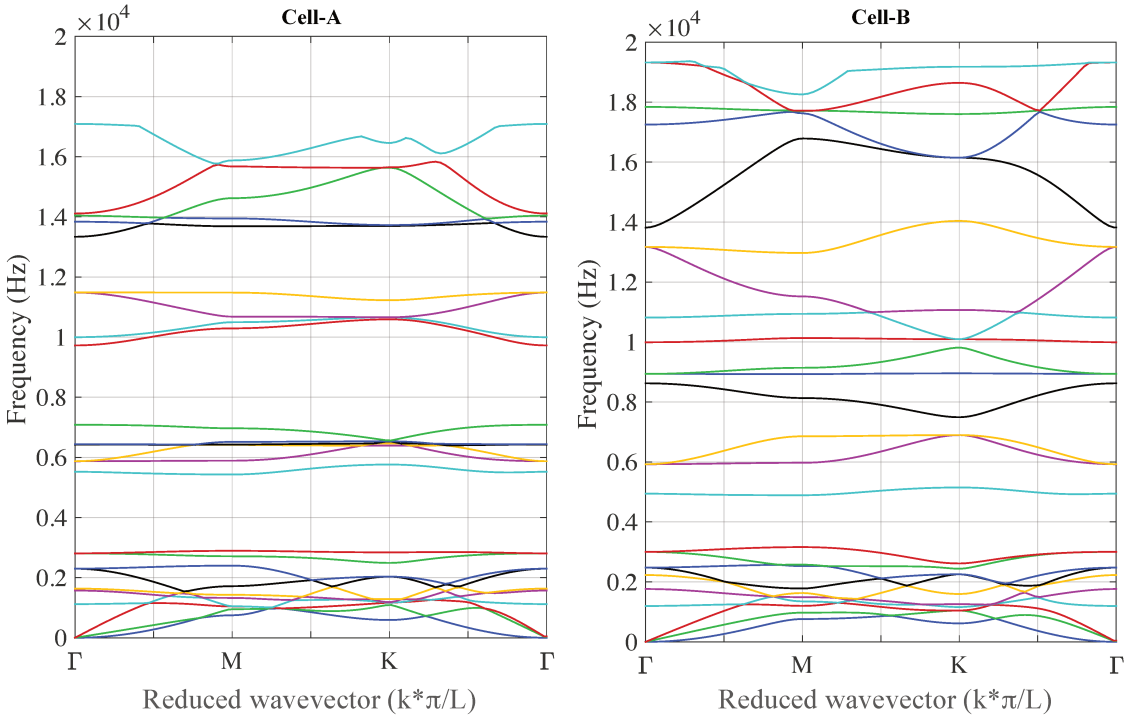

Figure 5.8: Band diagrams of infinite lattices: (left) unit cell A, (right) unit cell B

row gap at 11000 Hz, just before the next wide stop band at 12000−13800 Hz.

The dispersion diagram of the combined (mixed periodic) A-B structure show some similarities with a combination of the dispersion diagrams of the single cells shown in Fig.5.8. Cell A provides interesting dynamics properties with a few wide band gaps. Cell B has more band gaps, but with narrow frequency width. The combination of the two in a periodic formation provides a large number of gaps, the largest ones being almost as wide as cell A, while keeping a number of gaps comparable to cell B. In the next section, FRFs will be computed for finite structures, in order to first validate the applicability of the gaps for real structures, and second to check whether or not a quasi-periodic arrangement can provide added value for engineering applications.

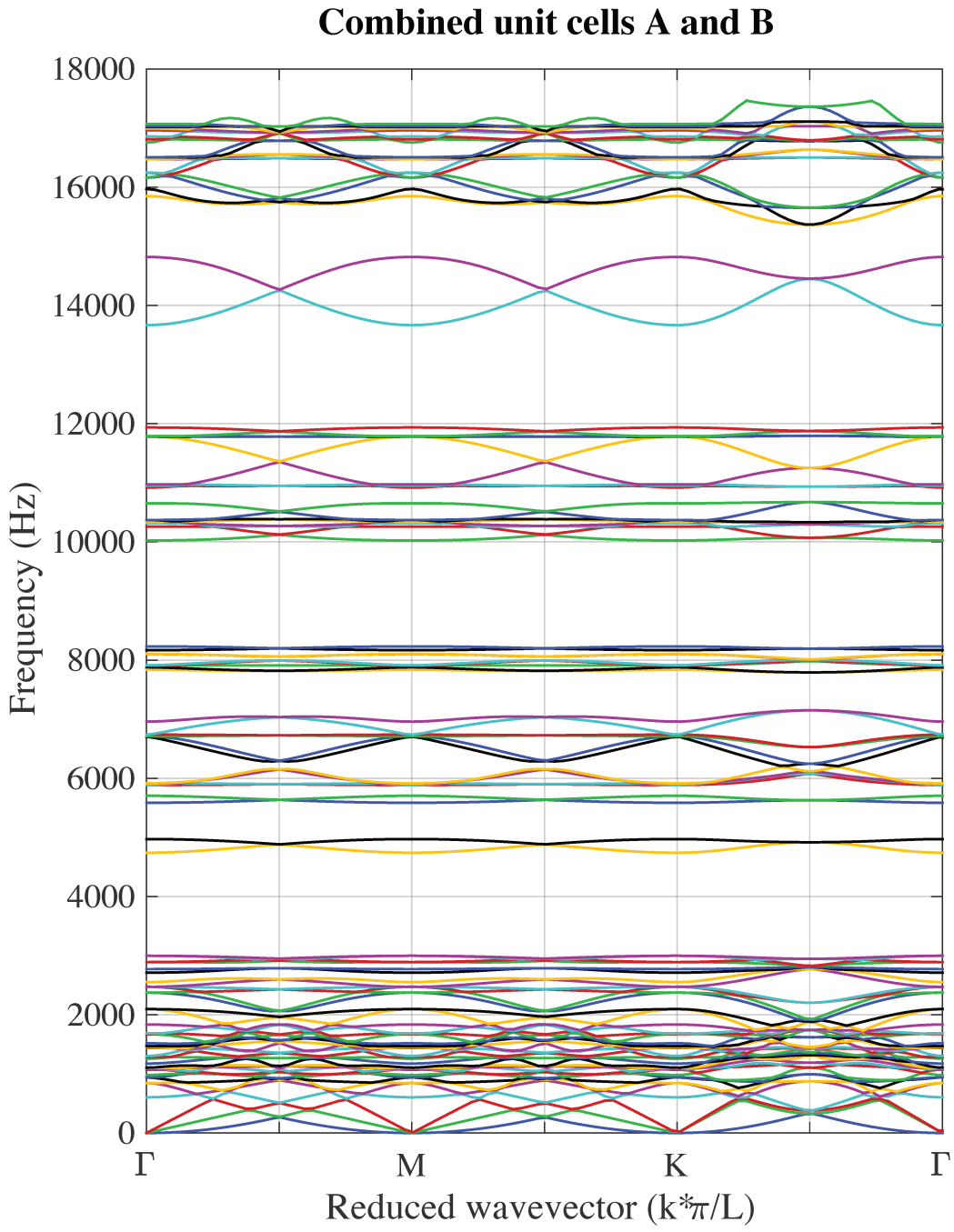

Figure 5.9: Band diagram of combined A-B lattice

5.4 Experimental measurements

In this section, the simulated results of the dynamic response of the lattice are validated by comparison with experimental results. The quasi-periodic panel is manufactured by laser cutting as shown in Fig.5.10. The material properties of this test-article are already reported in Table. 5.1.

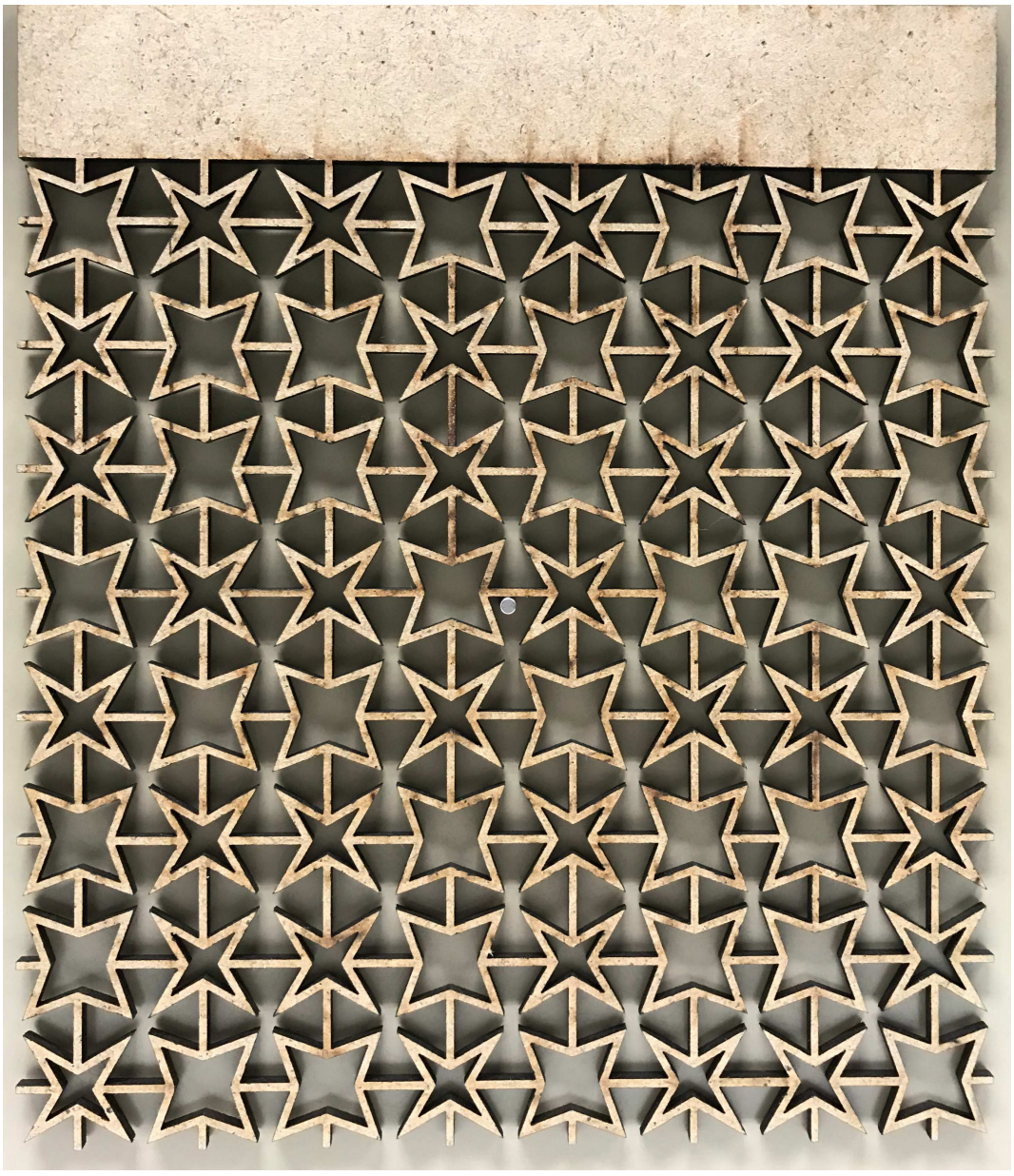

Figure 5.10: Design of meta-material prototype for experimental testing.

For the experimental tests, the lattice has an extra flat panel part that is used as a boundary support during the dynamic tests. The lattice is vertically positioned and clamped with the fasteners, as shown in Fig. 5.11. The shaker is attached to the structure on the left corner at a position that is very close to the boundary support. A white noise excitation source generates signal from 1 kHz to 11 kHz. The measurements are recorded using a laser vibro-meter as shown in Fig. 5.11.

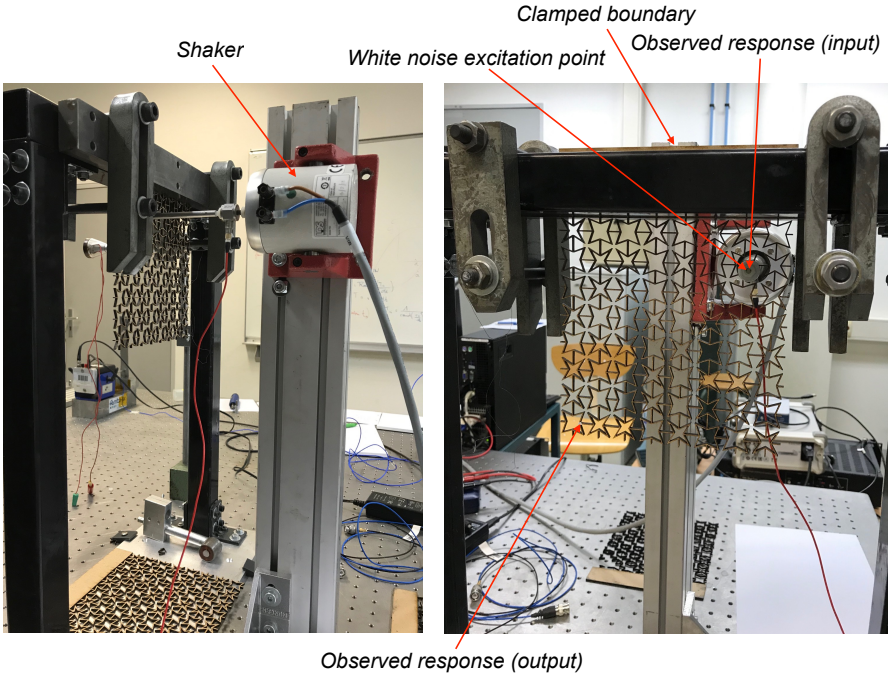

Figure 5.11: Manufactured prototype of quasi-periodic metamaterial under experimental measurement

The first eigenfrequencies of the structure are characterized with the numerical modal analysis of the quasi-periodic configuration to predict the values of the material and geometrical properties.

Fig. 5.12 shows the FRF measured between $0-100$ Hz. On this figure, the eigenfrequencies of the numerical model are shown using vertical lines. The first 3 modes are very well correlated in terms of frequency, which means that the low frequency behavior of the structure is well captured by the FE model. Then, measurements are performed up to 10.9 kHz. The corresponding FRFs are shown in Fig. 5.13.

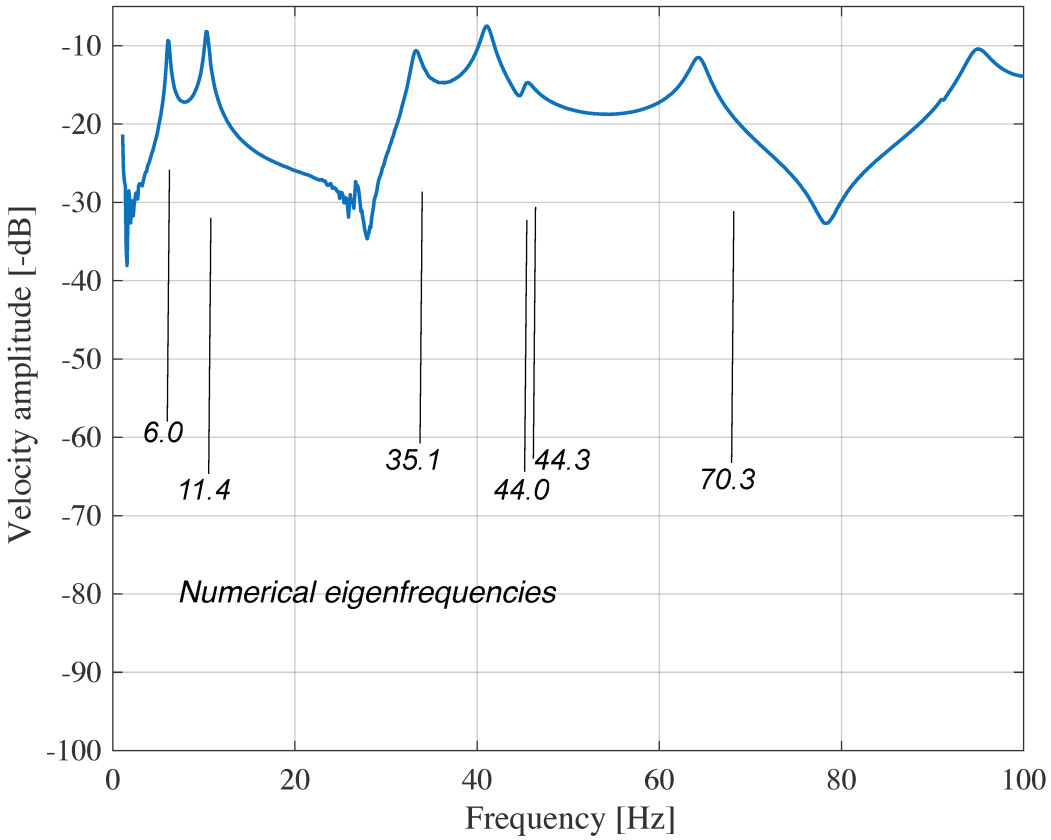

Figure 5.12: Measured FRF in low frequencies

Three subplots in Fig. 5.13 represents the amplitude, phase angle and coherence. The response is measured at the input point.

Similarly, the experimental FRF of the output reference point is shown in Fig. 5.14. It can be seen that there is a loss of elastic wave propagation while measuring the far field response. The coherence plot shows some falls of the noise level meaning that some background noise is measured that corresponds to possible band gaps. For instance the first stop band appears from 2.5 to 5.2 kHz with a peak in the middle of the attenuation zone, the second is from 7 to 8 kHz, and the last stop band starts after 8.2 kHz and continues up to the maximum frequency that can be reached by the experimental setup (11 kHz).

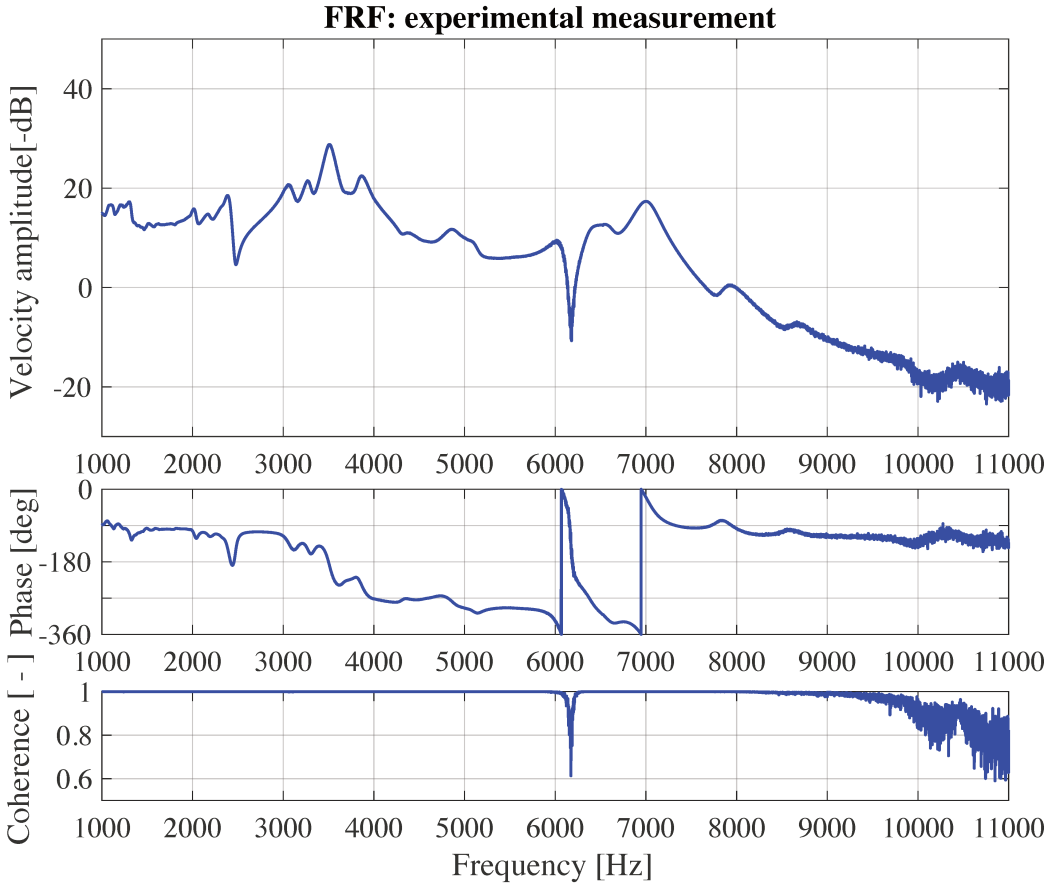

Figure 5.13: Velocity response measured in the input point

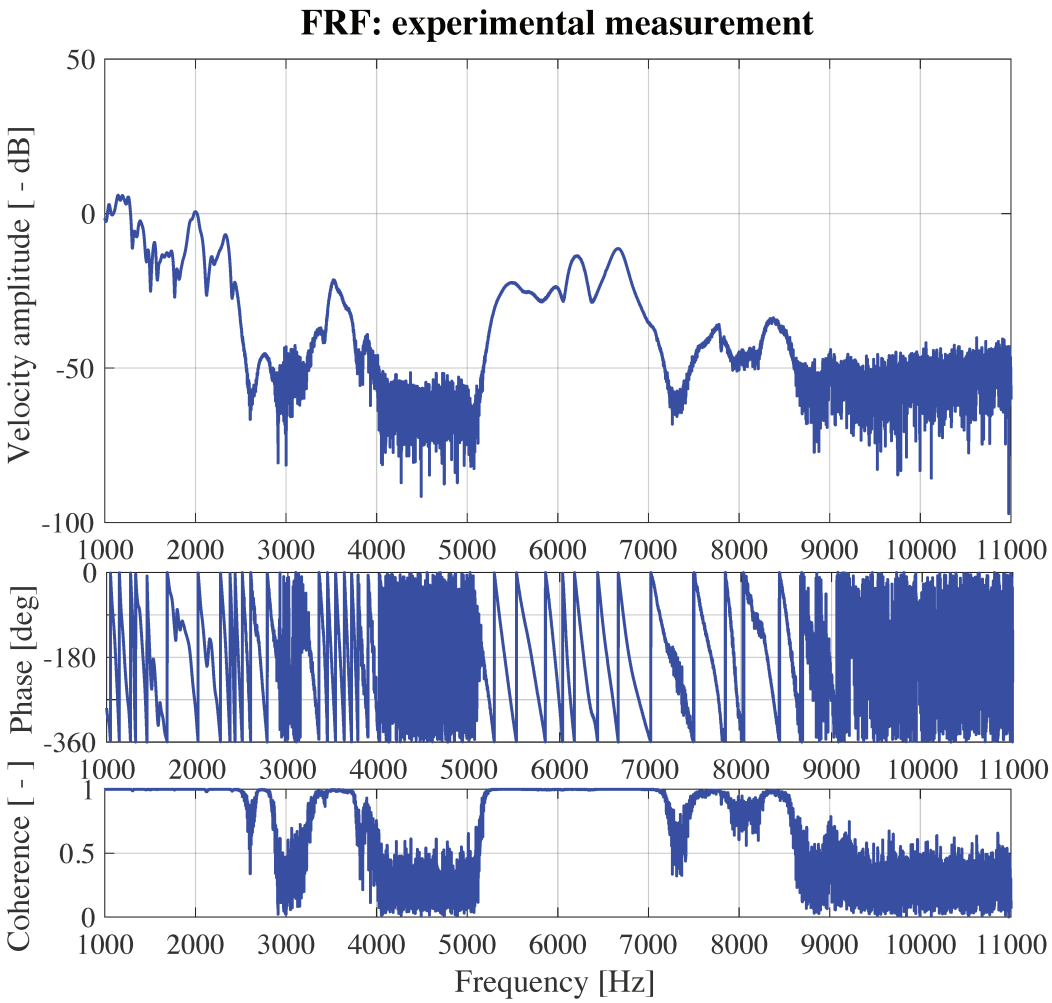

Figure 5.14: Velocity response measured in the output point

5.5 Finite element analysis

In this section, two periodic and one quasi-periodic lattices are considered. The first two periodic lattices are modelled as finite meta-materials made of cell A and cell B in two separate lattices. The aim is to verify whether those stop bands predicted in the previous section are maintained for this specific finite element configuration, i.e., with a finite domain. Secondly, the quasi-periodic meta-material in Fig. 5.15 is compared with a structure formed from a combination of cell A and cell B (periodic lattice). Finally, an FRF of a meta-structure (filter junction) with a pure quasi-periodic lattice is described.

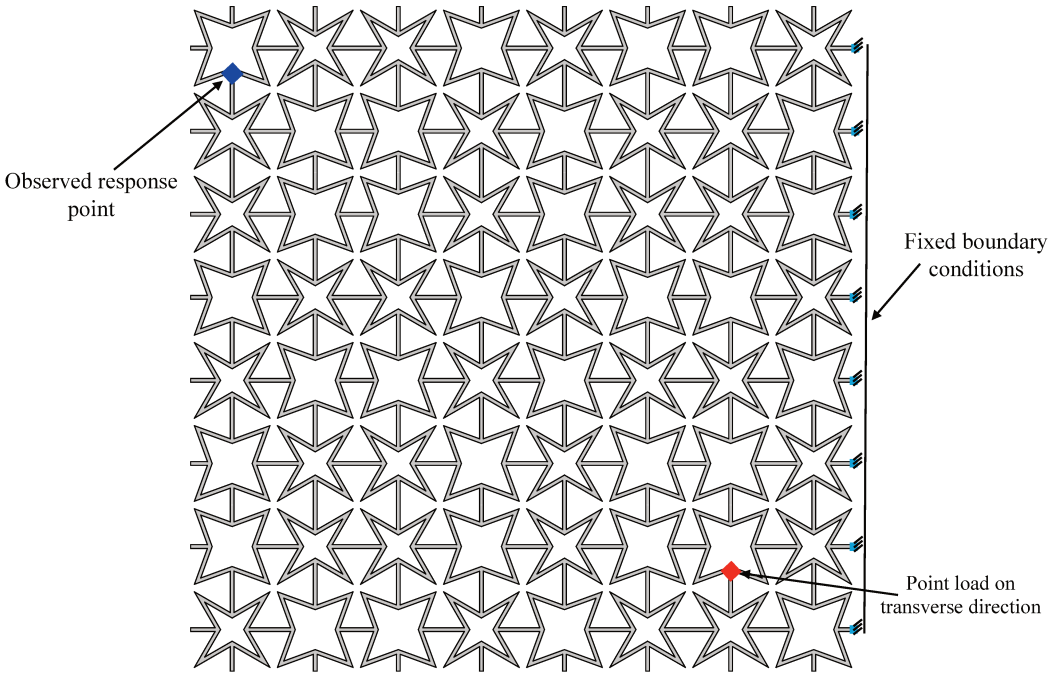

Figure 5.15: Quasi-periodic lattice, numerical model setup for FRF analysis

5.5.1 Frequency response of meta-materials

The FRFs are computed by considering three cases. Case A, B and quasi-periodic (combined A & B). All these cases contain finite panels with 64 unit cells. The models were numerically analyzed. It was considered that they were clamped on the right edges and a harmonic point force is applied in the region close to the fixed boundary condition with a frequency ranging

from $0 - 35$ kHz. The model is meshed by 1061 free tetrahedral and 840 bi-quadratic triangle elements with 6 nodes each. A frequency range of 35 kHz is selected for all the FRFs to check how the various cases behave at higher frequencies. The response is observed in the location marked with a dark blue spot in Fig. 5.15. Fig. 5.16 shows the FRFs for the three types of lattices. It can be seen that the predicted band gaps in the dispersion diagram of the periodic lattices (Fig. 5.8) have similarities with the FRFs of their finite counterparts. There are basically four full band gaps, which are associated with the resonant and Bragg-type band gaps.

There is no generic theoretical definition to classify the types of band gaps in this dispersion diagram; however, at least the first band gap in all cases are resonant band gaps. Fig. 5.16 shows four band gaps marked as BG1, BG2, BG3, and BG4. For BG1, the response is almost the same for all the cases. BG2 has almost the same width for all the cases. It is the widest gap, but possesses a localized mode in the middle for case A. The quasi-periodic case shows the same width as for case B but starts at lower frequency. The BG3 band gap is only fully visible for case A, very narrow for the quasi-periodic case, but not visible for case B.

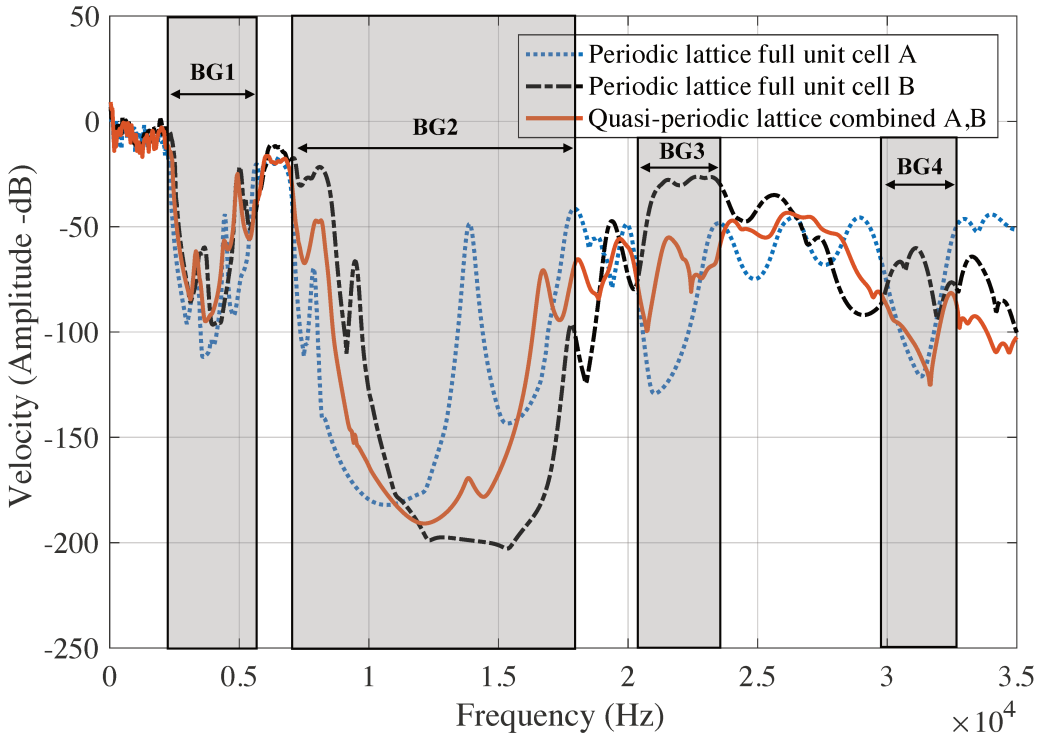

Figure 5.16: FRF of the two periodic and a quasi-periodic lattices

BG4 has almost the same width for case A and the quasi-periodic case, but the quasi-periodic fall starts before than case A, and no band gap exists at this position for case B. In conclusion, the quasi-periodic case can be seen as a good *compromise* between case A and case B.

So, after analyzing the data sets, it is apparent that all periodic and quasi-periodic lattices have specific performances in terms of band gaps. In the next step, the combined (periodic) A & B case is compared to the quasi-periodic arrangement. The FRFs are shown in Fig. 5.17. The two lattices are similar in terms of in-plane dimension and volume fraction. The responses provided in Fig. 5.17 in terms of velocity (amplitude -dB) show similar dynamic effects with only slight differences. The first observed difference is higher depth of around 15-dB for the quasi-periodic case (blue line) compared to the strictly periodic cases (red line). The second difference is the wider frequency stop bands around $8 - 16$ kHz. The quasi-periodic curve has lower peaks starting from 16 kHz and continues up to higher frequencies around 25 kHz. In conclusion, both design have similar dynamic effects, but with important differences. The generated combination of quasi-periodicity in the lattice could give reduced response in the attenuation level at $3.5 - 5$ kHz compared with the regular periodic combination. It also has a similar band gap width in the medium frequency range of $8 - 16$ kHz, with lower attenuation level and peaks after 25 kHz.

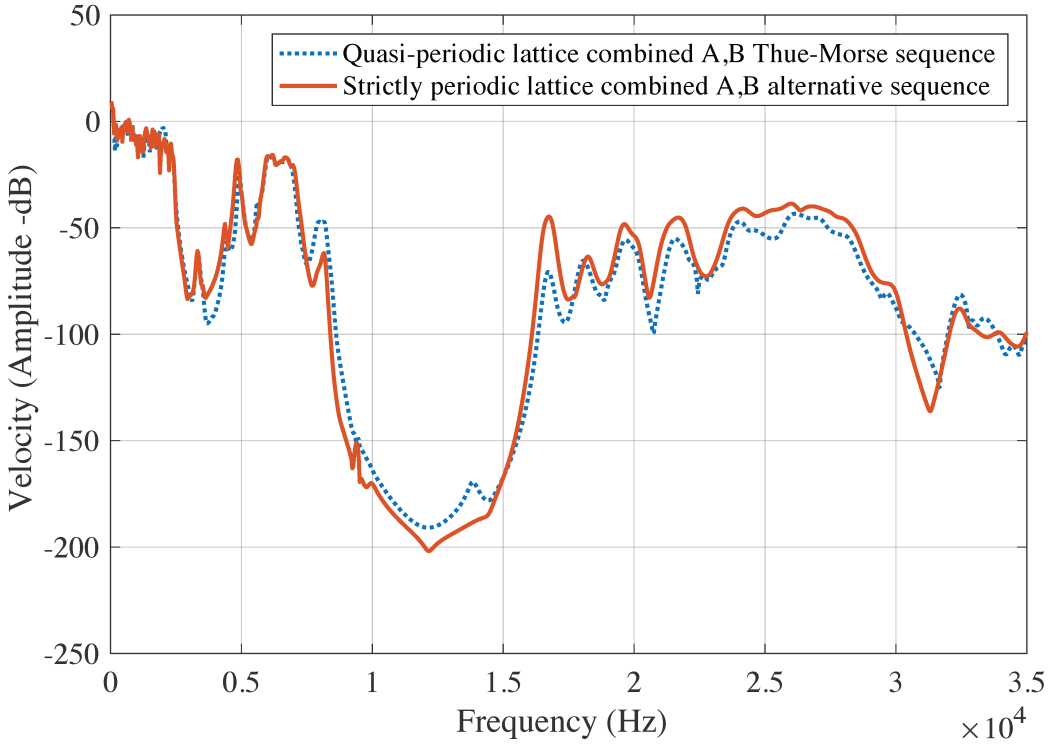

Figure 5.17: FRF of the periodic and quasi-periodic lattices

5.5.2 Frequency response of a meta-structure

In order to illustrate the applicability of the quasi-periodic arrangement for wave filtering, a meta-structure that filters the elastic wave propagation from one component to another is proposed. The meta-structure is located at the interface between two flat panels. In Fig. 5.18. the design of the setup and meta-structure is shown. In this model the connection between the meta-material and two panels are made by linking the side branches of the meta-material lattice with the side walls of the panels at the right and left sides respectively. The cross-sectional area of each branch of the star-shape meta-material is $1 \times 3mm^2$. In total there are 16 links, consisting of 8 connections on the right and 8 connections on the left with the bare panels. Two cases are investigated. First, the dynamic response in terms of Root Mean Squared (RMS) of velocity (amplitude -dB) over all nodes of the panels, is computed. Secondly, four specific frequencies are selected, and the response is calculated to visualize the elastic energy transfer from one side of the panel to the other side. A harmonic point force is applied in the transverse direction on the first component and the response is computed in

the first and second components shown in Fig. 5.18.

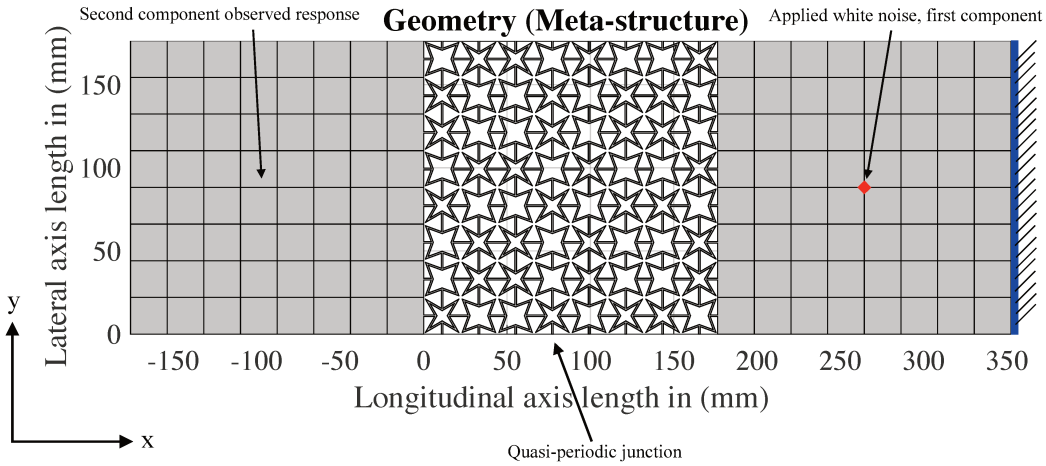

Figure 5.18: Geometrical model of the meta-structure

Fig. 5.19 shows the structural response of the meta-structure. The orange curve corresponds to the RMS response, in terms of velocity amplitude of the first component of the meta-structure where the point load is applied. It can be seen that the elastic energy is totally confined in the first component, by the meta-material blocking some frequency bands and preventing transfer to the neighboring flat panel.

The frequency stop bands starts from 2.5 kHz and it continues up to 6 kHz. A short peak appears around $6-7$ kHz, and after the level of attenuation drops down back and continues to higher frequencies up to 19 kHz. Two other small full stop bands can be observed from $20-24$ kHz, and $28-33$ kHz. Ultimately, the quasi-periodic interface creates stop band effects and reduces the elastic wave propagation in the above-mentioned frequency ranges when the wave energy crosses the filter junction.

In the second case, four points of the selected frequency bands are studied and observed by operational deflections modes. The first point is at the beginning of the first frequency stop band at 2.54 kHz, following the second, third, and fourth at 6 kHz, 7.3 kHz, and 19 kHz, respectively. As per Fig. 5.18, the excitation point is on the right panel and the receiving panel the left one. Fig. 5.20 shows operative deformed modes. It can be observed from Fig. 5.20 that the energy is partially transported by the meta-material to the other side (second bare panel) in the low frequency band gap. On the contrary as the frequency increases, within the second band gap that starts at

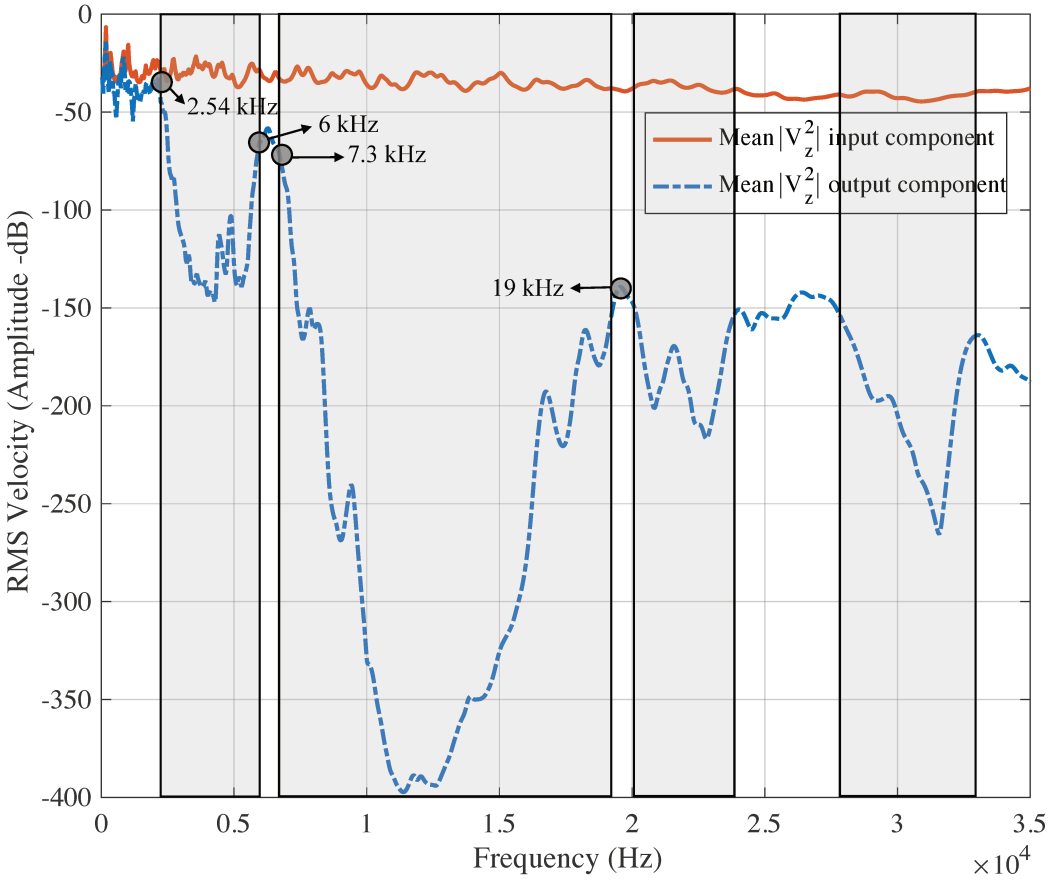

Figure 5.19: FRF of the meta-structure

6 kHz, energy is transferred partially to the left panel. In the third operative deformed mode at 7.3 kHz, the energy does not pass the meta-material and no vibration is observed in the second bare panel. In the fourth operative deformed mode at 19 kHz, the elastic energy transfer to the second bare panel is highly reduced, more than the third mode.

Fig. 5.21 shows the contours of the iso-surface of the meta-structure for three specific frequencies. The iso-surface shows the wave front by blue lines that crosses the meta-material. The color bar in the right-hand side of each iso-surface curve shows the velocity amplitude for the first frequency step at 35 Hz, the second frequency step at 70 Hz, and the start point of the first frequency stop band at around 2520 Hz. It can be seen from Fig. 5.21 that the contour of the iso-surface propagates as the wave front starts crossing the meta-material and continues to the end of meta-structure. For the second case at 70 Hz, wave energy with circular shapes propagates and crosses the

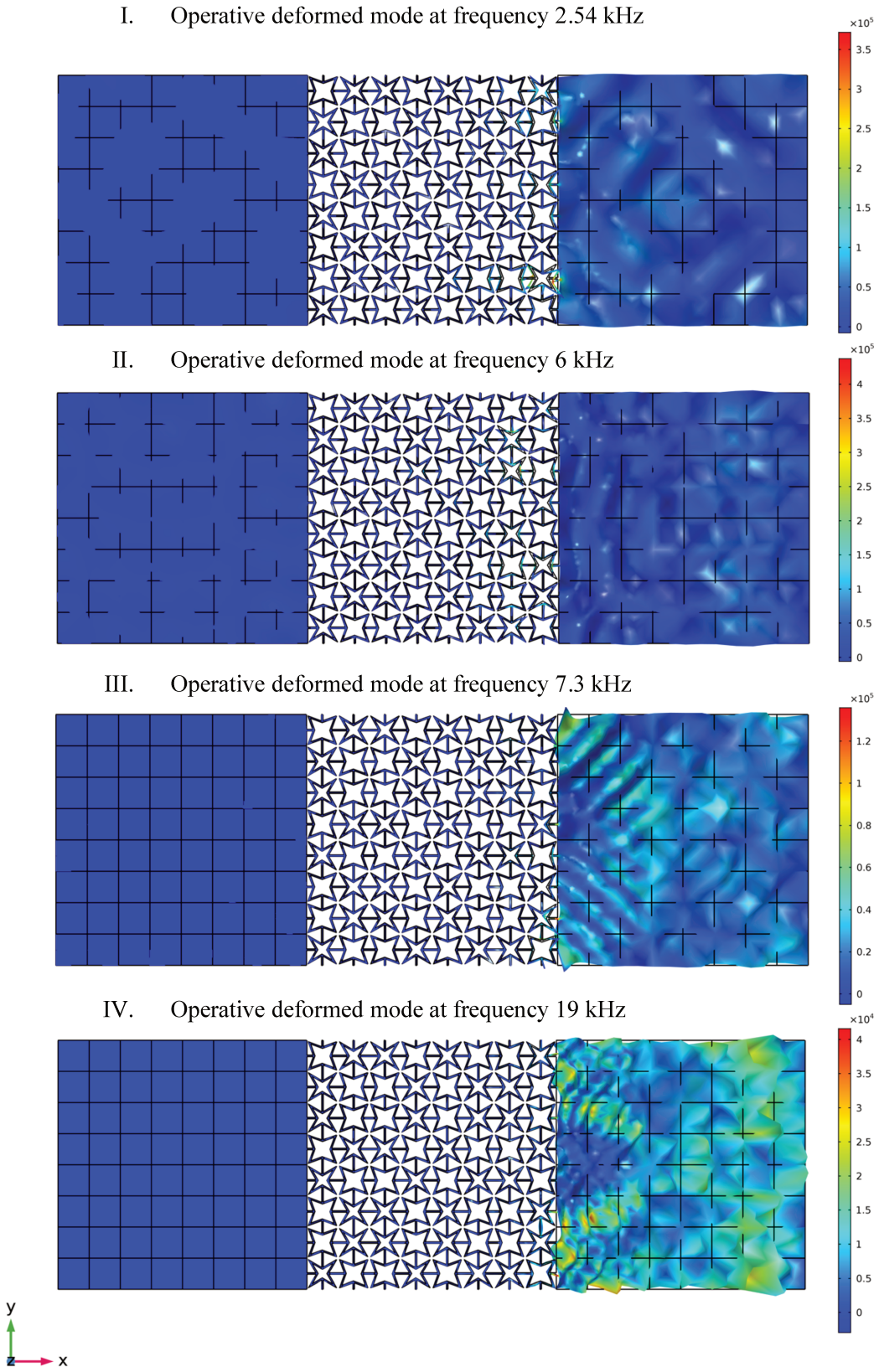

Figure 5.20: Operative deformed modes of the meta-structure in four selected frequencies (2.54 kHz, 6 kHz, 7.3 kHz, and 19 kHz), for visualization of elastic energy transfer from one bare panel to the next one by crossing the quasi-periodic mata-material panel.

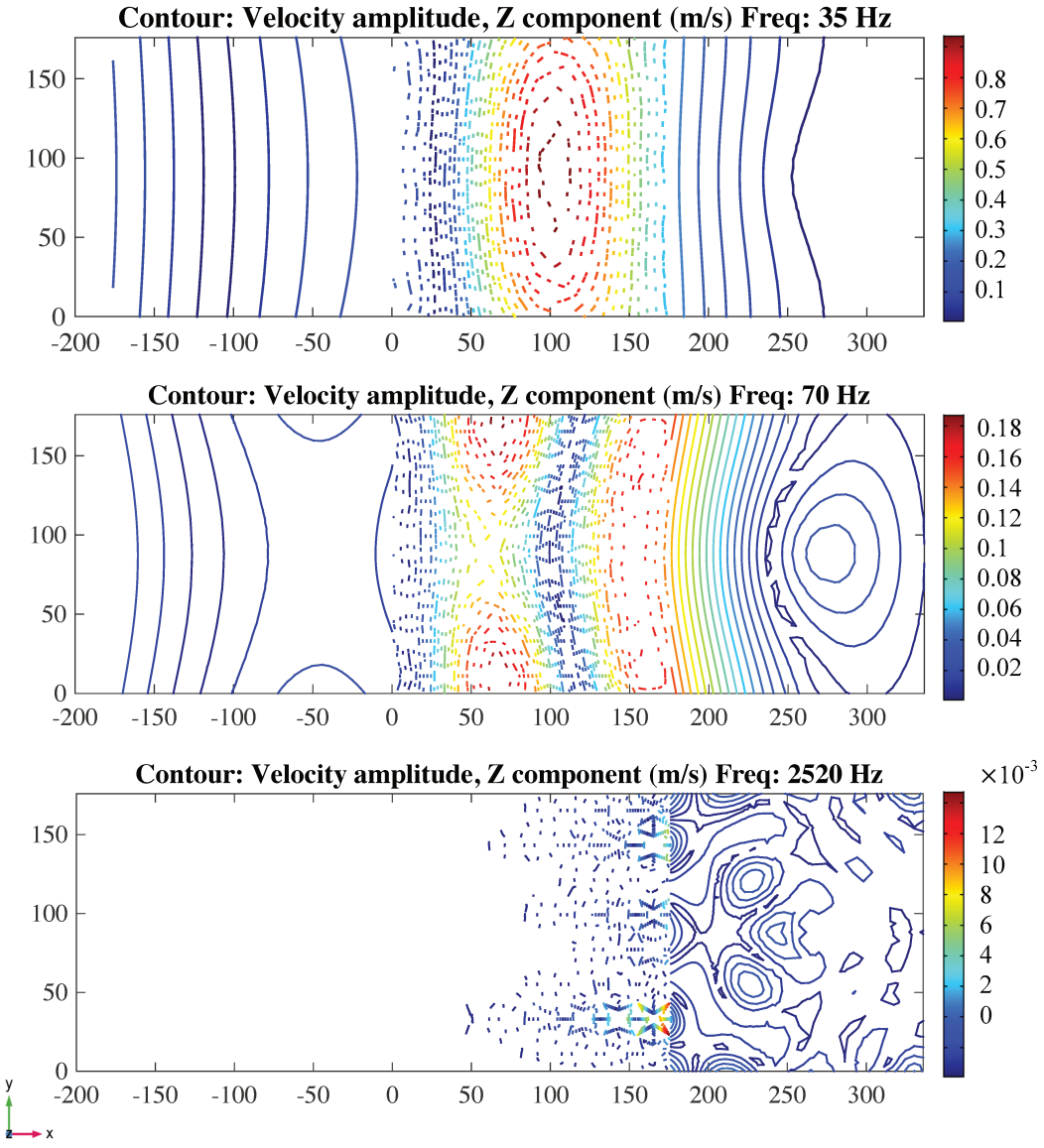

Figure 5.21: Iso-surface of three selected response frequencies

meta-material again. When the frequency reaches 2520 Hz, the first band gap starts and the induced energy is confined in the right panel with a partial crossover to the meta-material and has completely stopped propagating by the mid-point of the meta-material (i.e., stop band effects are evident).

A comparison between the numerical models and the measurements is given in Fig. 5.22. Two band gaps can be seen in the plot for both numerical and experimental cases. The first band gap between 2.5 and 5 kHz is almost similar in terms of width for both cases but with a lower attenuation in the experimental results. The second band gap that starts from 8.1 kHz and continues to higher frequencies over 10.9 kHz is similar too, for both cases. As can be seen, the second band gap in the experimental measurement has again lower attenuation compared to the numerical one. The different depth of numerical and experimental band gaps can be a function of many concurrent parameters.

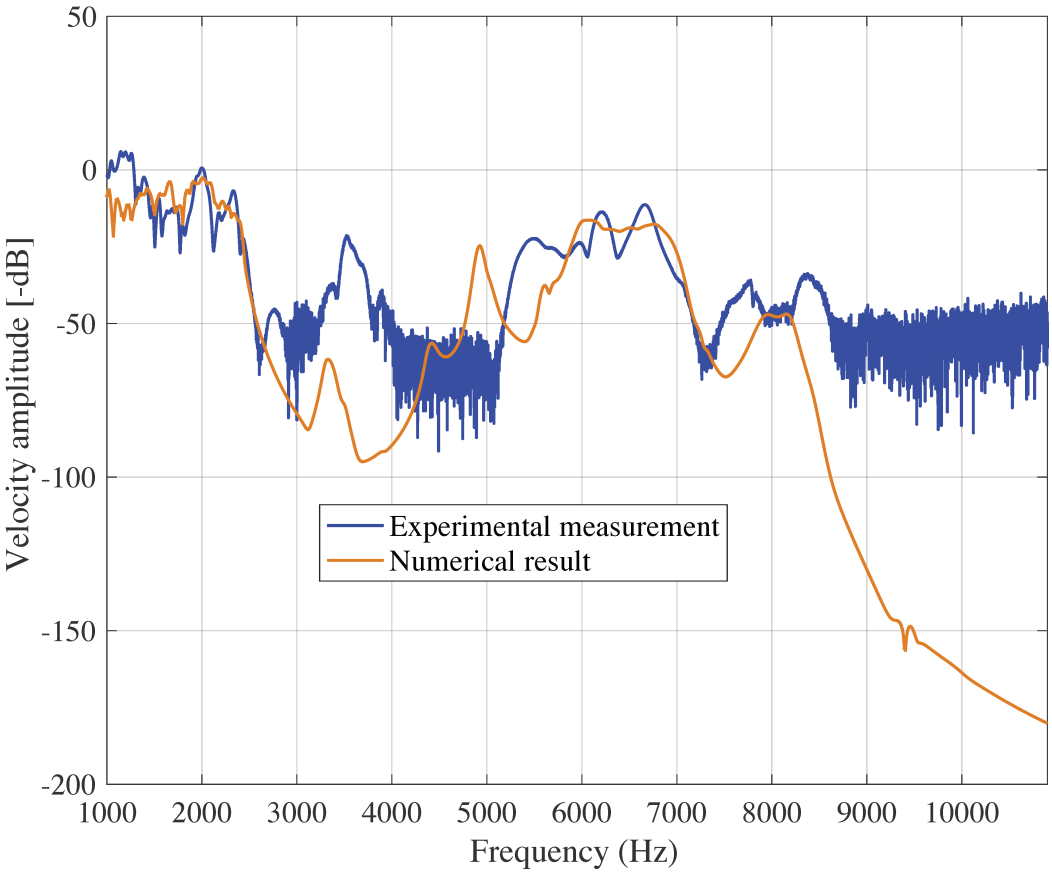

Figure 5.22: Comparison of numerical and experimental FRFs

For example, for every response amplitude in the experimental measurements, the measured data are strongly influenced by the fundamental noise. On the contrary, in the numerical model the computed reduction of the structural response is simply a function of the numerical approximations.

5.6 Concluding remarks

This chapter contains an analysis of meta-materials and meta-structures for vibroacoustic applications. The modelling strategy provides key factors to increase the order of quasi-periodicity in two dimensions in order to create lattices based on a quasi-periodic sequence.

Numerical simulations are performed using FE analysis both for dispersion diagram and harmonic response analyses. According to the numerical analysis, the predicted stop bands in the dispersion diagram of infinite lattice match the response in experimental measurements. Experimental measurement is used to validate the numerical results obtained by the developed model. The possibility of observing frequency stop bands in the lattice is performed by post processing of FRFs for lower, medium, and high frequencies. White noise excitation response shows a high degree of consistency between the predicted numerical and experimentally measured results. The velocity amplitude and coherence plots show that even with a different excitation sources like coil/voice, and shakers the results are comparable in terms of validation.

In the last section, the structural dynamic behavior of a quasi-periodic lattice is computed by FE analysis and compared with experimental results. The results show acceptable agreement. In another case study, the FE model of a quasi-periodic lattice is embedded as a junction filter between two bare panels. The induced vibration energy is transferred through the meta-material junction, and it filters the elastic waves due to the impedance mismatch in the star-shaped unit cells. The FRF of RMS of velocity amplitude provides evidence that this novel design can reduce unwanted vibration from the host structure.

The star-shaped unit-cell sequences can thus be considered as a viable starting point for optimization of the final configurations for designing structures with desired frequency stop bands.

Part V

Conclusions

Chapter 6

Conclusion

In this thesis we have demonstrated that structures with irregularity (quasi-periodicity) will have impact in the dynamical behavior. These impact are the results of the numerical simulations in the framework of WFEM. The effects of manufacturing issues are too analyzed by manufacturing a quasi-periodic lattice made of polymers with irregular cores.

The research undertaken in this study initially focused on the development of algorithms to numerically evaluate wave finite element models of 1D and 2D quasi-periodic beams and panels. The modelled beam has a finite number of cells but it is deterministically designed to embed a Fibonacci sequence up to a certain order. Beam prototypes designed according to 4^{th}-order up to 11^{th}-order Fibonacci were modelled, for which the length of the beam with a cross section of $20 \times 20mm^2$ reached 8.9 m. Increasing the Fibonacci order impacts the harmonic response of the structure. Spectral analysis of completely periodic beams, and quasi-periodic beams containing a super-unit-cell (identical unit cell having different properties inside each cell), is introduced to predict the stop bands. The results in 1D structures are satisfactory and are highlighted in the following.

- The effects of dynamic behavior of the finite beam-spans when increasing the number of cells following Fibonacci orders is emphasized by this analysis.
- The effectiveness of case M1(geometrical impedance mismatch) compared to case M2 (material impedance mismatch) depends on sound velocity of property of materials. The sound velocity of case M2 with constant cross-sections and material variation is simply the ratio between modulus of elasticity and density. On the contrary, the sound

velocity of case M1 with constant material and cross-section variation is the ratio of modulus of elasticity with respect to density multiplied by the square of the height of the cross section. Thus, it explains why M2 is less efficient in terms of change in the impedance mismatch.

- Spectral analysis of periodic beams with four types of geometrical variations in identical 6^{th}-order Fibonacci sequence super-unit-cells and double unit cells/patterns were analyzed. The results shows larger (Δf) for the beam with unit cells whose composition follows a Fibonacci sequence.

- A quasi-periodic beam is designed using the 6th-order Fibonacci sequence is placed in a super unit cell for FB waves analysis. Four types of cross-section variations in the beams are considered. The main results, obtained for the 6^{th}-order case, show that a larger difference between the cross-sections (i.e., cross-section (A) is much larger than cross-section (B)) leads to three main effects: i) change in extension/enlargement of frequency band gaps, ii) shift of frequency band gaps to lower frequency, and iii) an increase in the depth of amplitude attenuation level of frequency band gaps.

The second thrust of this study was to analyze a similar case study in 2D quasi-periodic panels. A lattice made of a limited number of unit cells is designed following a Thue-Morse sequence. This mathematical sequence is capable of designing a 2D panel with an irregular repetition of unit cells in the x- and y-directions. This quasi-periodic meta-material is then numerically modelled and physically manufactured. The numerical 2D model is validated experimentally and it shows that response of combined cells with Thue-Morse characteristics can improve performances in terms of band gaps without weight penalty. The results in 2D panels are satisfactory and the achievements are highlighted in the following.

- A vibroacoustic frequency analysis is performed of meta-materials and meta-structures. The modelling strategy provides key factors to increase the order of quasi-periodicity in two dimensions in order to create lattices based on a quasi-periodic sequence.

- Numerical simulations are performed using FE analysis both for dispersion diagram and harmonic response analyses. According to the numerical analysis, the predicted stop bands in the dispersion diagram of the infinite lattice match the response in experimental measurements.

- The FE analysis shows that the dynamic response of the quasi-periodic lattice has efficient results, therefore a numerical test case for building a meta-structure is also computed. The FRF of RMS of velocity amplitude provides evidence that this novel design can reduce unwanted vibration from the host structure.

- Degree of consistency between numerical & experimental results are highly predicted.

Experimental measurement is used to validate the numerical results obtained by the developed model. The possibility of observing frequency stop bands in the lattice is performed by post processing of FRFs for lower, medium, and high frequencies. White noise excitation response shows a high degree of consistency between the predicted numerical and experimentally measured results. The velocity amplitude and coherence plots show that even with a different excitation sources like coil/voice or shakers the results are comparable in terms of validation. The star-shaped unit-cell sequences can thus be considered as a viable starting point for optimization of the final configurations for designing structures with desired frequency stop bands. This will be the focus of the future work undertaken after that completed for this study.

Bibliography

[1] D. Mead, Wave propagation in continuous periodic structures: research contributions from southampton, 1964–1995, Journal of sound and vibration 190 (3) (1996) 495–524.

[2] K. F. Graff, Wave motion in elastic solids, Courier Corporation, 2012.

[3] L. Cremer, M. Heckl, Structure-borne sound: structural vibrations and sound radiation at audio frequencies, Springer Science & Business Media, 2013.

[4] R. DiTaranto, Theory of vibratory bending for elastic and viscoelastic layered finite-length beams, Journal of Applied Mechanics 32 (4) (1965) 881–886.

[5] D. Mead, S. Markus, The forced vibration of a three-layer, damped sandwich beam with arbitrary boundary conditions, Journal of sound and vibration 10 (2) (1969) 163–175.

[6] V. S. Sokolinsky, S. R. Nutt, Consistent higher-order dynamic equations for soft-core sandwich beams, AIAA journal 42 (2) (2004) 374–382.

[7] G. Kurtze, B. Watters, New wall design for high transmission loss or high damping, The Journal of the Acoustical Society of America 31 (6) (1959) 739–748.

[8] J. A. Moore, Sound transmission loss characteristics of three layer composite wall constructions, Ph.D. thesis, Massachusetts Institute of Technology (1975).

[9] C. L. Dym, M. A. Lang, Transmission of sound through sandwich panels, The Journal of the Acoustical Society of America 56 (5) (1974) 1523–1532.

[10] C. L. Dym, D. Lang, Transmission loss of damped asymmetric sandwich panels with orthotropic cores, Journal of Sound and Vibration 88 (3) (1983) 299–319.

[11] A. C. Nilsson, Wave propagation in and sound transmission through sandwich plates, Journal of Sound and Vibration 138 (1) (1990) 73–94.

[12] J. N. Reddy, Mechanics of laminated composite plates and shells: theory and analysis, CRC press, 2003.

[13] S. Ghinet, N. Atalla, H. Osman, The transmission loss of curved laminates and sandwich composite panels, The Journal of the Acoustical Society of America 118 (2) (2005) 774–790.

[14] R. Kumar, R. Stephens, Dispersion of flexural waves in circular cylindrical shells, Proceedings of the Royal Society of London. A. Mathematical and Physical Sciences 329 (1578) (1972) 283–297.

[15] C. Fuller, The effects of wall discontinuities on the propagation of flexural waves in cylindrical shells, Journal of Sound and Vibration 75 (2) (1981) 207–228.

[16] D. G. Karczub, Expressions for direct evaluation of wave number in cylindrical shell vibration studies using the flügge equations of motion, The Journal of the Acoustical Society of America 119 (6) (2006) 3553–3557.

[17] J. Banerjee, Development of an exact dynamic stiffness matrix for free vibration analysis of a twisted timoshenko beam, Journal of Sound and Vibration 270 (1-2) (2004) 379–401.

[18] L. Brillouin, Wave propagation in periodic structures: electric filters and crystal lattices, Courier Corporation, 2003.

[19] M. Collet, M. Ouisse, M. Ruzzene, M. Ichchou, Floquet–bloch decomposition for the computation of dispersion of two-dimensional periodic, damped mechanical systems, International Journal of Solids and Structures 48 (20) (2011) 2837–2848.

[20] D. Mead, A general theory of harmonic wave propagation in linear periodic systems with multiple coupling, Journal of Sound and Vibration 27 (2) (1973) 235–260.

[21] K. Billon, I. Zampetakis, F. Scarpa, M. Ouisse, E. Sadoulet-Reboul, M. Collet, A. Perriman, A. Hetherington, Mechanics and band gaps in hierarchical auxetic rectangular perforated composite metamaterials, Composite Structures 160 (2017) 1042–1050.

[22] S. Gonella, A. Spadoni, M. Ruzzene, F. Scarpa, Wave propagation and band-gap characteristics of chiral lattices, in: ASME 2007 International Design Engineering Technical Conferences and Computers and Information in Engineering Conference, American Society of Mechanical Engineers Digital Collection, 2009, pp. 505–515.

[23] V. Velasco, J. Zárate, Elastic waves in quasiperiodic structures, Progress in Surface Science 67 (1-8) (2001) 383–402.

[24] D. Shechtman, I. Blech, D. Gratias, J. W. Cahn, Metallic phase with long-range orientational order and no translational symmetry, Physical review letters 53 (20) (1984) 1951.

[25] L. Bindi, P. J. Steinhardt, N. Yao, P. J. Lu, Natural quasicrystals, science 324 (5932) (2009) 1306–1309.

[26] Z. V. Vardeny, A. Nahata, A. Agrawal, Optics of photonic quasicrystals, Nature photonics 7 (3) (2013) 177.

[27] Y. E. Kraus, O. Zilberberg, Quasiperiodicity and topology transcend dimensions, Nature Physics 12 (7) (2016) 624.

[28] Y. E. Kraus, Y. Lahini, Z. Ringel, M. Verbin, O. Zilberberg, Topological states and adiabatic pumping in quasicrystals, Physical review letters 109 (10) (2012) 106402.

[29] Y. E. Kraus, Z. Ringel, O. Zilberberg, Four-dimensional quantum hall effect in a two-dimensional quasicrystal.

[30] J. Fikar, Al-cu-fe quasicrystalline coatings and composites studied by mechanical spectroscopy, Tech. rep., EPFL (2003).

[31] M. Kalman, The quasicrystal laureate, Massachusetts Institute of Technology (MIT) Technology Review, Cambridge.

[32] J.-M. Dubois, S. S. Kang, A. Perrot, Towards applications of quasicrystals, Materials Science and Engineering: A 179 (1994) 122–126.

[33] J.-B. Suck, M. Schreiber, P. Häussler, Quasicrystals: An introduction to structure, physical properties and applications, Vol. 55, Springer Science & Business Media, 2013.

[34] Z. Hou, F. Wu, Y. Liu, Acoustic wave propagating in one-dimensional fibonacci binary composite systems, Physica B: Condensed Matter 344 (1-4) (2004) 391–397.

[35] H. Aynaou, E. El Boudouti, B. Djafari-Rouhani, A. Akjouj, V. Velasco, Propagation and localization of acoustic waves in fibonacci phononic circuits, Journal of Physics: Condensed Matter 17 (27) (2005) 4245.

[36] A.-L. Chen, Y.-S. Wang, Study on band gaps of elastic waves propagating in one-dimensional disordered phononic crystals, Physica B: Condensed Matter 392 (1-2) (2007) 369–378.

[37] P. King, T. Cox, Acoustic band gaps in periodically and quasiperiodically modulated waveguides, Journal of applied physics 102 (1) (2007) 014902.

[38] Z. Wu, F. Li, C. Zhang, Band-gap analysis of a novel lattice with a hierarchical periodicity using the spectral element method, Journal of Sound and Vibration 421 (2018) 246–260.

[39] Z.-J. Wu, F.-M. Li, Spectral element method and its application in analysing the vibration band gap properties of two-dimensional square lattices, Journal of Vibration and Control 22 (3) (2016) 710–721.

[40] Z.-J. Wu, F.-M. Li, C. Zhang, Vibration band-gap properties of three-dimensional kagome lattices using the spectral element method, Journal of Sound and Vibration 341 (2015) 162–173.

[41] M. Gei, Wave propagation in quasiperiodic structures: stop/pass band distribution and prestress effects, International Journal of Solids and Structures 47 (22-23) (2010) 3067–3075.

[42] E. M. Barber, Aperiodic structures in condensed matter: fundamentals and applications, CRC Press, 2008.

[43] S. Mester, H. Benaroya, Periodic and near-periodic structures, Shock and Vibration 2 (1) (1995) 69–95.

[44] D. Mead, A. Bansal, Mono-coupled periodic systems with a single disorder: Free wave propagation, Journal of Sound and Vibration 61 (4) (1978) 481–496.

[45] K. H. Matlack, A. Bauhofer, S. Krödel, A. Palermo, C. Daraio, Composite 3d-printed metastructures for low-frequency and broadband vibration absorption, Proceedings of the National Academy of Sciences 113 (30) (2016) 8386–8390.

[46] C. Claeys, N. G. R. Melo Filho, L. Van Belle, E. Deckers, W. Desmet, Design and validation of metamaterials for multiple structural stop bands in waveguides, Extreme Mechanics Letters 12 (2017) 7–22.

[47] M. Ouisse, M. Collet, F. Scarpa, A piezo-shunted kirigami auxetic lattice for adaptive elastic wave filtering, Smart Materials and Structures 25 (11) (2016) 115016.

[48] A. Madeo, M. Collet, M. Miniaci, K. Billon, M. Ouisse, P. Neff, Modeling phononic crystals via the weighted relaxed micromorphic model with free and gradient micro-inertia, Journal of Elasticity 130 (1) (2018) 59–83.

[49] P. Martinsson, A. Movchan, Vibrations of lattice structures and phononic band gaps, Quarterly Journal of Mechanics and Applied Mathematics 56 (1) (2003) 45–64.

[50] M. Ruzzene, L. Mazzarella, P. Tsopelas, F. Scarpa, Wave propagation in sandwich plates with periodic auxetic core, Journal of intelligent material systems and structures 13 (9) (2002) 587–597.

[51] D. Qing-Tian, Y. Zhi-Chun, Wave propagation in sandwich panel with auxetic core, J Solid Mech 2 (4) (2010) 393–402.

[52] G. Carta, M. Brun, A. B. Movchan, T. Boiko, Transmission and localisation in ordered and randomly-perturbed structured flexural systems, International Journal of Engineering Science 98 (2016) 126–152.

[53] M. Ichchou, F. Bouchoucha, M. B. Souf, O. Dessombz, M. Haddar, Stochastic wave finite element for random periodic media through first-order perturbation, Computer Methods in Applied Mechanics and Engineering 200 (41-44) (2011) 2805–2813.

[54] C. Pierre, E. Dowell, Localization of vibrations by structural irregularity, Journal of sound and Vibration 114 (3) (1987) 549–564.

[55] C. Hodges, J. Woodhouse, Vibration isolation from irregularity in a nearly periodic structure: theory and measurements, The Journal of the Acoustical Society of America 74 (3) (1983) 894–905.

[56] I. Harari, A survey of finite element methods for time-harmonic acoustics, Computer methods in applied mechanics and engineering 195 (13-16) (2006) 1594–1607.

[57] V. Cotoni, R. Langley, P. Shorter, A statistical energy analysis subsystem formulation using finite element and periodic structure theory, Journal of Sound and Vibration 318 (4-5) (2008) 1077–1108.

[58] B. R. Mace, E. Manconi, Modelling wave propagation in two dimensional structures using finite element analysis, Vol. 318, Elsevier, 2008, pp. 884–902.

[59] S. Ham, K.-J. Bathe, A finite element method enriched for wave propagation problems, Computers & structures 94 (2012) 1–12.

[60] F. Moser, L. J. Jacobs, J. Qu, Modeling elastic wave propagation in waveguides with the finite element method, Ndt & E International 32 (4) (1999) 225–234.

[61] J.-M. Mencik, M. Ichchou, Multi-mode propagation and diffusion in structures through finite elements, European Journal of Mechanics-A/Solids 24 (5) (2005) 877–898.

[62] O. Doutres, M. Ouisse, N. Atalla, M. Ichchou, Impact of the irregular microgeometry of polyurethane foam on the macroscopic acoustic behavior predicted by a unit-cell model, The Journal of the Acoustical Society of America 136 (4) (2014) 1666–1681.

[63] M. Ouisse, M. Ichchou, S. Chedly, M. Collet, On the sensitivity analysis of porous material models, Journal of Sound and Vibration 331 (24) (2012) 5292–5308.

[64] G. Petrone, V. D' Alessandro, F. Franco, S. De Rosa, Numerical and experimental investigations on the acoustic power radiated by aluminium foam sandwich panels, Composite Structures 118 (2014) 170–177.

[65] S. Timorian, G. Petrone, S. De Rosa, F. Franco, M. Ouisse, N. Bouhaddi, Spectral analysis and structural response of periodic and quasi-periodic beams, Proceedings of the Institution of Mechanical Engineers, Part C: Journal of Mechanical Engineering Science 233 (23-24) (2019) 7498–7512.

[66] S. Timorian, M. Ouisse, N. Bouhaddi, S. De Rosa, F. Franco, Numerical investigations and experimental measurements on the structural dynamic behaviour of quasi-periodic meta-materials, Mechanical Systems and Signal Processing 136 (2020) 106516.

[67] L. Pisano, L. Sigler, Fibonacci's liber abaci: a translation into modern english of the book of calculation, Sources and Studies in the History of Mathematics and Physical Sciences, Sigler, Laurence E., trans, Springer.

[68] J. Berstel, Combinatorics on words: Christoffel words and repetitions in words, Vol. 27, American Mathematical Soc., 2009.

[69] J.-P. Allouche, J. Shallit, The ubiquitous prouhet-thue-morse sequence, in: Sequences and their applications, Springer, 1999, pp. 1–16.

[70] M. S. KUSHWAHA, Band gap engineering in phononic crystals.

[71] M. S. Kushwaha, P. Halevi, L. Dobrzynski, B. Djafari-Rouhani, Acoustic band structure of periodic elastic composites, Physical review letters 71 (13) (1993) 2022.

[72] M. Sigalas, E. N. Economou, Band structure of elastic waves in two dimensional systems, Solid state communications 86 (3) (1993) 141–143.

[73] Y. Sun, Y. Yu, Y. Zuo, L. Qiu, M. Dong, J. Ye, J. Yang, Band gap and experimental study in phononic crystals with super-cell structure, Results in Physics 13 (2019) 102200.

[74] M. Petyt, Introduction to finite element vibration analysis, Cambridge university press, 2010.

[75] A. Kutsenko, A. Nagy, X. Su, A. Shuvalov, A. Norris, Wave propagation and homogenization in 2d and 3d lattices: A semi-analytical approach, The Quarterly Journal of Mechanics and Applied Mathematics 70 (2) (2017) 131–151.

[76] L. Arnold, H. Crauel, J.-P. Eckmann, Lyapunov exponents: proceedings of a conference held in Oberwolfach, May 28-June 2, 1990, Springer, 2006.

[77] M. I. Hussein, M. J. Leamy, M. Ruzzene, Dynamics of phononic materials and structures: Historical origins, recent progress, and future outlook, Applied Mechanics Reviews 66 (4) (2014) 040802.

[78] A. Spadoni, M. Ruzzene, S. Gonella, F. Scarpa, Phononic properties of hexagonal chiral lattices, Wave motion 46 (7) (2009) 435–450.

[79] S. Timorian, M. Ouisse, N. Bouhaddi, S. De Rosa, F. Franco, Band diagram and forced response analysis of periodic and quasi-periodic panels, in: 9th ECCOMAS Thematic Conference on Smart Structures and Materials (2019), Paris, France, 2019, pp. 1085 – 1095.

[80] S. Timorian, F. Franco, M. Ouisse, S. De Rosa, N. Bouhaddi, Investigation for the analysis of the vibrations of quasiperiodic structures, in: 28th International Conference on Noise and Vibration engineering (ISMA 2018 2018), Leuven, Belgium, 2018, pp. 4451 – 4462.

[81] G. A. Bécus, Wave propagation in imperfectly periodic structures: a random evolution approach, Zeitschrift für angewandte Mathematik und Physik ZAMP 29 (2) (1978) 252–261.

[82] S.-Y. Chang, C.-D. Chen, J.-Y. Yeh, L.-W. Chen, Elastic wave propagation of two-dimensional metamaterials composed of auxetic star-shaped honeycomb structures, Crystals 9 (3) (2019) 121.

[83] A. Krushynska, M. Miniaci, F. Bosia, N. Pugno, Coupling local resonance with bragg band gaps in single-phase mechanical metamaterials, Extreme Mechanics Letters 12 (2017) 30–36.

[84] C. Hakoda, J. Rose, P. Shokouhi, C. Lissenden, Using floquet periodicity to easily calculate dispersion curves and wave structures of homogeneous waveguides, in: AIP Conference Proceedings, Vol. 1949, AIP Publishing, 2018, p. 020016.

[85] J. Kook, Investigation of bandgap structure in coupled acoustic-mechanical system, in: INTER-NOISE and NOISE-CON Congress and Conference Proceedings, Vol. 253, Institute of Noise Control Engineering, 2016, pp. 2608–2615.